DESIGN AID FOR SHEAR STRENGTHENING OF REINFORCED CONCRETE T-JOINTS USING CARBON FIBER REINFORCED PLASTIC COMPOSITES

By

Ioan Gergely, Ph.D.

Chris P. Pantelides, Ph.D., P.E.

July 13, 1998

Earthquake Research Program
Research Report UUCE 98-02
Department of Civil and Environmental Engineering
University of Utah
Salt Lake City, Utah 84112

ABSTRACT

The research presented in the present work focuses on the shear strengthening of beam column joints using carbon fiber composites, a material considered in seismic retrofit in recent years more than any other new material. The design and field application research on reinforced concrete cap beam-column joints includes analytical investigations using pushover analysis; design of carbon fiber layout, experimental tests and field applications.

Several beam column joints have been tested recently with design variables as the type of composite system, fiber orientation and the width of carbon fiber sheets. The surface preparation has been found to be critical for the bond between concrete and composite material, which is the most important factor in joint shear strengthening. The final goal of this research is to develop design aids for retrofitting reinforced concrete beam column joints.

Two bridge bents were tested on the Interstate-15 corridor. One bent was tested in the as-is condition. Carbon fiber reinforced plastic composite sheets were used to externally reinforce the second bridge bent. By applying the composite, the displacement ductility has been doubled, and the bent overall lateral load capacity has been increased as well.

TABLE OF CONTENTS

LIST OF FIGURES

LIST OF TABLES

ACKNOWLEDGEMENT

The work presented in this report was performed at the University of Utah and was partially funded by the U.S. National Science Foundation under Grant No. CMS9712761, the Federal Highway Administration, the Utah Department of Transportation, and the Idaho National Engineering and Environmental Laboratory. In-kind contributions were made by Xxsys Technologies, Inc., and Geopier Foundation, Inc.

CHAPTER 1

INTRODUCTION

As the nation's infrastructure is deteriorating, there is a need for effective rehabilitation methods for structures. A new retrofit method involving the use of fiber reinforced plastics (or composites) has been in the center of attention in the last decade.

These composites offer advantages over structural steel, reinforced concrete or timber. Some of the advantages are the superior resistance to corrosion, high stiffness-to-weigth and strength-to-weigth rations, and the ability to control the material's behavior by selecting the proper orientation of the fibers (Swanson, 1997). All of these make the carbon fiber composites a highly engineered material, suitable in infrastructure applications, in spite of the fact that the cost of carbon fibers is much higher than the cost of conventional construction materials.

The applications of this technology include reinforced concrete circular and rectangular columns, beams, slabs, tilt-up walls, bridge decks, unreinforced masonry walls and glulam beams. Composites are being used to provide external and internal reinforcement in the form of external continuous jackets or woven fabrics, as bending reinforcement, as prestressing tendons and as closed stirrups.

From over half a million highway bridges in the country, about forty percent are classified according to the Federal Highway Administration's criteria, as deficient and in

need of rehabilitation or replacement. The lateral load capacity of concrete structures is of major interest due to potential catastrophic failures in large earthquakes. In the 1994 Northridge earthquake, all bridge collapses were associated with poor performance of older shear-critical columns and short seat widths (EERI, 1995).

Therefore, the initial experiments were conducted on typical bridge columns. However, at the present time, a large variety of applications are being explored, including parking garages, concrete and masonry structural elements.

1.1 Literature review

Research on retrofit techniques on multiple column bents has been conducted at the University of California, Berkeley since 1990. A three-span segment of the standing portion of the Cypress Street viaduct was tested to check existing retrofit techniques. It was found by Bollo et al. (1990), that retrofitting had little effect on overall stiffness, but increased strength and displacement ductilities.

Extensive research on retrofit of columns has been done at the University of California - San Diego by Sun et al. (1993), by Seible et al. (1994), by Priestley et al. (1996), by Seible et al. (1997). Circular, square and rectangular bridge columns have been strengthened using continuously wrapped carbon fiber reinforced plastic (FRP) composites and steel jacketing. The confinement, the ductility and the shear effects were studied and design guidelines were developed.

These retrofitted columns exhibited large displacement ductilities while maintaining a constant load capacity level, without significant cyclic capacity degradation. The tests showed that the carbon fiber reinforced plastic jacket was as effective as a comparable

steel jacket system.

Five full-scale circular bridge columns were retrofitted with carbon fiber jackets in 1995 at the Santa Monica viaduct (Policelli, 1995), and three columns and the cap beam were strengthened on the Interstate-80 at the Highland Drive overpass (Gergely et al., 1997). The purpose of the full-scale demonstration projects was to monitor the long-term performance of the repair, and to demonstrate the technical and commercial viability of the retrofit system.

Nine circular reinforced concrete columns were tested by Gamble and Hawkins (1996). The columns, part of an old bridge system built in the mid-1960s, were designed with no consideration of seismic effects. Three of the columns were retrofitted using tensioned steel bands, while two were glass FRP jacketed. All the baseline columns failed due to poor confinement of the lap splice region. However, none of the strengthened columns could be failed.

An experimental investigation was conducted by Saadatmanesh et al. (1996), to study the seismic performance of reinforced concrete columns retrofitted with composite straps. The retrofitted columns had a superior ductility (up to 6) compared to the low ductility level of 1.5 observed for the baseline specimens. The composite straps confined the concrete in the plastic hinge region, and prevented the column longitudinal reinforcement from buckling at higher displacements.

A theoretical study (Gergely et al., 1998) showed that the stress-strain curve for the confined concrete is bilinear. The first part of the curve is the unconfined concrete. However, the second part of the curve depends on the shape of the column (circular versus square), the composite material properties and number of confining layers, and the

radius of the corners for the noncircular columns. These findings correlate well with the experimental findings by Picher et al. (1996).

Concrete cylinders wrapped with composite materials were tested by Hoppel et al. (1994) and by Howie and Karbhari (1995). The composite jacket provided a confining pressure for the cylinders and the columns with similar retrofit. Once the concrete begun to fail, the wrap could hold the column together and allowed it to deform while the structural integrity of the member was maintained.

A series of twelve concrete beams were tested by Chajes et al. (1994), to study the effectiveness of composite fabrics applied externally to improve the member's shear capacity. Carbon, glass and aramid FRP were used to study the influence of stiffness and strength of these materials. An increase in the beam's ultimate strength of 60 to 150% was achieved.

In the study performed by Triantafillou (1998), experimental and analytical results are compared. from externally strengthened beams. The composite sheets were applied to the surface of the beams following different layouts and orientations. The failure of these beams was due to composite delamination from the concrete surface, at very low composite strain levels (in the range of 0.05 to 0.17%).

Five rectangular reinforced concrete beams were strengthened and analyzed by Saadatmanesh and Ehsani (1991). The glass FRP plates were applied to the tension face of beams subjected to four-point bending. The epoxy bonded plates increased the flexural capacity of the beams, and improved the cracking behavior of the specimens by delaying the formation of visible cracks.

The parametric study performed by An et al. (1991) on the same specimens

showed that because of the elastic behavior of the composite plates, failure of the beams could be reached by the rupture of the plates, crushing of the concrete or failure of the concrete cover between the reinforcing steel and composite plates. Similar research has been conducted by Norris et al. (1997).

Nanni and Norris (1995) experimentally investigated the behavior of concrete members laterally confined with FRP composites. Specimens with circular cross-section subjected to flexure showed a better performance compared to the rectangular shaped sections.

Reinforced concrete beams have been tested by Ritchie et al. (1991). Plates of glass, carbon and aramid fiber reinforced plastics were bonded to the tension side of the beams. A significant increase in ultimate strength and stiffness was observed.

The paper by Thomas et al. (1996) describes the applications of externally bonded composite sheets in the repair of concrete and masonry structures. Examples are presented of retrofitted beam-to-column and slab-to-column connections. Their practical experience led to the conclusion that the surface preparation is 90% of the job.

A prestressed concrete bridge girder hit by a truck was repaired in West Palm Beach, Florida. The girder was repaired using epoxy-impregnated carbon fiber sheets bonded to the member's surface (ENR, 1995).

Al-Salloum et al. (1996) used the design formulas of the current ACI-318 (1995) code to evaluate concrete beams reinforced with internal glass FRP bars. The results showed that the beam's flexural capacity can be estimated using the ultimate design method. However, the code underestimates the deflections of beams reinforced with internal composite bars.

The effectiveness of FRP external prestressing on concrete beams was tested by Arduini et al. (1996). The flexural behavior of the beams was similar to that expected with steel prestressing tendons.

A recent study by Karbhari (1996) summarizes a few concepts related to the importance of the bond between the composite and the concrete substrate as applicable to infrastructure repair. Some of these factors include external influences (humidity, moisture, temperature and aggressive environment), interfacial influences (moisture entrapment), and internal influences (chemical activity, electrochemical activity and stress level).

Karbhari and Engineer (1996) have studied the short term durability of composite applications. It was observed that by using carbon fibers and a higher T_g (glass transition temperature) resin composite, a more durable retrofit system was obtained.

Twenty prestress concrete beams pretensioned by carbon fiber composite cables were tested by Domenico et al. (1998). As it was expected, the load transfer length was in function of the diameter of the composite strands. However, the amount of concrete cover had no influence on the transfer length (the cover was about 3.3 to 6 times the diameter of the strands).

A new approach for seismic retrofitting of lightly-reinforced precast concrete walls is presented by Ehsani and Saadatmanesh (1997). Field application of the fiber reinforced plastic fabric in repairing a precast wall building, which was severely damaged during the 1994 Northridge earthquake, provided a unique economical solution for the retrofitting of the building.

Ten prestressed concrete wall assemblies have been tested by Pantelides et al.

(1998). First, the panels were tested with the welded connections, than two layers of carbon FRP sheet were applied to provide adequate in-plane shear capacity. Superior performance was achieved by water jetting the concrete surface, and by applying a thin layer of high strength structural adhesive (Sikadur 31), before the composite was placed.

Composite retrofit is applicable not only to reinforced concrete elements, but also to wood and masonry structures. A hybrid concrete-wood-CFRP beam system was investigated by Chajes et al. (1996). The experiments showed that CFRP plates and concrete could be used to increase the strength and stiffness of engineered wood beams. However, the bond between wood and concrete was found to be inadequate, as compared to the bond between wood and CFRP plates.

Dolan et al. (1997) investigated the behavior of glulam beams strengthened by kevlar FRP sheets added between the laminations. The beam's performance was further enhanced by pretensioning the composite layers. The fibers were glued using commercially available resin wood glues with satisfactory results. There was no apparent difference in the behavior of the beam by using a more expensive epoxy resin.

The repair of reinforced structural masonry walls was investigated by Innamorato (1994). The specimens were tested twice, once to generate the desired mode of failure, and again after the application of the composite overlay to examine the structural performance of the composite repair.

It can be seen from this section, that there were no previous analytical or experimental studies performed to strengthened reinforced concrete T-joints using externally applied composite materials. However, there are a few studies available focused on the behavior of beam-column joints.

The joint shear stresses recommended by ACI 352R-91 (1991) are valid for newly constructed beam-column joints. Values are given for exterior and interior joints, linear and nonlinear joints. but these allowable stresses are based on a properly confined concrete joint with adequate joint shear reinforcement.

However, older concrete structures do not meet these criteria, and based on experimental studies, the T-joints designed three decades ago, fail at a much lower stress level (Nilsson and Losberg (1976), and Priestley et al. (1997)). When the diagonal tensile stresses reach the concrete's tensile strength, diagonal cracks appear. By further increasing the cyclic load. significant joint damage and failure were observed.

To strengthened these weak joints, several methods are already available. In the research performed by Lowes and Moehle (1995), for one of the specimens, the section of the joint was increased and special dowels were provided. For the last specimen, additional post-tensioning rods were included in the increased section, and an axial force was applied to the member. In both cases a ductile beam-column behavior was observed, an improvement compared to the linear results from the baseline specimens.

The strength of frame connections has been increased by jacketing the joint region in the study performed by Alcocer and Jirsa (1993). Similar improvements were obtained by applying corrugated steel jackets around the beam-column connection (Biddah et al. (1993)). A method was formulated to design the corrugated steel jacket thickness and depth.

1.2 Objectives

Strengthening of concrete beam-column joints is desirable for concrete bridges, and other concrete structures, built before the 1980-s that may have corrosion or seismic problems. The present research focuses on a retrofit technique based on externally applied carbon FRP composite sheets, as opposed to the methods presented in the previous section.

In order to study the behavior of concrete T-joints, fifteen specimens were designed, built and tested. There were four baseline specimens tested in the as-built condition. The column reinforcement ensured that the columns would have superior shear and flexural capacity compared to the beam.

The remaining specimens were externally reinforced using composite woven sheets. The following variables have been considered: the composite curing process, the carbon FRP layout, and the surface preparation of the concrete specimens. First, an elevated temperature cure system was used, which was replaced by a room temperature cure system. There was no difference observed between these two methods.

To examine the effect of number and orientation of composite layers, a balanced and unsymmetrical layout was applied to the beam's surface. This layout was changed to a balanced and symmetric one, which proved to be superior.

In order to study the effect of the surface preparation, some of the specimens were only wire brushed, and the resin was used as adhesive. Two of the specimens however, were water jetted, and a high strength adhesive was applied to the rough surface as adhesive for the composite material.

The experimental results were compared with the analytical findings from the finite

element analysis using DRAIN-2DX (1992). Based on the increase in the strength of the specimens and by analyzing the joint shear stresses, a design equation is given for the retrofit of beam-column joints with small axial load.

The analytical findings from the T-joint specimens combined with the published design equations for the composite material, were used to retrofit a bridge bent on the Interstate-15 corridor. The goal was to double the ductility of the structure, compared to the baseline test which was performed in the as-is condition.

To achieve this, the shear capacity of the joint was increased, and the confining of the plastic hinge and the lap splice region was provided.

CHAPTER 2

CFRP PROPERTIES AND THEIR MEASUREMENT

As the potential of using composite materials in construction grows, so the need to understand the material properties increases as well. Being a highly engineered material, an efficient and economical FRP (fiber reinforced plastic) repair involves a minimum knowledge of the material behavior.

The selection of the repair system will depend on the type of the structure, the base material, the condition of the structural elements, the targeted performance level, and the availability of composite material.

2.1 Material description

The fiber reinforced plastics are defined as a polymer matrix reinforced by fibers. The polymer matrix can be thermosetting (polyester, vinyl ester, epoxy, phenolic) or thermoplastic (nylon, PET). The polymer matrix used in the present project was a mixture of an epoxy resin and a hardener. Being a thermosetting polymer, once cured, its shape can not be changed by applying heat and force, as opposed to thermoplastics.

The fiber materials considered in structural repairs are the carbon, the glass and the aramid fibers. Among these fibers, the carbon fiber costs the most and has the highest strength and modulus. However, the glass fiber is the least expensive but also has the

lowest tensile strength. Carbon fiber was used in the present research, resulting in the full name of the composite as carbon fiber reinforced plastic or CFRP.

Fibers are commercially available in the form of tows or bundles of parallel fibers. The number of individual fibers in a tow ranges from 1000 to 200000 fibers. These tows could be applied individually using a wrapping machine, or could be woven in sheets and applied manually. The fiber orientation in these woven sheets can be unidirectional, multidirectional or sheets with random fiber orientation.

Unidirectional tows, having 48000 fibers per tow, woven in 152 to 457 mm wide sheets (fabrics) were used here. The fiber material was Zoltek PANEX33-0048 carbon fiber. The number of tows per 25.4 mm of sheet (pitch) was around 6 to 7. The latter weaving resulted in a denser sheet, making it more difficult for the resin to penetrate uniformly the entire thickness of the fiber tows. Therefore, later in the project, a looser material was ordered with a pitch equal to 6.

Figure 1 shows the geometry of the carbon fiber sheets. The width of these sheets was 406 mm for the beam-column joint specimens; for the bridge tests two widths were used, 152 mm and 457 mm. The width of the material is a function of the member dimensions and the design requirements for the composite application. To enable the weaving of the material, cross-stitches are used throughout the length of the material. These cross-stiches (here E-glass fibers), due to their inferior mechanical properties and the limited amount applied, are ignored in the strength evaluation of the material.

By choosing the hardener in the matrix, the curing procedure needs to be specified also. An elevated temperature curing system requires an incremental increase in the composite temperature up to 154 ^{0}C, followed by a curing time of approximately 90

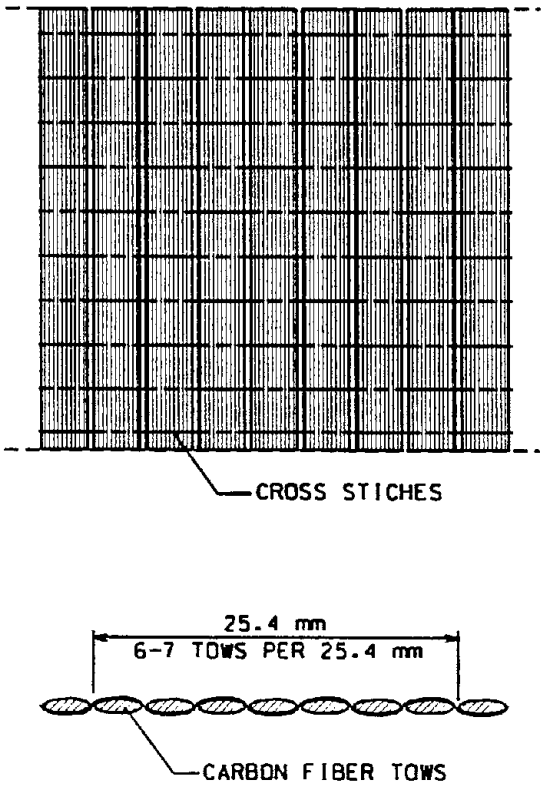

Figure 1. Woven carbon fiber sheets

minutes, and finished by gradually decreasing the temperature. This procedure needs a controlled environment, best achieved in an autoclave. However, the construction field conditions require the use of heat blankets. These blankets cover the repaired surface, and by providing the external heat, cure the composite material.

The curing process for this system does not start until the temperature is increased significantly. This fact provides an opportunity to prepreg the fiber material, in a controlled way, with the premixed resin and hardener. Thus, the specified matrix volume fraction is monitored during fiber impregnation by measuring the amount of matrix added to the fiber. The prepreg composite material could be stored for a limited time until the application process begins.

As opposed to the elevated temperature system, a room temperature curing system cures in the ambient temperature (room temperature). The curing time required depends on the resin and the hardener used, and also on the ambient temperature. By changing the resin or the hardener, the viscosity can be changed, which proved to be critical in the densely woven material and using the room temperature curing system.

Both curing systems have been investigated in the present study. To some of the specimens the carbon fiber sheets were preimpregnated with a mixture of Shell Epon 828 resin and Shell Epirez Epicure curing agent. After the composite sheets were applied to the concrete surface, the specimens were placed in a curing chamber and cured in a temperature controlled environment.

For the majority of the test specimens and for the repair of the bridge bents however, a room temperature cure system was used. In this case, a Shell Epon 826 resin combined with Shell 3379 Epicure hardener was applied to the "dry" woven sheets. The

mixture consisted of two parts by weight of resin and one part of curing agent. In this application, the curing time was approximately seven days.

This system proved to be more suitable for the construction industry from the application point of view. There was no need for thermally controlled heat blankets. However, from the few studies available, the long-term durability of the thermally cured composite is expected to be superior.

2.2 Material properties

Like with any other construction material, it is essential to know the basic material properties of the CFRP. Among the numerous composite material properties used by the structural engineer, the in-plane tensile properties and the composite fiber content were evaluated in the present research.

To evaluate these properties, the samples were prepared according to ASTM specification, and the test results compiled at the University of Utah. The Composite Materials Research Group at the University of Wyoming tested the specimens and provided the recorded test data.

2.2.1 Composite fiber content

The composite fiber content determines the composite's in-plane tensile properties. As the reinforcement in the matrix, the amount of fibers is directly proportional to the tensile strength in the fiber direction of the composite material. The accepted fiber volume content in the civil industry is in the range of 50 %.

This yields a required matrix volume fraction of 50 % (neglecting the volume of

voids). The role of the matrix, besides providing the in-plane shear strength of the composite material, is to provide an adequate load transfer (by shear) between the fibers. As the composite specimen is loaded in tension in the fiber direction, the load lost by the rupture of a single fiber is recovered by shear transfer in the matrix within a distance of eight times the fiber diameter.

It has been proven, that an all fiber sample would fail at about half of the load of a composite sample, with the same amount of fibers, but providing adequate matrix content. The matrix in a composite, besides the above mentioned strength effects, provides a protective coating to the fibers. This will affect the short-term and the long-term durability of the composite application.

To determine the carbon fiber volume content of the specific composite material, the ASTM D-3171 Standard ("Test Method for Fiber Content of Resin-Matrix Composites by Matrix Digestion") was followed. The three samples were obtained from a composite unidirectional sheet (fabric). The average of three tests resulted in the following:

- fiber volume fraction – V_f = 35.3 % (with a standard deviation of 0.8 %);
- matrix volume fraction – V_m = 64.7 %.

The composite fiber content is lower than the expected 50 %, however, it was within acceptable range.

2.2.2 In-plane tensile properties

In determining the tensile properties of the composite material, the ASTM D-3039 specifications ("Standard Test Method for Tensile Properties of Polymer Matrix

Composite Materials") were followed.

Two types of specimens were prepared. For Specimens 1-5 ("unidirectional"), six tows from a fabric have been separated for each specimen, after they were epoxy impregnated. These tows were laid in a machined mold (two layers of three tows for each specimen) and cured in room temperature. Before laying the composite, a thin layer of mold release (Frekote) was sprayed on the mold. By using this mold, it was possible to control the straightness of the tows, and the dimensions of the specimens.

For Specimens 6-9 ("fabric"), a larger woven composite sheet (one layer) was prepared and cured on a flat surface. After the sheet has been cured, a water-cooled rock-saw was used to cut the specimens to the required dimensions. Even though these were unidirectional samples as well, the designation fabric suggests that the tows, due to weaving, are not straight in the transverse direction of the composite sheets (through the thickness). This is also illustrated in Figure 1.

For all the fabric specimens, there has been observed a misalignment of 2^0 from the direction of loading due to a sample cutting error. This problem did not influence significantly the overall test results.

To all the tensile specimens, special glass fiber reinforced plastic tabs were attached at both ends, to provide a good grip for the testing machine, and an even distribution of the clamping forces. The dimensions of the tensile samples, including the tabs, are shown in Figure 2, and are tabulated for each specimen in Table 1.

All the dimensions in Table 1 are measured values, except the thickness of the fabric specimens (column (5)). Due to the difficulty in measuring the thickness of an uneven fabric material, these values (t) were calculated using Equation (1):

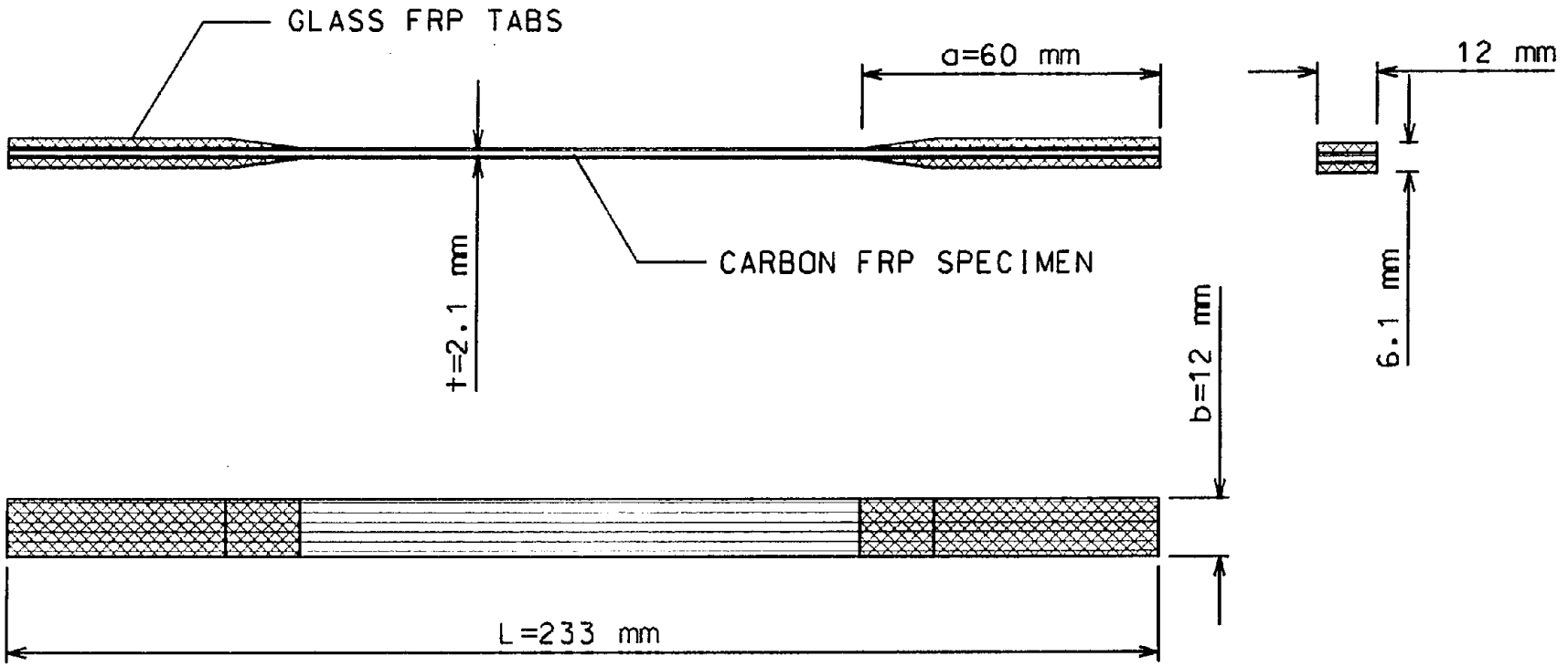

Figure 2. Carbon FRP composite tensile specimens

Table 1. Composite tensile specimens – measured dimensions

Material Type (1)	Specimen (2)	Total Length (L) (mm)[1] (3)	Tab Length (a) (mm)[1] (4)	Thickness (t) (mm)[1] (5)	Width (b) (mm)[1] (6)
Unidirectional	1	233.8	60.7	2.1	12.1
	2	232.3	59.8	2.1	12.1
	3	232.3	59.9	2.0	12.1
	4	233.7	60.7	2.1	12.0
	5	232.4	60.0	2.1	12.1
Fabric	6	222.1	62.4	1.3	12.3
	7	222.0	61.3	1.3	13.3
	8	222.0	61.6	1.3	12.4
	9	222.1	61.8	1.3	12.4

Note: [1] Dimensions defined in Figure 1.

$$t = \frac{A_{tow}}{V_f} \times N_{tow} \times C \qquad (1)$$

where:

t – the calculated specimen thickness;

A_{tow} – the cross-sectional area of the carbon tows, $A_{tow} = 1.968$ mm^2;

V_f – the composite fiber volume fraction, $V_f = 0.353$;

N_{tow} – the number of tows per 25.4 mm, $N_{tow} = 6$ tows/25.4mm;

C – the number of plies. C = 1.

Substituting these values into Equation (1), the calculated fabric specimen thickness is t = 1.32 mm.

Figure 3 shows the stress-strain curves for the unidirectional (molded) specimens. At a stress level of about 800 MPa, all the specimens showed a strange behavior. This was probably the result of a sudden movement or slippage of the strain reading instrument (extensometer) during the test, caused by failure initiation in the specimen. This could have been avoided by using strain gages attached to the specimens.

The dotted line represents the average elastic modulus. It can be seen, that this line covers very well the lower portion of the recorded data, and is parallel with the test curves at the upper segment.

The stress-strain curves for the fabric specimens are shown in Figure 4. The family of test curves is in good agreement with the average elastic modulus line. The upper segment shows again the same problem, observed at the previous test results.

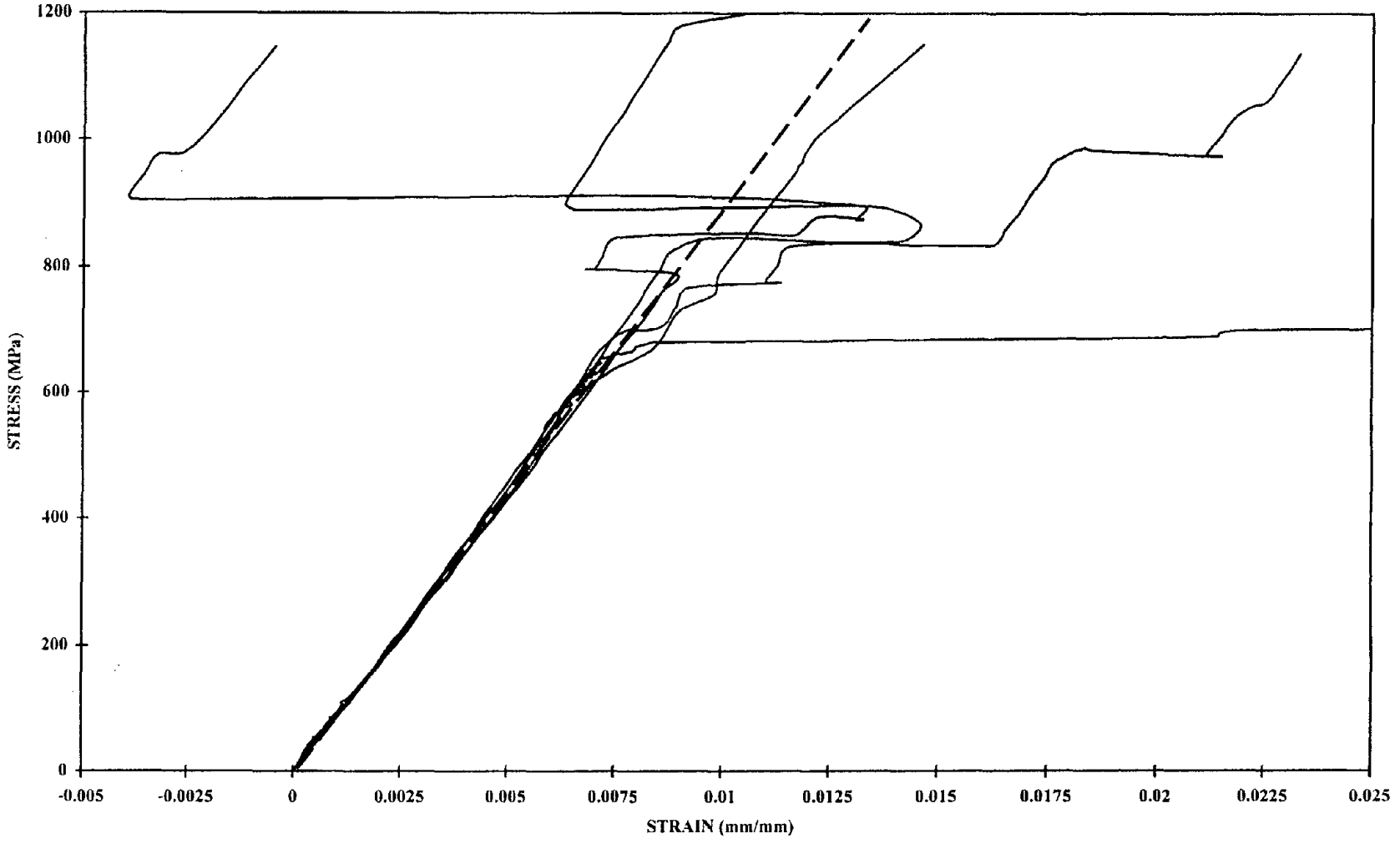

Figure 3. Stress-strain curves for the unidirectional specimens

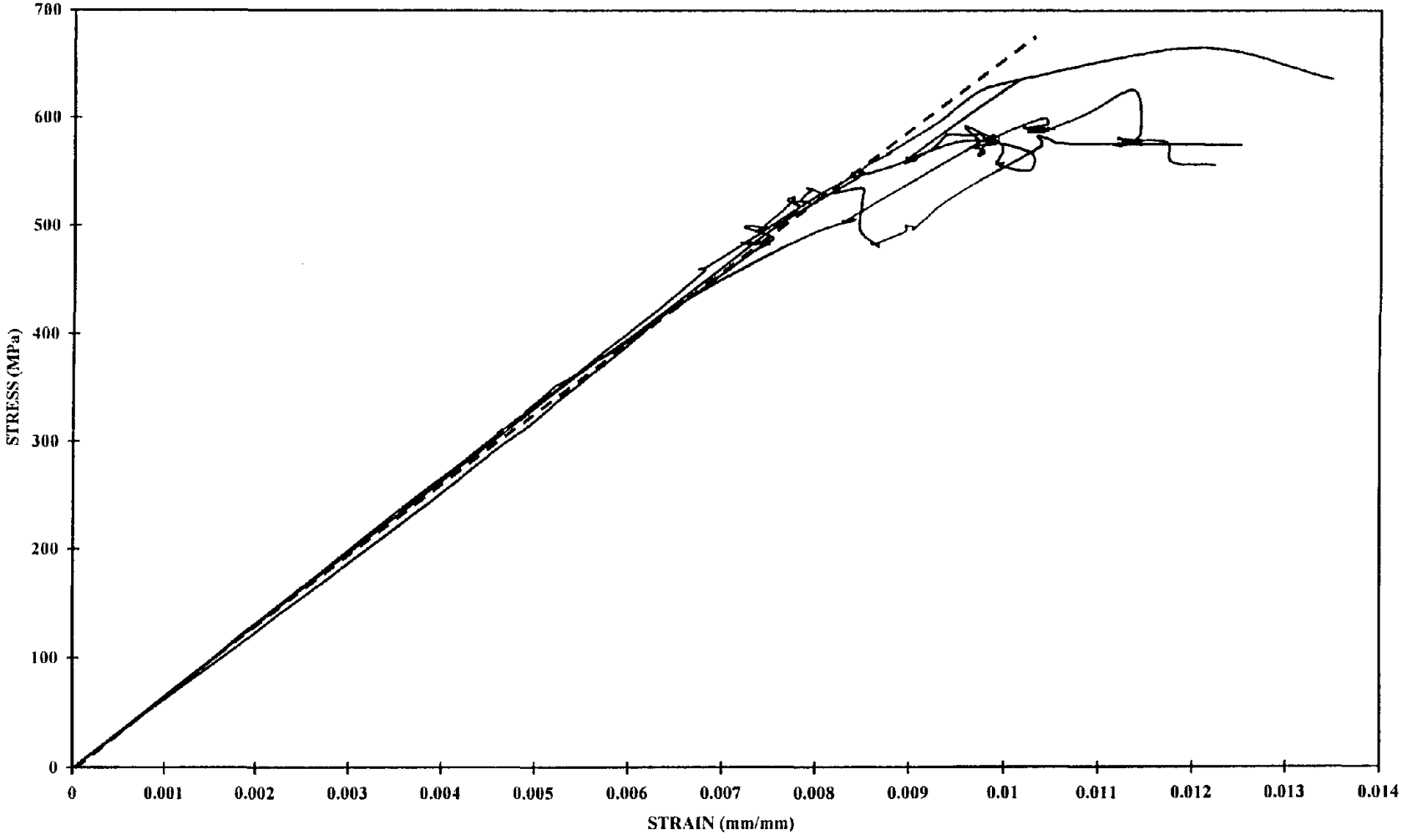

Figure 4. Stress-strain curves for the fabric specimens

The elastic modulus in the fiber direction was calculated at the lower segment of the stress-strain curves using Equation (2):

$$E = \frac{\sigma_2 - \sigma_1}{\varepsilon_2 - \varepsilon_1} \tag{2}$$

where:

ε_2 – a recorded strain reading close to 1.60E-3 mm/mm;

ε_1 – a recorded strain reading close to 8.00E-4 mm/mm;

σ_2 – the recorded stress level corresponding to the strain ε_2;

σ_1 – the recorded stress level corresponding to the strain ε_1.

The strain and stress levels, as well as the calculated elastic modulus for each specimen are given in Table 2. The strain values are selected based on available readings close to the specified values.

The tensile test results for both types of specimens (unidirectional and fabric) are summarized in Table 3. The ultimate tensile stress (given in column (3)) for Specimen 1. and the Poisson's ratio (column (6) in Table 3) for Specimen 6 were not recorded. Therefore, the results from Specimen 1 were not included in the statistical data.

The sample average, standard deviation and the coefficient of variation is calculated for each material type separately. This allows a direct comparison between the performance of the unidirectional and the fabric specimens. As expected, the average elastic modulus for the unidirectional specimens was higher by 32 %.

However, the average ultimate tensile stress of the fabric was only 55 % of the ultimate for the unidirectional specimens. This was due to the stress concentration inside

Table 2. Composite tensile specimens – calculated elastic modulus

Specimen (1)	ε_1 (mm/mm) (2)	ε_2 (mm/mm) (3)	σ_1 (MPa) (4)	σ_2 (MPa) (5)	$\Delta\varepsilon$ (mm/mm) (6)	$\Delta\sigma$ (MPa) (7)	E (GPa) (8)
1	7.77E-4	1.546E-3	71.53	130.06	7.69E-4	58.53	76.11
2	8.05E-4	1.628E-3	67.98	139.27	8.23E-4	71.28	86.62
3	7.63E-4	1.727E-3	67.74	150.54	9.64E-4	82.80	85.89
4	7.76E-4	1.553E-3	65.14	133.50	7.77E-4	68.36	87.98
5	8.15E-4	1.873E-3	77.68	163.53	1.058E-3	85.85	81.14
6	6.58E-4	1.722E-3	40.75	105.42	1.064E-3	64.67	60.78
7	9.59E-4	1.632E-3	60.07	104.81	6.73E-4	44.74	66.48
8	0.00E-4	1.521E-3	0.01	98.37	1.521E-3	98.36	64.67
9	9.57E-4	1.920E-3	61.87	126.36	9.63E-4	64.49	66.97

Table 3. Composite tensile specimens – test results

Material Type (1)	Specimen (2)	Ultimate Tensile Stress σ_{ult} - (MPa) (3)	Elastic Modulus E - (GPa) (4)	Poisson's Ratio ν (5)	Specimen Failure Code[1] (6)
Unidirectional	1[4]	Not Recorded	76.11	0.60	SGM[2]
	2	1147	86.62	0.59	SGM
	3	1200	85.89	0.31	SGM
	4	1137	87.98	0.26	SGM
	5	1152	81.14	0.28	SGM
	Average (Mean)	1159	85.41	0.36	
	Standard Deviation	28.0	3.0	0.15	
	Coefficient of Variation (%)	2.4	3.5	43.0	
Fabric	6	583	60.78	Not Recorded	LIT[3]
	7	635	66.48	0.44	LIT
	8	626	64.67	0.40	LIT
	9	666	66.97	0.82	LIT
	Average (Mean)	628	64.73	0.55	
	Standard Deviation	34.3	2.8	0.23	
	Coefficient of Variation (%)	5.5	4.3	41.9	

Note: [1] Using the failure codes given in the ASTM D-3039 specifications
[2] SGM: Longitudinal Splitting-Gage-Middle
[3] LIT: Lateral-Inside Grip/Tab-Top/Bottom
[4] Results from Specimen 1 are not used in the statistical data

the grip, which caused an early sample failure.

The failure mode for each specimen is given in column (6) of Table 3, using the failure codes from the ASTM D-3039 standard. The unidirectional specimens failed by longitudinally splitting through the entire sample. However, the fabric specimens failed inside the grip at one of the sample ends.

The average measured Poisson's ratios given in column (5) of Table 3 are outside the usual range of $\nu = 0.28$-0.30. Taking into account only the results from Specimens 3-5 for the unidirectional samples, the average of these three values is $\nu = 0.28$, which is acceptable and will be used throughout this research.

The values for the fabric specimens are much higher, and probably are due to difficulties in reading the transverse strain on the fabric material. One would expect to have a slightly lower Poisson's ratio for this material, compared to the unidirectional samples, because of the glass fibers applied (during weaving) perpendicular to the main fiber direction.

It can be seen from Figures 3 and 4 that is nearly impossible to determine the ultimate strain, an important composite property, from the data recorded. To overcome this problem, Equation (3) was used to estimate the ultimate strain:

$$\varepsilon_{ult} = \frac{\sigma_{ult}}{E} \tag{3}$$

where:

ε_{ult} – the calculated ultimate strain in the fiber direction;

σ_{ult} – the recorded ultimate tensile stress;

E – the calculated average elastic modulus.

Using the data from Table 3, the following values were obtained:

- unidirectional samples: ε_{ult} = 1159/85.41E+3 = 0.013 = 1.3 % ;
- fabric samples: ε_{ult} = 628/64.73E+3 = 0.010 = 1.0 % .

CHAPTER 3

BEAM-COLUMN JOINTS – SPECIMEN DESIGN AND TEST SETUP

In order to study the behavior of reinforced concrete beam-column T-joints, fifteen joint specimens were designed, built and tested in two phases. These specimens had identical dimensions and reinforcement. After the first nine tests (Phase I), it has been decided to build and test six more specimens (Phase II). This was necessary in order to check the repeatability of the test results from Phase I, and introduce a new variable, the concrete surface preparation.

Two of these specimens in each phase (a total of four specimens) were tested in the as-built condition. The remaining specimens (eleven specimens) were externally reinforced using carbon fiber reinforced plastic (CFRP) sheets attached to the surface of the concrete beam-column joints. The following variables have been considered, tested and analyzed:

- the composite curing process;
- the CFRP layout;
- the surface preparation of the concrete specimens.

3.1 Design and construction of baseline specimens

Figure 5 shows the dimensions and reinforcement of the reinforced concrete specimens. The specimens were tested in an inverted position, compared to the existing position in a reinforced concrete structure. The location of the T-joints in a multi-column bridge bent is shown in Figure 6a. The specimens were designed to represent a third scale compared to the typical bent dimensions. However, T-joints can also be part of a planar frame R/C building (see Figure 6b), in which case the dimensions of the specimens are close to the actual size of the elements.

In Phase I. 27.58 MPa concrete has been ordered; however, the compressive strength of the concrete was found to be only 19.65 MPa. To match this strength, in Phase II, 20.68 MPa concrete has been ordered; however, the measured compressive strength was 33.92 MPa. This inconsistency in the delivered concrete made it later difficult to compare the test results from the two phases.

It was assumed that the yield strength of the longitudinal and transverse reinforcement for all the specimens was 413.67 MPa. This assumption was made based on the experience that the yield strength of reinforcing bars does not have a variation of more than ±5%.

To be able to identify how much each of the resisting components (concrete, reinforcing steel and CFRP sheets) contributes to the overall shear capacity of the joint, the transverse reinforcement in the beam and the beam-column joint region was entirely omitted. However, in order to position the flexural reinforcement in the beam, there were two ϕ = 13 mm closed stirrups provided at the ends of the beam.

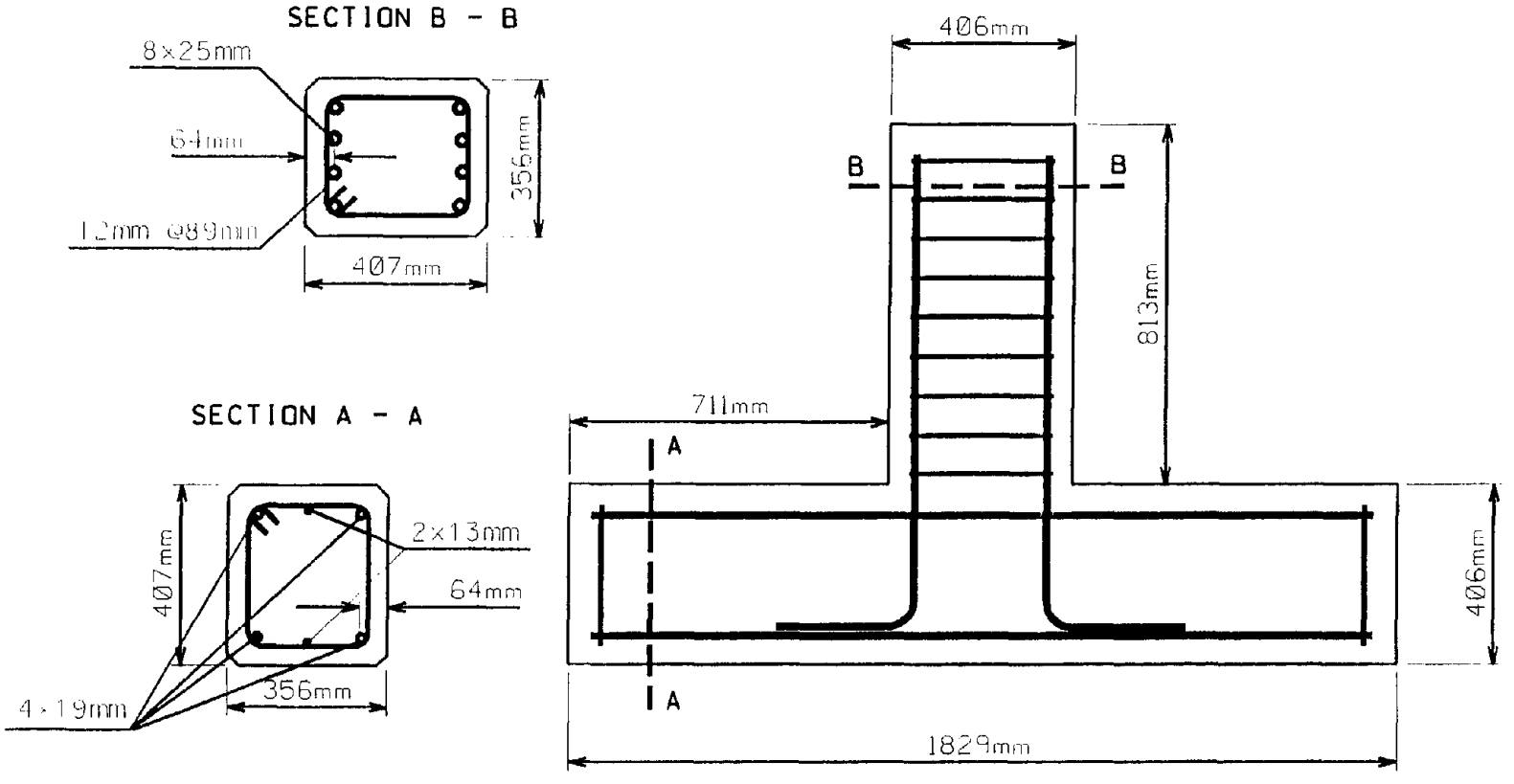

Figure 5. Beam-column joint specimen dimensions and reinforcement

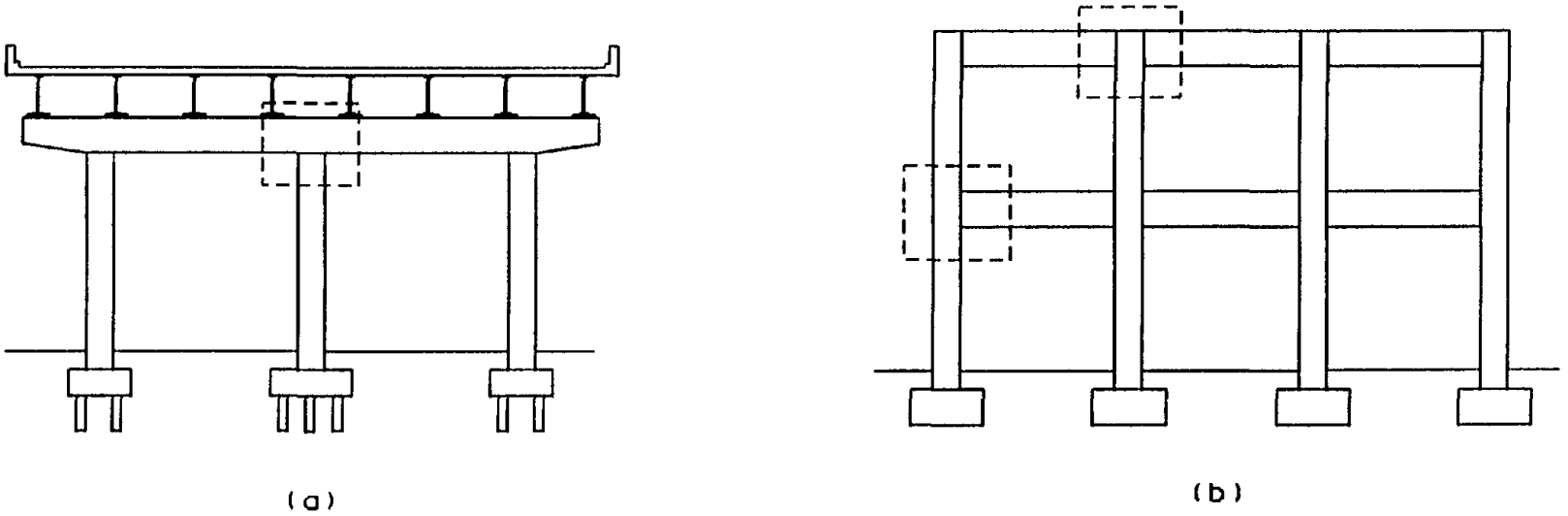

Figure 6. Location of T–joints in bridge bents (a), and in planar frame R/C buildings (b)

The beam longitudinal reinforcement consisted of two ϕ = 19 mm and one ϕ = 13 mm bars at the top and the bottom of the beam. The longitudinal rebars were placed with a 64 mm clear cover from the face of the concrete. The column longitudinal reinforcement consisted of four ϕ = 25 mm bars at each face, located at 64 mm from the face of the column. This reinforcement was extended into the joint, and a standard 90^0 bar hook was provided at the end to satisfy the development length requirement. The ϕ = 13 mm closed ties are placed at a distance of 89 mm o.c. throughout the column, starting at the face of the beam.

The amount of longitudinal and transverse reinforcement provided in the column was sufficient to ensure that the lateral load corresponding to the flexural and shear capacity of the column, exceeds the load corresponding to the shear capacity of the beam and the joint. Table 4 summarizes the nominal shear and flexural strength of the columns and beams (for both phases), and the lateral load corresponding to these capacity values. The lateral load corresponding to the flexural capacity of the elements are calculated based on the fact, that the maximum bending moment in the column and the beam will develop at the face of the joint.

It is evident from these values that the baseline specimens' weakness is in the shear strength of the beam and the joint region. This will result in a brittle shear failure for the specimens, rather than reaching the flexural capacity and develop a ductile behavior. It was found from previous studies that the effectiveness of composite sheets applied to rectangular concrete sections greatly depends on the level of stress concentration in the composite material at the corners. Therefore, a 38 mm chamfer was formed and grinded at the corners of the specimens.

Table 4. Beam-column specimens' shear and flexural capacities

Phase (Concrete Strength) (1)	Element (2)	Shear Strength		Flexural Strength	
		Nominal Capacity[1] (kN) (3)	Corresponding Lateral Load (kN) (4)	Nominal Capacity[1] (kN-m) (5)	Corresponding Lateral Load (kN) (6)
I	Beam	90	144	92	241
(f'_c=19.65 MPa)	Column	450	450	229[2]	282
II	Beam	119	190	95	249
(f'_c=33.92 MPa)	Column	479	479	255[2]	314

Note: [1] Nominal shear and flexural capacity values
[2] Flexural capacity at no axial load

3.2 Application of CFRP composite materials

Seven specimens in Phase I, and four specimens in Phase II were strengthened by externally applied CFRP composite woven sheets. Figure 7 gives a general composite layout, and in Figure 8 the additional layers for Specimen 15 are shown. For each specimen, the dimensions L_i, the fiber orientations, the curing temperatures and the surface preparation are summarized in Table 5.

3.2.1 Surface preparation

As in every repair procedure involving externally attached materials to existing members, here too, the bond between the concrete surface and the composite sheets is critical. The quality of the concrete surface, from the adhesion point of view, depends greatly on:

- the quality of the finish;
- the concrete strength;

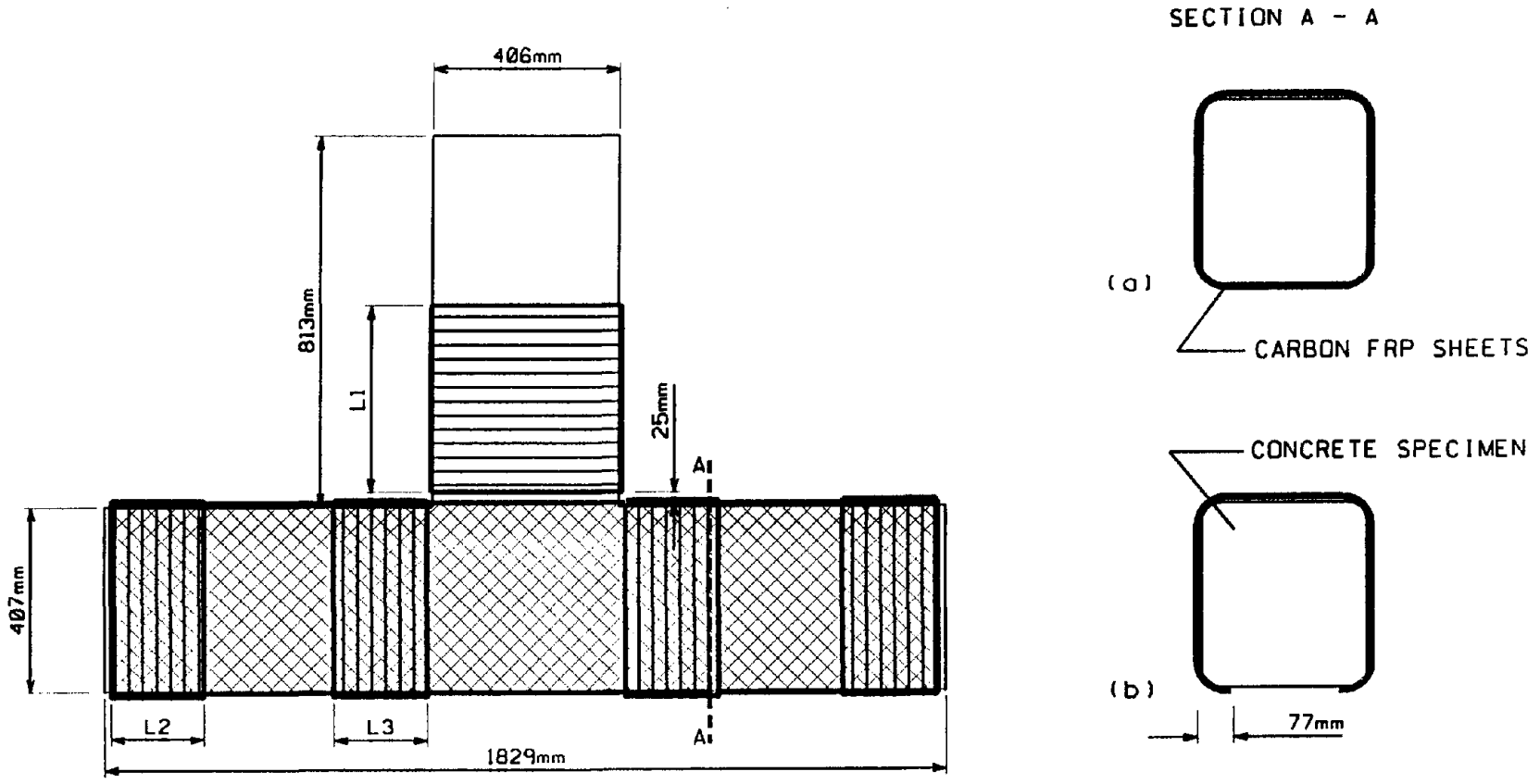

Figure 7. Carbon FRP layout on four (a), and three sides (b) of the beam

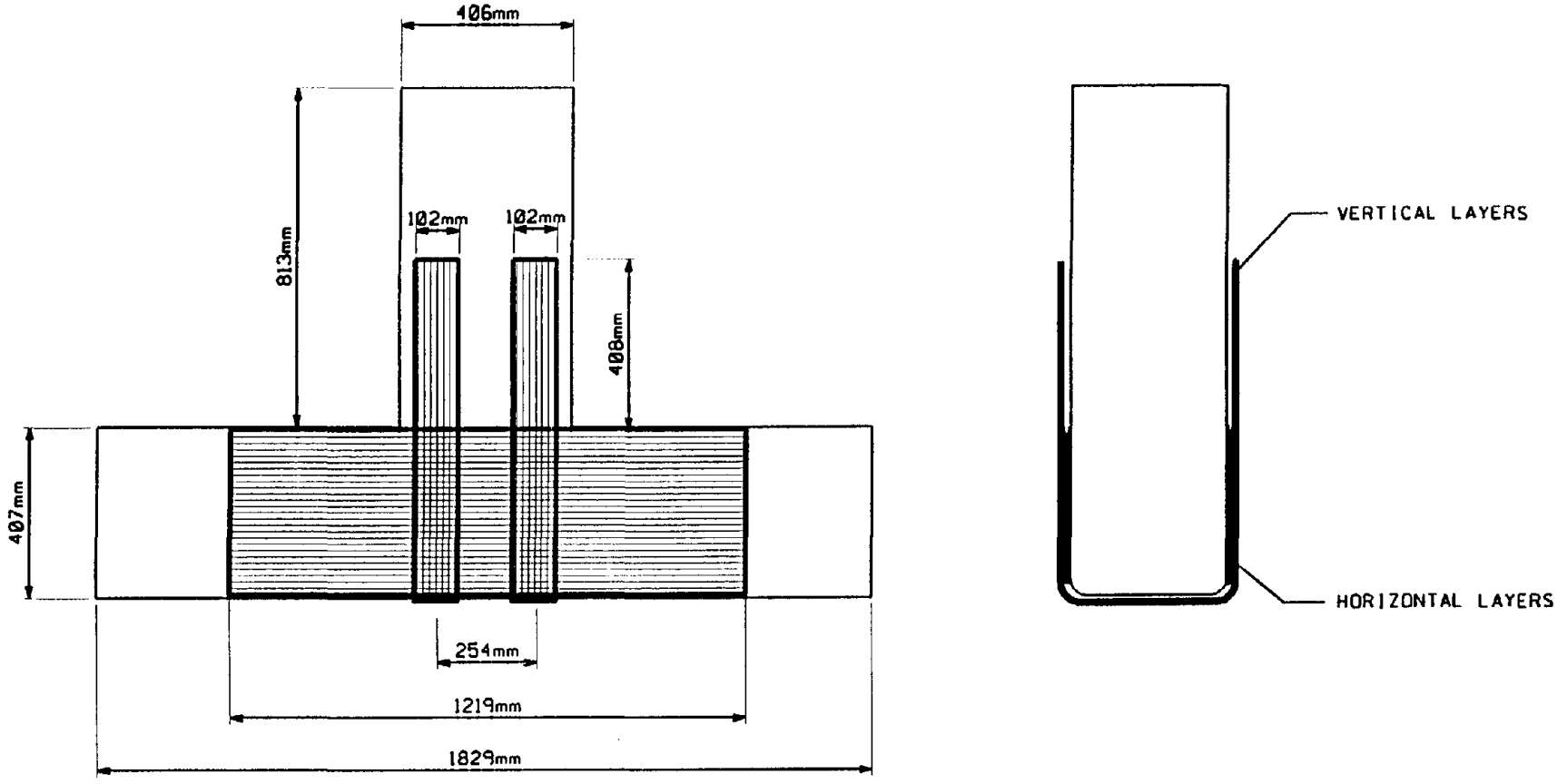

Figure 8. Additional carbon FRP layout on Specimen 15

Table 5. Beam-column joint specimen CFRP layout

Phase (1)	Specimen (2)	Surface Preparation (3)	CRFP Layout[3] (4)	Curing Temperature (5)	L_1 (mm) (6)	L_2 (mm) (7)	L_3 (mm) (8)
I	1[1]	N/A	N/A	N/A	N/A	N/A	N/A
	2[1]	N/A	N/A	N/A	N/A	N/A	N/A
	3	Wire Brush	[45]	Elevated	0	178	0
	4	Wire Brush	[±45]	Elevated	0	178	0
	5	Wire Brush	[45]	Room	0	229	0
	6	Wire Brush	[45]	Room	432	229	406
	7	Wire Brush	[45]	Room	432	229	406
	8	Wire Brush	[±45]	Room	0	203	0
	9	Wire Brush	[±45]	Room	406	229	203
II	10[1]	N/A	N/A	N/A	N/A	N/A	N/A
	11[1]	N/A	N/A	N/A	N/A	N/A	N/A
	12	Wire Brush	[±45]	Room	406	203	406
	13	Wire Brush	[±45]	Room	406	203	406[5]
	14	Water Jet[2]	[±45]	Room	406	203	406[5]
	15	Water Jet[2]	[±45][4]	Room	406	203	406[5]

Note:
[1] Baseline specimens
[2] Water jet and Sikadur 31
[3] CFRP layout on each vertical face of the beam
[4] Additional layers are shown in Figure 11b
[5] Only on three sides

- the presence of materials deposited on the surface (paint, dust, oil, loose material, etc.).

In Phase I, the specimens were wire brushed until any loose material was removed. However, this method was proved to be unsatisfactory by a study performed at XXsys Technologies, Inc., San Diego, CA. To improve the bond between concrete and composite material, in Phase II a powerful water jet was used to remove loose and weak material from the surface of the beam-column specimens. The 275.79 MPa pressure water grinded into the specimen up to 3 mm deep, and resulted in a rough and evenly hard surface.

3.2.2 The matrix and the curing process

The matrix in a composite material has two components, the resin and the curing agent. The mixture of these two provides a strong and effective bond between single fibers in a tow, and between the composite sheets and the surface to which is applied. A Shell Epon 828 resin was used in Phase I. Because of the dense weaving of the carbon fiber material (7 tows per 25.4 mm), and the higher viscosity of this type of resin, it was more difficult to ensure a satisfactory resin content in the composite.

To eliminate this problem, a Shell Epon 826 resin in combination with a looser weaving (6 tows per 25.4 mm) was used in Phase II. This combination resulted in a more uniform matrix volume fraction throughout the application, and an easier product to work with. As a comparison, the concrete with a higher slump, among other effects, increases the workability.

The two types of curing agents used in this project, necessitated different

procedures. The first type of curing agent (Shell Epirez Epicure) required a cure temperature of 154 ^{0}C for 90 minutes, and a cooling ramp of 30 minutes. These specimens were shipped and cured in a large curing oven at Thiokol, UT. Because of the curing agent type, it was possible to prepreg the fiber material with the resin beforehand in a closely monitored production environment.

The second type of curing agent (Shell 3379 Epicure) required only room temperature to cure for approximately seven days. This procedure made it impossible to prepreg the carbon fiber sheets, because curing would have started the same time as the matrix components were mixed together.

3.2.3 Application of composite material

In the present study, Zoltek PANEX33-0048 carbon fiber was delivered in unidirectional woven sheets for all the specimens. The width of these sheets was 406 mm. which allowed an easier application for these reduced scale specimens. However, if larger surface needs to be covered, a wider sheet could be used. The thickness of the carbon sheets was about 1 mm.

Before applying the composite material, the specimen was thoroughly wire brushed and vacuumed. For two of the specimens in Phase II, the surface was prepared by water jetting, and a thin layer of Sikadur 31 was spread over the surface. This was necessary to obtain uniform and even surface, and to increase the bond and anchor capacity of concrete specimens.

As it was described in the previous section, the prepreg composite material already contained the necessary matrix volume (40-50%). The outline of the composite

layout was marked on the specimen, which made the application of the inclined layers easier. The composite sheets were then cut to the length previously determined. A thin layer of epoxy was applied to the prepared surface and the composite was laid following the design specification. The epoxy and composite layers were applied in this sequence as needed.

For the room temperature cure system, the precut carbon fiber sheets were first thoroughly impregnated by hand with epoxy using paint rollers and squeegees. It has been observed that if these freshly impregnated sheets were left on the table for a few minutes, they became soft and easy to use. The same procedure described in the last paragraph was followed to apply the composite sheets to the beam-column specimens.

The general layout is shown in Figure 7 for all the specimens, and a summary of the particular specimen layouts is given in Table 5. The layer L_1 on the lower part of the column had the effect of confining the peak bending moment region. It was necessary to apply CFRP bands at the ends of the beam (dimension L_2) in the transverse direction, to strengthen the beam at the location of the holding devices. The layer L_3 on both sides of the beam in the transverse direction served two purposes, to confine the maximum moment region in the beam, and to increase the effectiveness of the anchor for the composite layers applied in the beam-column joint region. Layers L_1 and L_3 were applied only to selected specimens.

A continuous composite layer was applied at 45^0 throughout the length of the beam, but only to three sides, top and the two lateral sides. However, this layer was turned back to the bottom of the beam approximately 76 mm. This was necessary to simulate the accessibility at the top of the cap beam, which is the bottom of the test

specimens, in the actual bridge bent (support for the girders), or in a reinforced concrete building where the slab is connected to the top of the beam.

The layer at 45^0 in the joint region was provided to enhance the shear capacity and to prevent the formation of diagonal shear cracks. To further increase the shear capacity and to prohibit the bar pullout of the column reinforcement anchored in the joint, additional horizontal and vertical layers were provided for Specimen 15, as shown in Figure 8.

3.3 Instrumentation and test procedures

3.3.1 Instrumentation

Various instruments have been used to monitor strain levels, displacements, forces and hydraulic pressures, as shown in Figures 9 and 10. The following instruments have been used:

- Strain gages (SG); the length of the strain gages varied from 6.4 mm to 51 mm, the resistance from 120Ω to 350Ω, depending on the surface quality and the material the strain gages is applied to.
- Displacement transducers (DT), with a working range of ±254 mm.
- Linear Variable Differential Transformers (LVDT), with a working range of ±51 mm and ±76 mm, respectively.
- Pressure transducers (PT), with a range of 0-20.68 MPa.

Strain gages have been used to monitor the variations of strain levels at the longitudinal reinforcement in the beam, and on the surface of the concrete and the composite. The strain gage on the beam reinforcement at the face of the column, at the

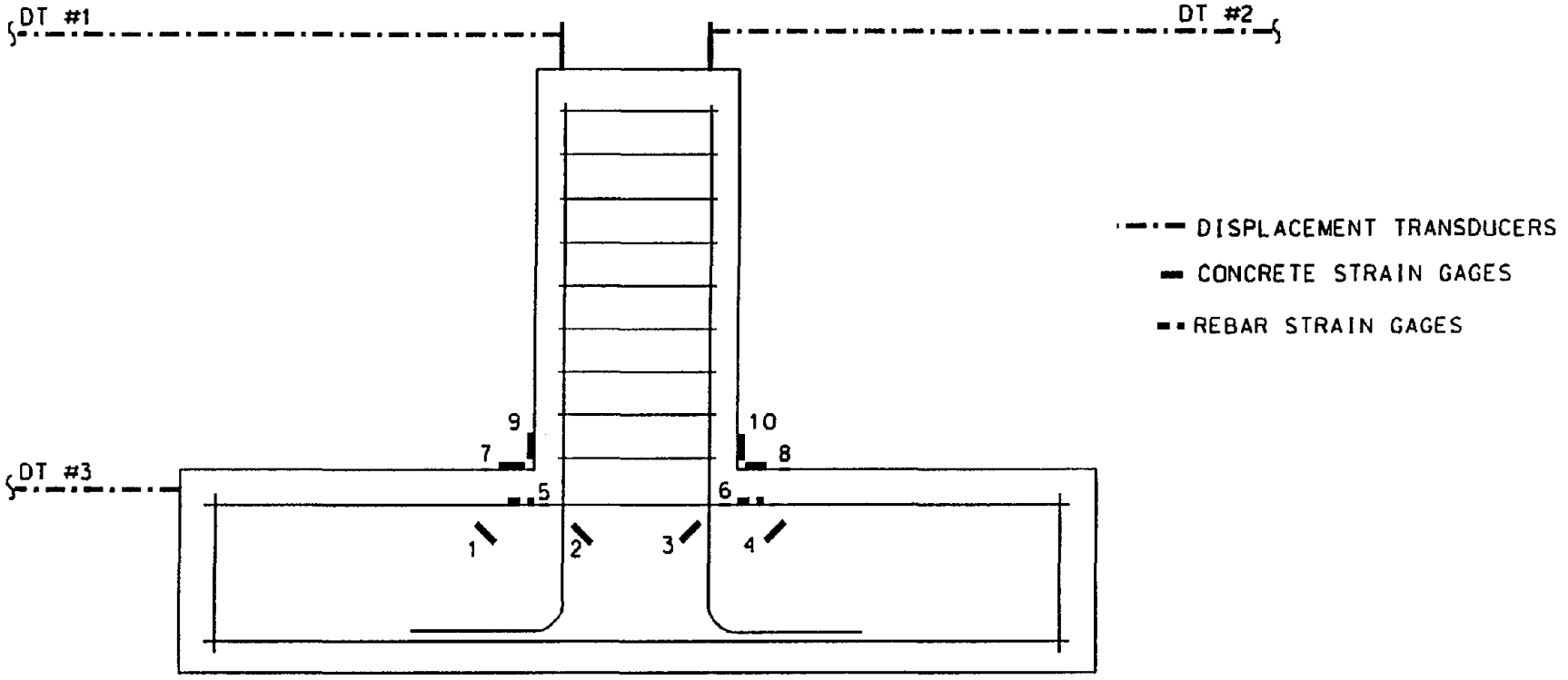

Figure 9. Location of DT, concrete and rebar strain gages

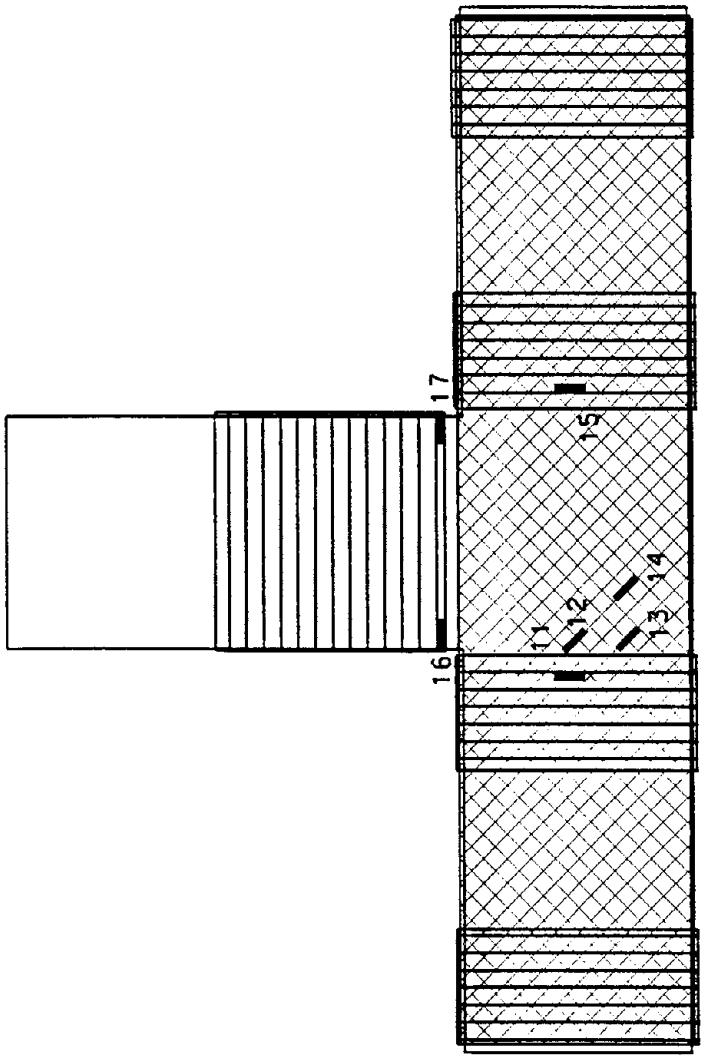

Figure 10. Location of stain gages on the composite

location of maximum bending moment in the beam, provided information about the stress level in the reinforcement.

Longer strain gages were attached to the surface of the concrete in the joint, oriented at 45^0 from the longitudinal axis of the beam, as shown in Figure 9. With this location and orientation, the recording of the maximum diagonal tension and compression in the joint was possible. Similar strain gages were placed on the columns at the face of the beam. The shorter strain gages applied to the CFRP surface measured the strain history of the composite sheets, along the fiber directions at the location of expected maximum tensile stresses.

Four strain gages were mounted on the force link between the hydraulic jack and the loading head attached to the top of the column. These provided the readings of the force that was applied to the specimens. Equation (4) was used to calculate the applied force:

$$F = \varepsilon \times E \times A \tag{4}$$

where:

F - the calculated applied force;

ε - the strain level measured by the strain gages;

E - the elastic modulus of the steel used for the force link, E = 199.94 GPa;

A - the area of the force link, A = 7742 mm^2.

To check the forces calculated using Equation (4), the hydraulic oil pressure in the cylinder was measured by pressure transducers and the force was calculated in the

hydraulic jack. The latter force was smaller by approximately 13 kN because of the pressure difference between the hydraulic power unit and the cylinder (due to the pressure loss at the valve and the hose fittings).

Strain gages were attached to the surface of the composite material in the fiber direction, as shown in Figure 10. The strain gages in the joint region were placed, wherever it was possible, approximately at the same location as the gages attached to the concrete, allowing a strain level comparison between these two surfaces. Additional strain gages were attached to the composite on the column in the hoop direction.

Displacement transducers were used to measure the horizontal movement of the specimen. The third transducer (DT#3) monitored the horizontal rigid body motion of the test specimen. This movement was observed as the beam length has been changed due to extensive cracking in the beam-column joint region. The displacement measurements from DT#1 and DT#2 were corrected by the value from DT#3 to give the true column deflection. However, this instrument was not available for the test specimens in Phase I.

In Phase II, LVDTs have been mounted to the specimen, to measure the average strain levels in three directions in the joint, and to calculate the principal stresses in the joint. However, these LVDTs were mounted to the surface in a rigid way, influencing the performance of these instruments, and the data collected could not be used in the present research. This problem was solved by the time the Interstate-15 bridge bents were tested.

3.3.2 Test procedures

Figure 11 shows the test setup, with details on the loading devices and fixtures. To eliminate the rotational restraint at the beam ends, rollers were provided in all the remaining degrees of freedom (i.e. the vertical and horizontal restraints). A pinned connection was obtained at the ends of the beam. The heavy welding (38 mm full penetration welding) of the loading head caused a misalignment of the loading device, and a small torsion has been introduced into the system; but the magnitude of this torsion was small and was not considered in the analytical study.

After all the instruments were connected to the data acquisition system, they were calibrated and zeroed following the procedures described in the SYSTEM 5000 software's user manual (from Measurements Group). Data were collected and stored from each instrument at a rate of one reading per second.

This rate was found to be more than adequate considering the time required to perform the entire test, which was about 2 to 3 hours. Even though there were sensor values recorded once a second, the results shown throughout this research were reduced by taking the average value from four to eight readings (depending on the test duration). The reduced recording frequency matched the recommended value of ten to fifteen readings per loading cycle

A cyclic, quasistatic lateral load was applied at the top of the column. The test was force controlled as the load was increased in each step from 44.5 kN with an increment of 22.2 kN. In each step there were three cycles, and each cycle consisted of a push and a pull segment from the column's neutral position. Figure 12 shows the displacement history followed for the tests.

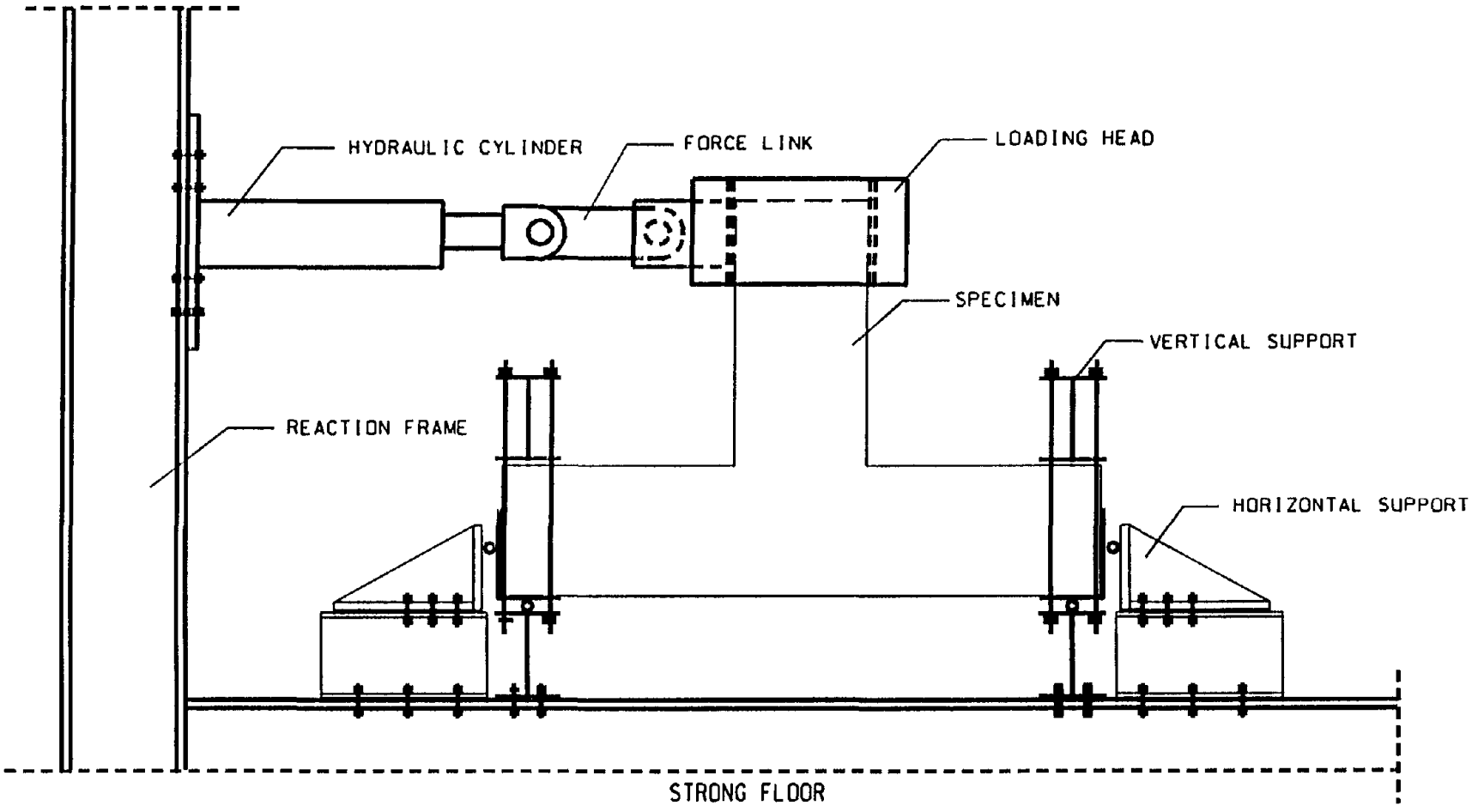

Figure 11. Beam-column joint specimen test setup

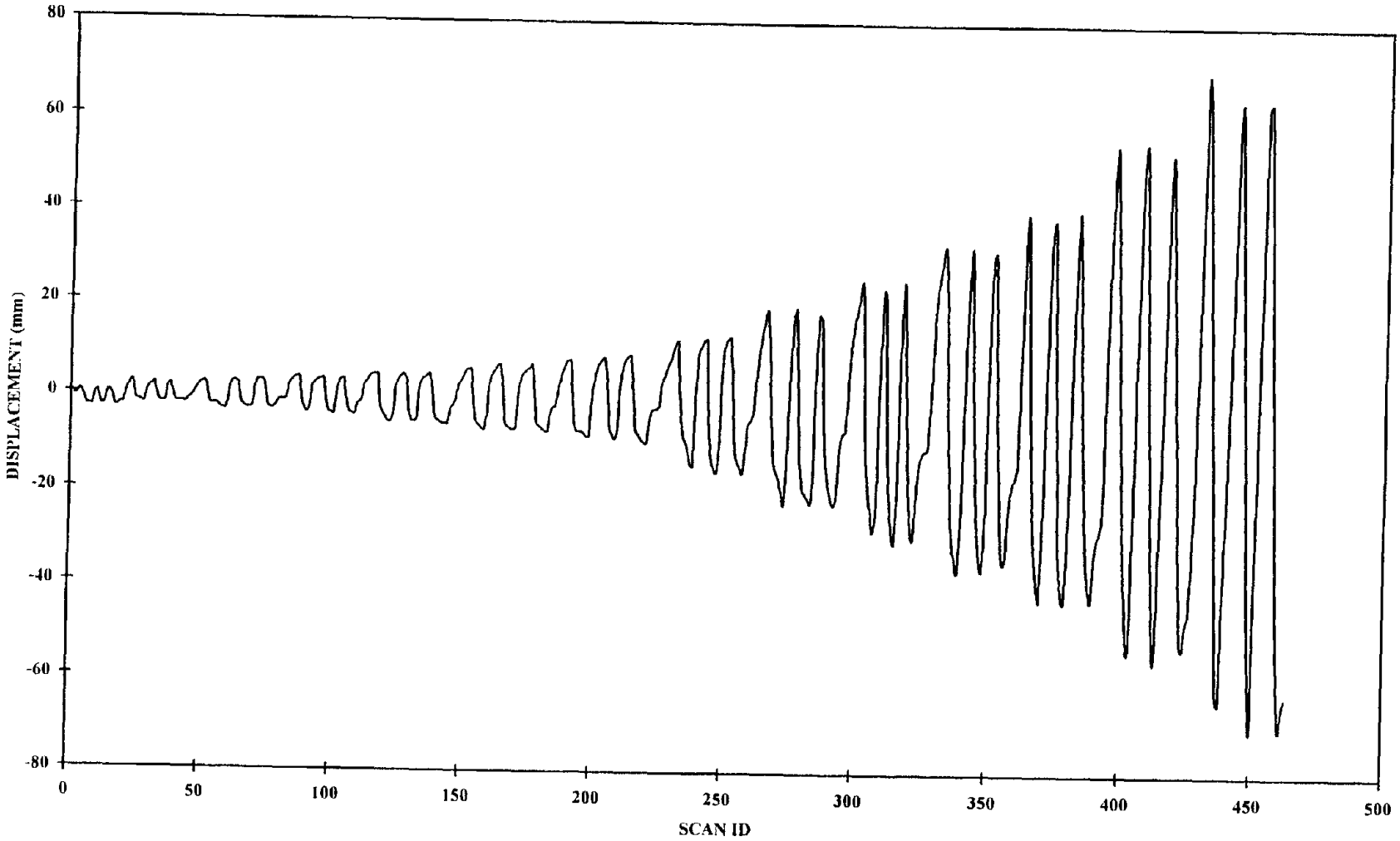

Figure 12. Displacement history for the beam-column joint tests

Following each load step the test was stopped. Pictures were taken, cracking and composite delamination were identified, marked and recorded. The test was progressed until a significant loss in strength was observed, due to cracking, bar pullout, or composite failure.

CHAPTER 4

BEAM-COLUMN JOINTS – EXPERIMENTAL RESULTS

Following the design and the construction of the T-joint specimens, and the test procedures described in the previous chapter, the 15 specimens were tested in two phases. These phases represent the two concrete types (with different compressive strength) used in the construction of the specimens.

The observed failure mode was a function of the composite layout, the surface preparation and the number of layers. For the baseline specimens, shear damage in the beam-column joint region caused failure at a low lateral load. For the strengthened specimens, the CFRP sheets gradually delaminated from the face of the beam, leaving the joint with no effective external reinforcement. This resulted in a similar but contained damage. However, the peak lateral load was significantly increased.

For each test, the peak horizontal load, and the ultimate deflection were recorded, and the failure mode was determined. The ultimate deflection (Δ_u) was assumed to be the displacement corresponding to a loss in the lateral load capacity of 20% compared to the peak load.

This chapter presents the experimental results for each beam-column joint specimen. These results include the :

- the load-displacement curves on the same scale to enable a direct comparison

between specimen performances;

- the strain history on the reinforcement, on the surface of the concrete and the carbon FRP sheets;
- the failure modes illustrated by sketches of cracks and the location of delaminated composite materials;
- the ultimate displacement, which is defined as the displacement at 80% of the maximum load.

4.1 Phase I - baseline specimens

In the first phase there were two baseline specimens tested. However, for Specimen 1, there were no strain readings available on the force link. So the only way the force could be calculated was by using the hydraulic pressure from one pressure transducer (showing the pressure in the system) mounted to the power supply. This problem was solved for the rest of the test program by providing two more pressure transducers into the outgoing and incoming hoses to the hydraulic power supply, and by attaching strain gages to the force link.

Figure 13 shows the load displacement response for Specimen 2. The positive displacements and forces correspond to the push segment in a given cycle or load step. During the push segment in the first cycle of the 44 kN load step, the test specimen was unintentionally subjected to a gradually applied quasistatic load approximately equal to the lateral load capacity of the system.

This unscheduled monotonic loading, however, provided a unique opportunity to observe the specimen's behavior during a pushover event. This pushover test, as shown

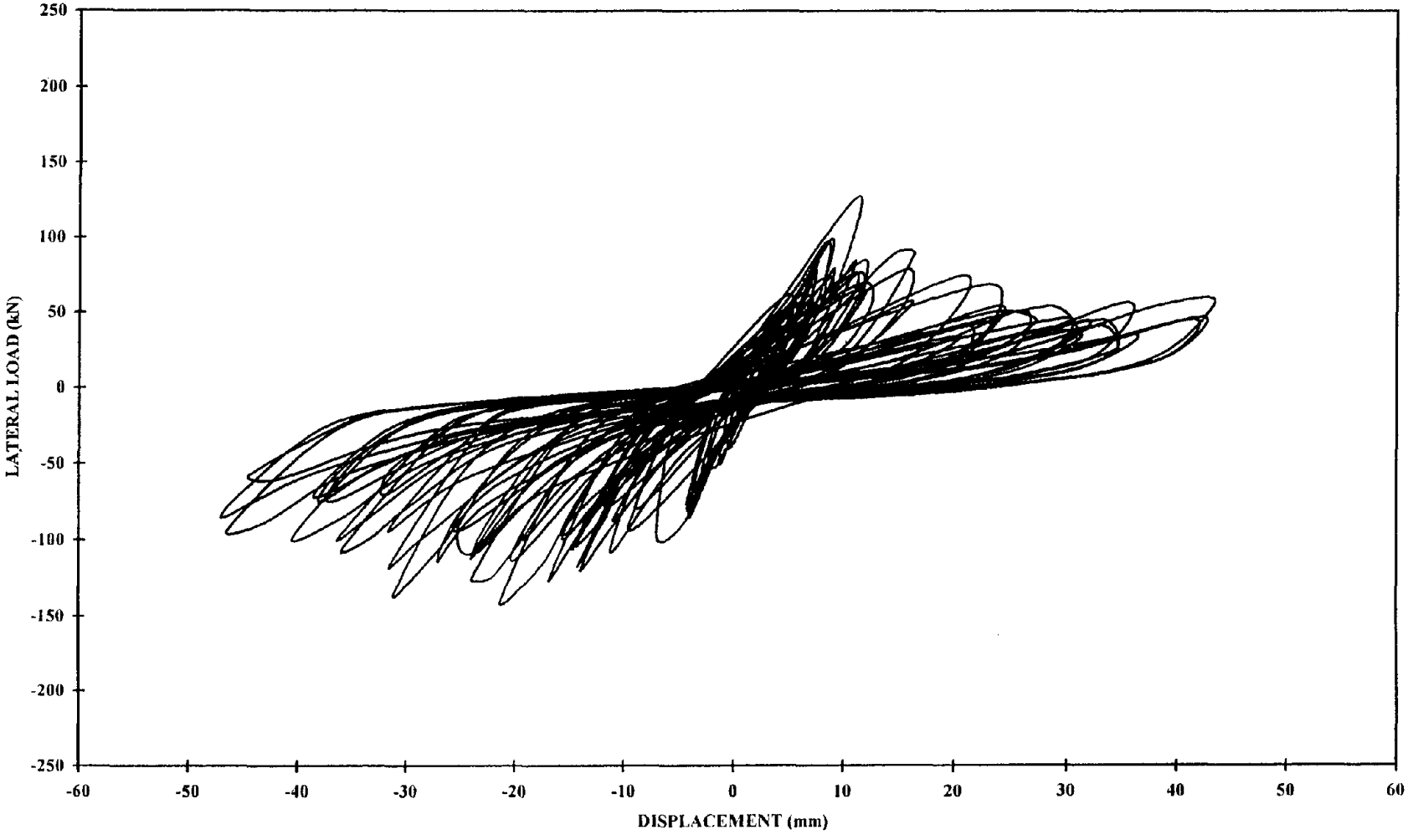

Figure 13. Beam-column joint tests - Load vs. displacement for Specimen 2

in Figure 14, has the characteristics of a beam-column joint tested in the linear range. The behavior of the joint following the maximum load is typical for damaged and cracked reinforced concrete elements with significant stiffness degradation. The theoretical analysis of this event, with a comparison of the recorded and predicted response, is given in the next chapter.

The diagonal tensile cracks formed during the push segment closed in the pull segment, and this preloading affected only the specimen's behavior in the push segment of the subsequent load steps. The pull segment shows a better performance (see Figure 13). The following behavior was observed for Specimen 2:

- The maximum load reached in the push segment was P_{max} = 129 kN. This was obtained during the pushover test, with a lower peak load in the subsequent cycles. For the pull segment a value of P_{max} = 142 kN was obtained and sustained for two more cycles, and was decreased gradually.
- The ultimate displacement in the push segment was found to be Δ_u = 16 mm, corresponding to a lateral load equal to 80% of P_{max}. However, in the pull segment a higher ultimate displacement was obtained (Δ_u = 32 mm).

Figure 15 shows the cracking pattern at the end of the test. Besides the diagonal tension cracks in the joint region, there are horizontal cracks in the beam starting at the face of the column. These cracks were developed due to bar pullout of the column longitudinal reinforcement (anchored in the beam-column joint), and to the poor confinement of the concrete in the joint.

The strain values recorded from two strain gages from the concrete surface (1 and 4) are shown in Figure 16. The other concrete strain gages were damaged during the

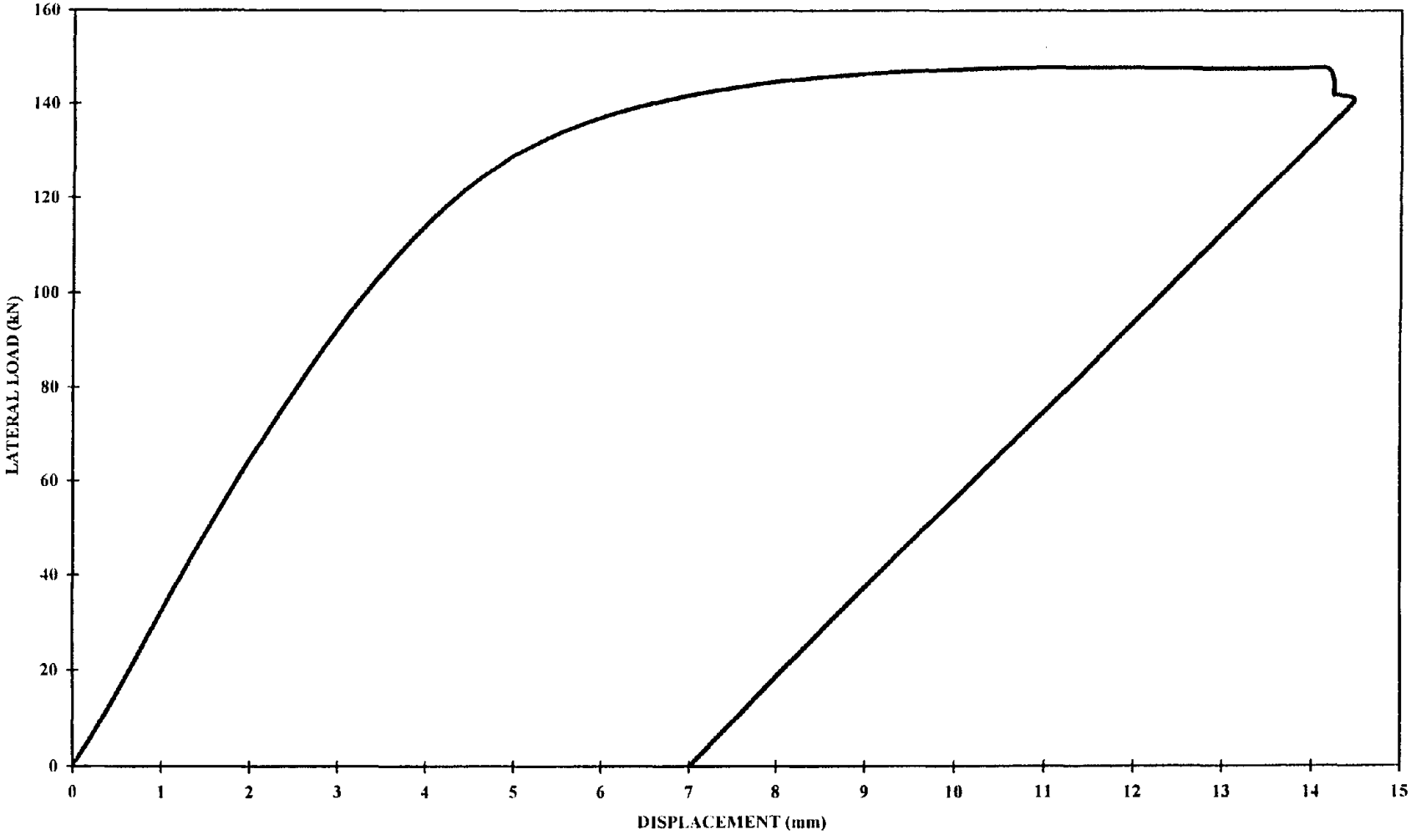

Figure 14. Pushover test of Specimen 2

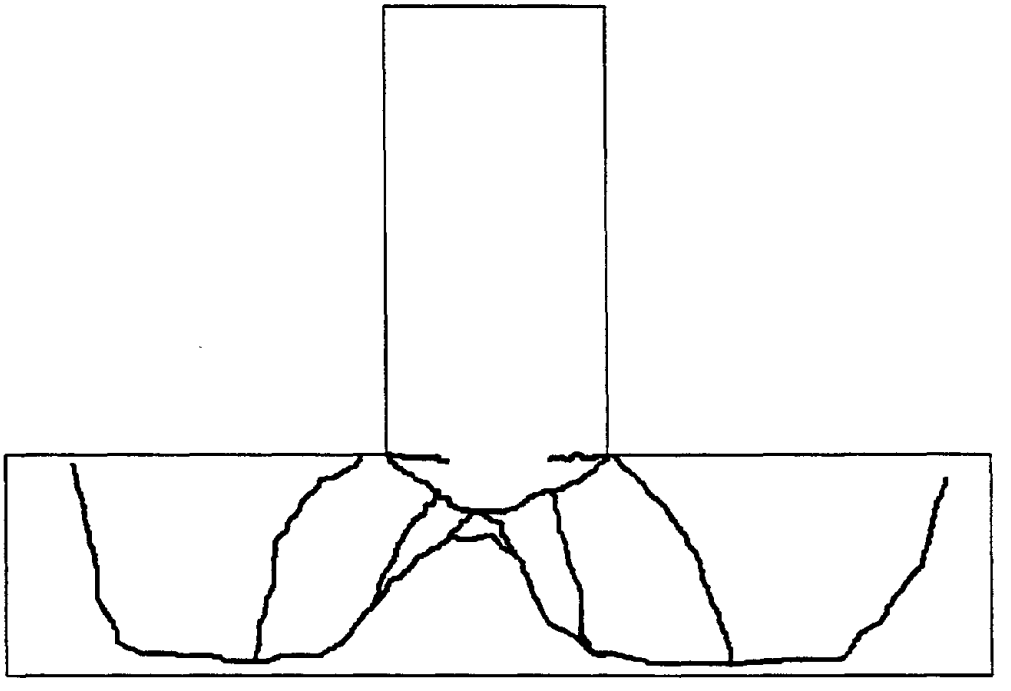

Figure 15. Crack pattern for Specimen 2

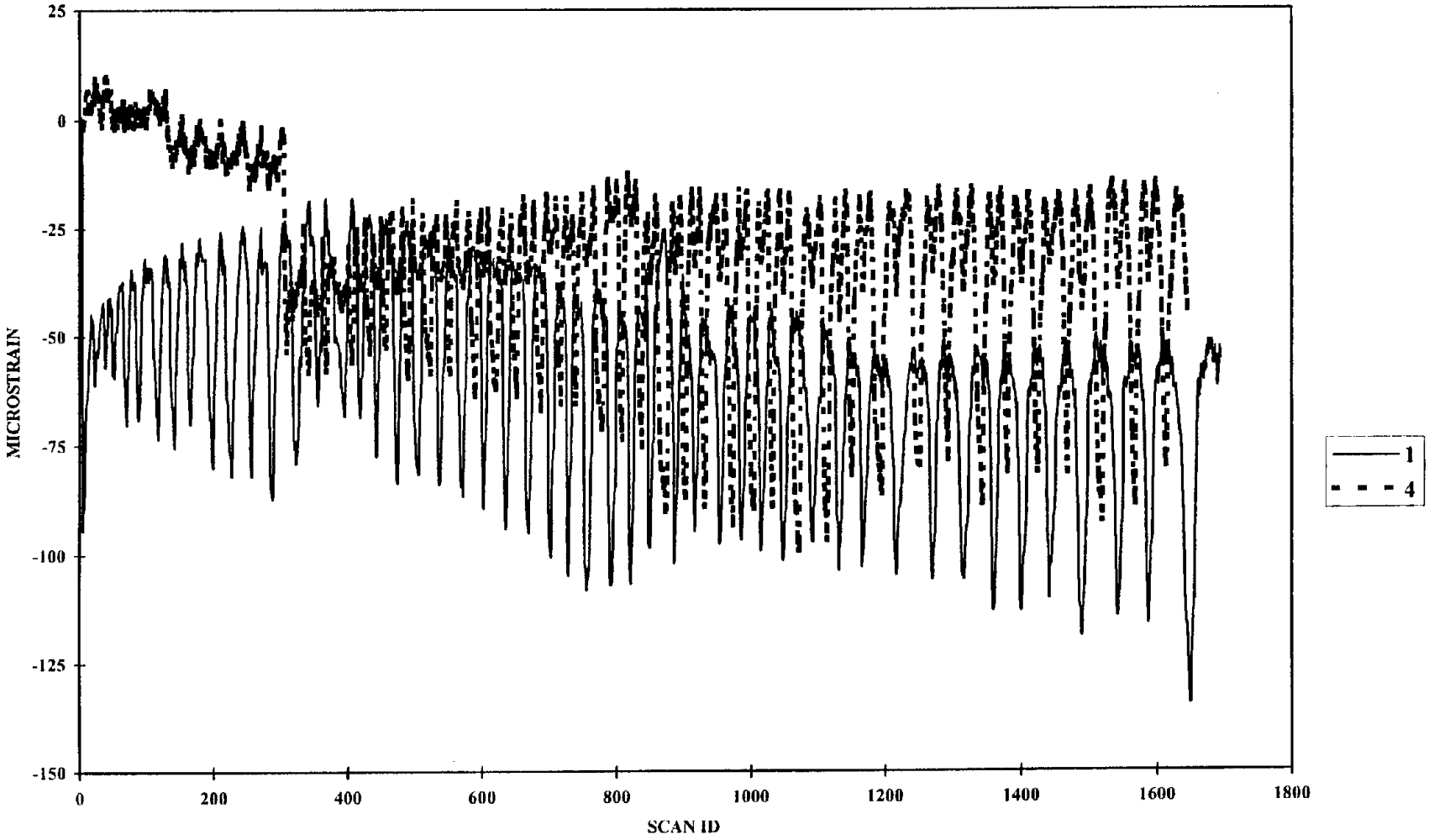

Figure 16. Beam-column joint tests - Strain readings on the concrete for Specimen 2

pushover test. The strain gages on the reinforcement show strain levels above the yield point (see Figure 17). However, this happened after extensive damage has occurred in the joint region, at a moment far bellow the bending capacity of the cross-section. This was the result of the outward force generated by the column longitudinal reinforcement bent towards the end of the beam.

4.2 Phase I – Specimens 3 and 4

These two specimens were strengthened with CFRP sheets using an elevated temperature cure system. The layout and dimensions are presented in Figure 7 and summarized in Table 5. The difference between these two specimens is the amount of the inclined composite applied to the beam's surface. For Specimen 3, one layer of composite was applied to both faces at an angle of 45^0. However, a second layer was added to both sides of Specimen 4 at an angle of -45^0.

As it can be seen in Figure 18, Specimen 3 developed unsymmetrical load displacement curves. The push segment behaved in the predicted manner. However, the pull segment (negative displacements and forces) shows a less effective repair and a behavior similar to the baseline specimens. This was due to an early delamination of composite sheets on one side of the beam starting from an "air pocket" developed during the thermal curing. Therefore, the composite sheet was stressed in compression and buckled during a push segment, resulting in an unbalanced stiffness in the push and in the pull direction. The following results were obtained for Specimen 3:

- The maximum load reached in the push segment was P_{max} = 182 kN. This value represents a 35% increase in strength over the baseline specimens. For the pull

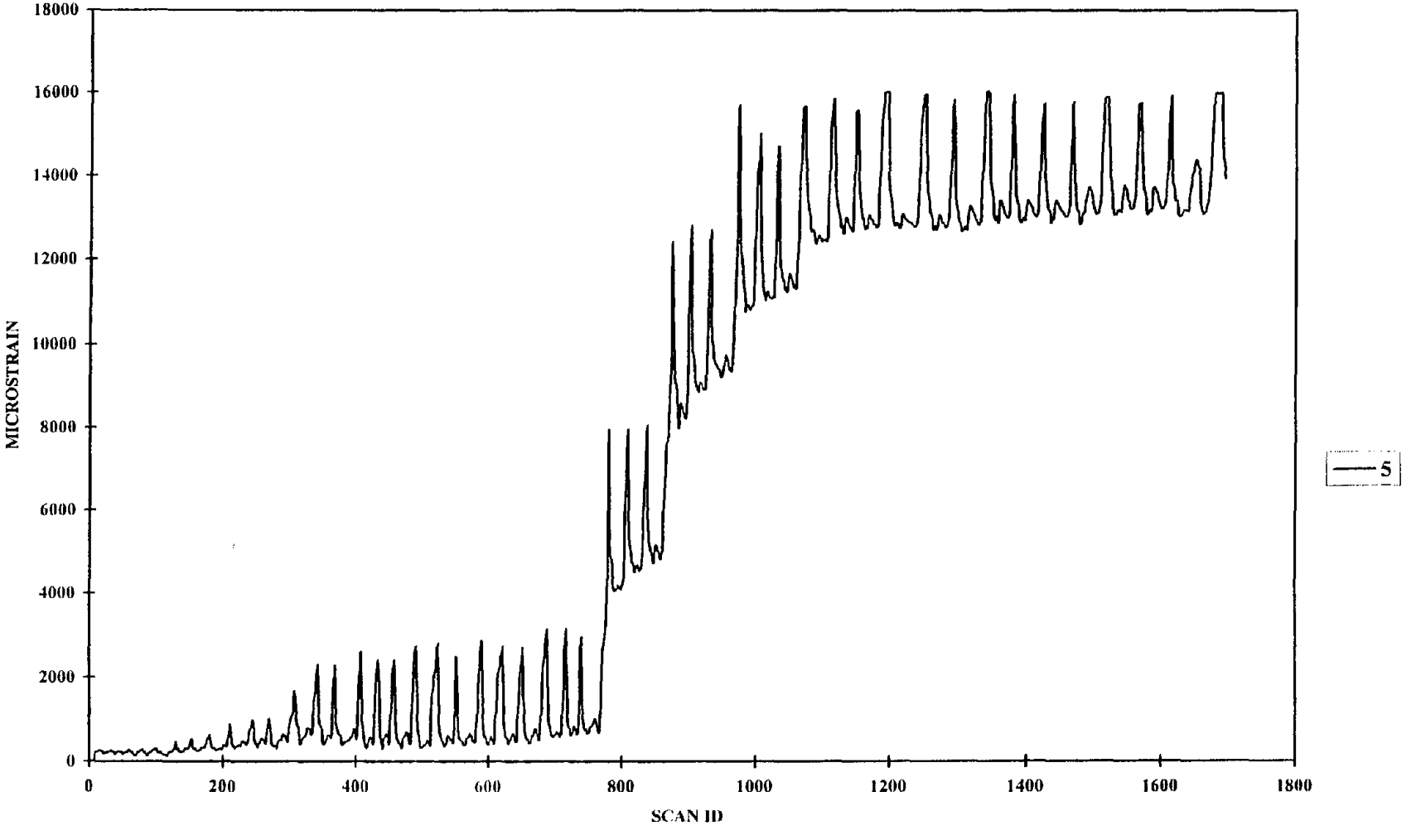

Figure 17. Beam-column joint tests - Strain readings on the reinforcement for Specimen 2

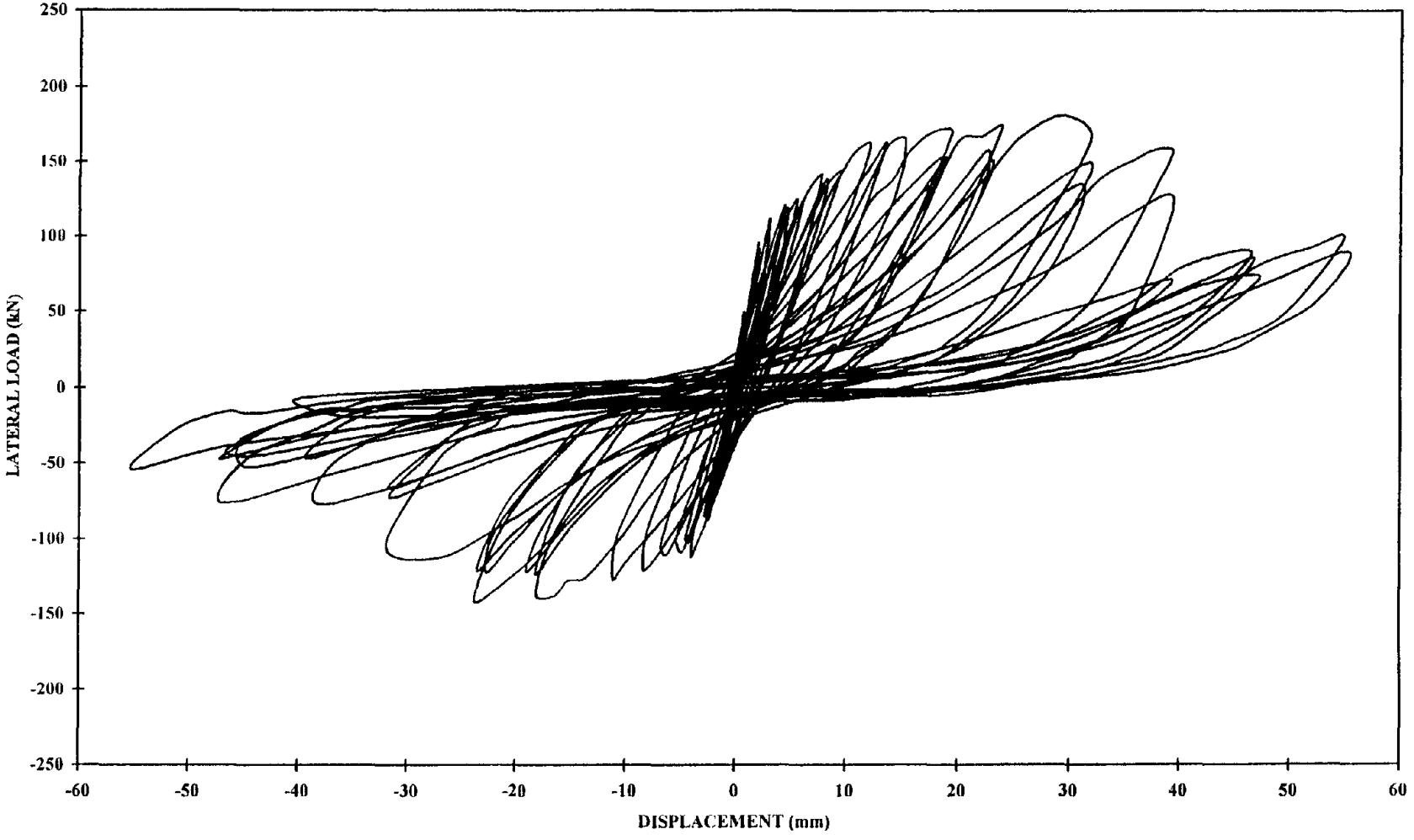

Figure 18. Beam-column joint tests - Load vs. displacement for Specimen 3

segment a value of P_{max} = 142 kN was obtained, a value similar to the ones obtained for the baseline specimens.

- The ultimate displacement in the push segment was found to be Δ_u = 39 mm. However, in the pull segment the displacement was Δ_u = 33 mm.

After the peak lateral load has been reached, the composite delaminated from the joint region. Figure 19 shows the approximate location and extent of composite delamination for Specimen 3. As mentioned in Chapter 2, composite unidirectionally woven sheets are the most effective in tension in the fiber direction.

Perpendicular to this direction, the composite's tensile capacity is governed by the matrix properties, which are similar to the concrete. As the cyclic load was applied, the direction of the principal tensile stresses changed from approximately $+45^0$ to -45^0, forcing the matrix to crack along the fiber direction (see Figure 19).

The effectiveness of the composite layers can be identified by comparing (see Figure 20) the strain values recorded outside the joint (1) and inside the joint (2), where the values from gage B' are higher throughout the test. The maximum strain value was approximately 0.8%. However, this high value was obtained after the composite delaminated, and lost most of its effectiveness in increasing the joint's shear capacity. At the peak lateral load, the tensile strain on the composite was approximately 0.57%.

Figure 21 shows the load-displacement curves for Specimen 4. Even though this specimen had twice the external composite sheets compared to Specimen 3, the force levels are similar in the push segments from that test. Because the composite layout is a balanced and symmetric, the symmetrical behavior shown in Figure 21 was expected, where the performance in the push and the pull segments is similar.

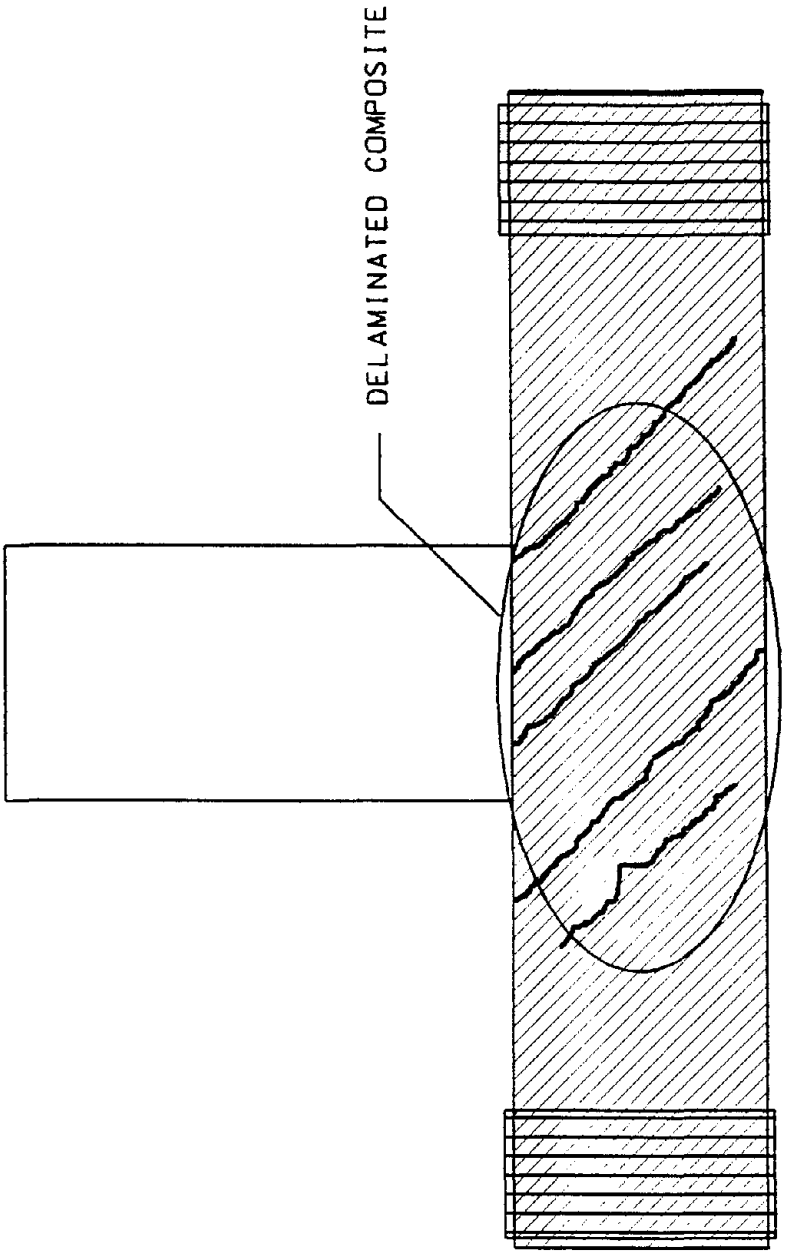

Figure 19. Location of cracks and delaminations in the composite for Specimen 3

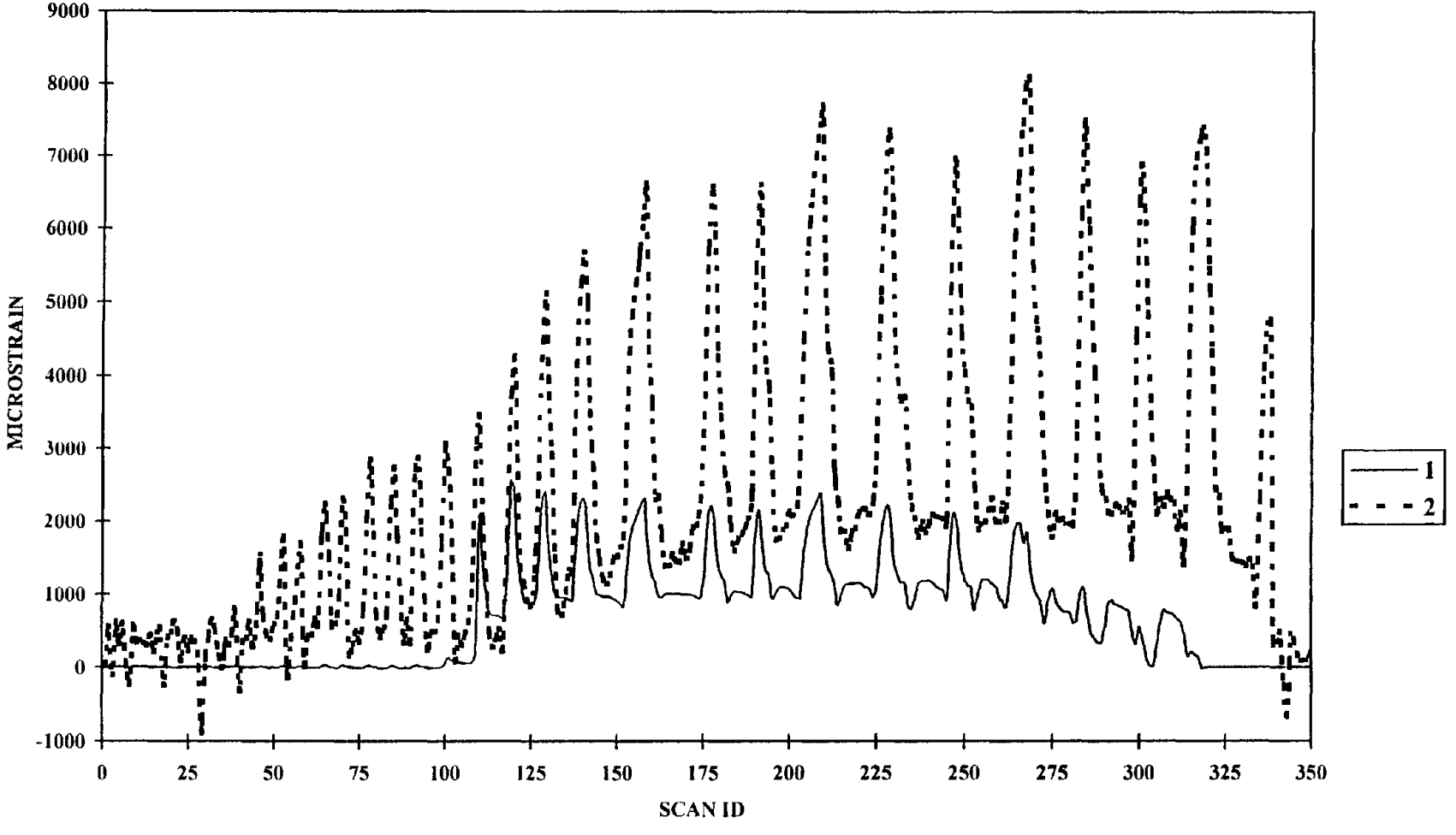

Figure 20. Beam-column joint tests - Strain readings on the composite for Specimen 3

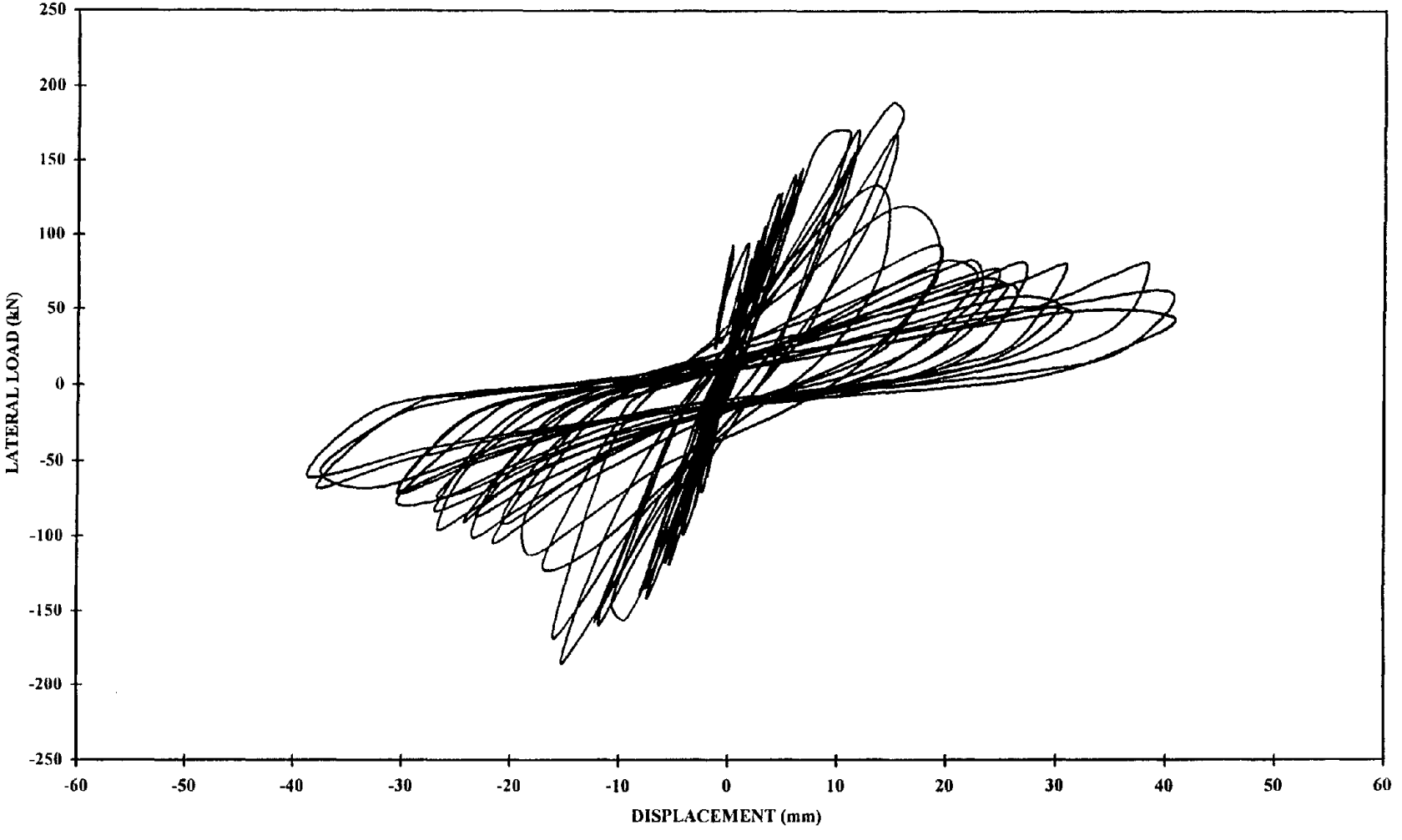

Figure 21. Beam-column joint tests - Load vs. displacement for Specimen 4

Inadequate surface preparation, and insufficient adhesive applied to the concrete surface, resulted in a weak CFRP-concrete bond. The outcome was an early composite delamination, which was observed simultaneously on both sides of the beam during the test. This prevented the external sheets to be fully developed.

The low efficiency of this repair is also evident from the low strain level (0.48%) recorded on the composite sheet (as shown in Figure 22). The sudden drop in the strain level (at a Scan ID of about 175) corresponds to the debonding of the composite sheets. The results for Specimen 4 are:

- The maximum load reached in the push and pull segments is P_{max} = 187 kN. This value represents a 40% increase in strength over the baseline specimens, but no change compared to the peak load for Specimen 3.
- The ultimate displacement in the push segment was found to be Δ_u = 19 mm. In the pull segment the displacement was Δ_u = 17 mm.

4.3 Phase I – Specimens 5, 6 and 7

Specimens 5, 6 and 7 have a composite layer on both sides of the beam at a 45^0 angle and one layer at 90^0 angle (with respect to the beam's longitudinal axis) at the supports. In addition, Specimens 6 and 7 have one layer around the column and the beams at a location adjacent to the joints (areas marked on Figure 7 with dimensions L_1 and L_3). These additional layers were provided to increase the confinement in the column at the maximum bending stress level, and to anchor the composite sheets laid at a 45^0 angle on the beam extended beyond the joint region.

All the subsequent repaired specimens (5 through 15) were strengthened with

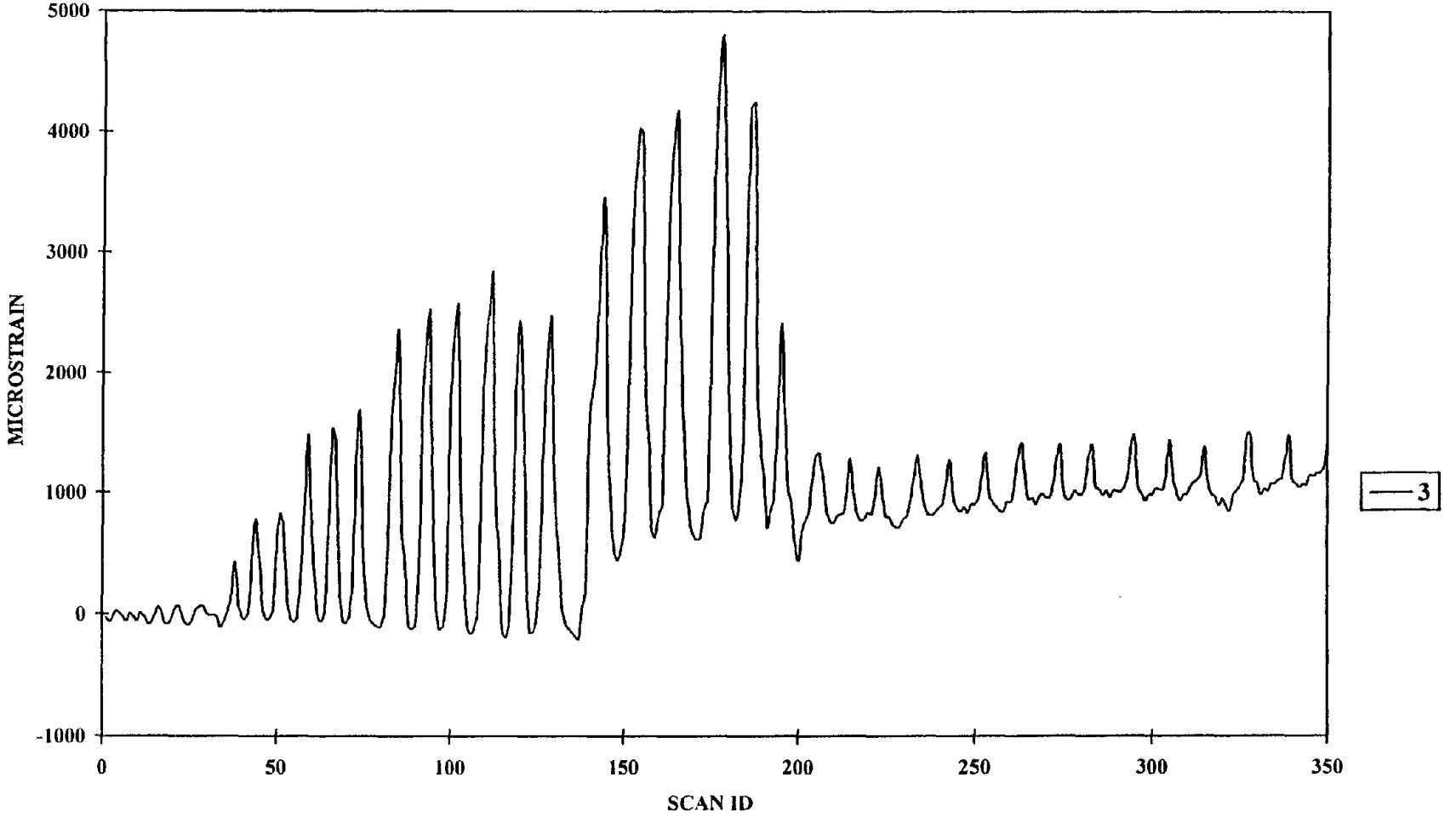

Figure 22. Beam-column joint tests - Strain readings on the composite for Specimen 4

CFRP sheets using a room temperature cure system. However, a relatively low matrix volume fraction has been observed in the composite material after the tests (in Phase I only). This was combined with a small amount of adhesive applied to the concrete surface, and resulted in early delamination and inferior bond strength.

Figure 23 shows the load-displacement curves for Specimen 5. This specimen had a similar CFRP layout to Specimen 3, the only difference being the curing process. The strain level recorded on the composite material was close to 0.19% for Gage 3 and 0.16% for Gage 4 (as shown in Figure 24). These values reflect a low stress value in the composite (20% of the tensile capacity), and compared to Specimen 3 an inferior beam-column joint capacity.

The recorded displacement and load results for Specimen 5 are:

- The maximum load reached in the push segments was P_{max} = 161 kN, and for the pull segment P_{max} = 154 kN. These values represent a decrease in strength compared to Specimen 3.
- The ultimate displacement was found to be Δ_u = 34 mm in the push segment, and Δ_u = 35 mm in the pull segment.

The crack pattern and the composite failure mode was similar to the one shown in Figure 19. Flexural cracks have been developed in the column near the joint. Matrix cracking and composite delamination was observed throughout the tests, leaving debonded sheets on the beam after the peak lateral load has been reached.

The load-displacement curves for Specimen 6 are shown in Figure 25. This specimen, in addition to the Specimen 5's composite layout, had the extra layers described earlier in this section (around the columns and beams). The increased

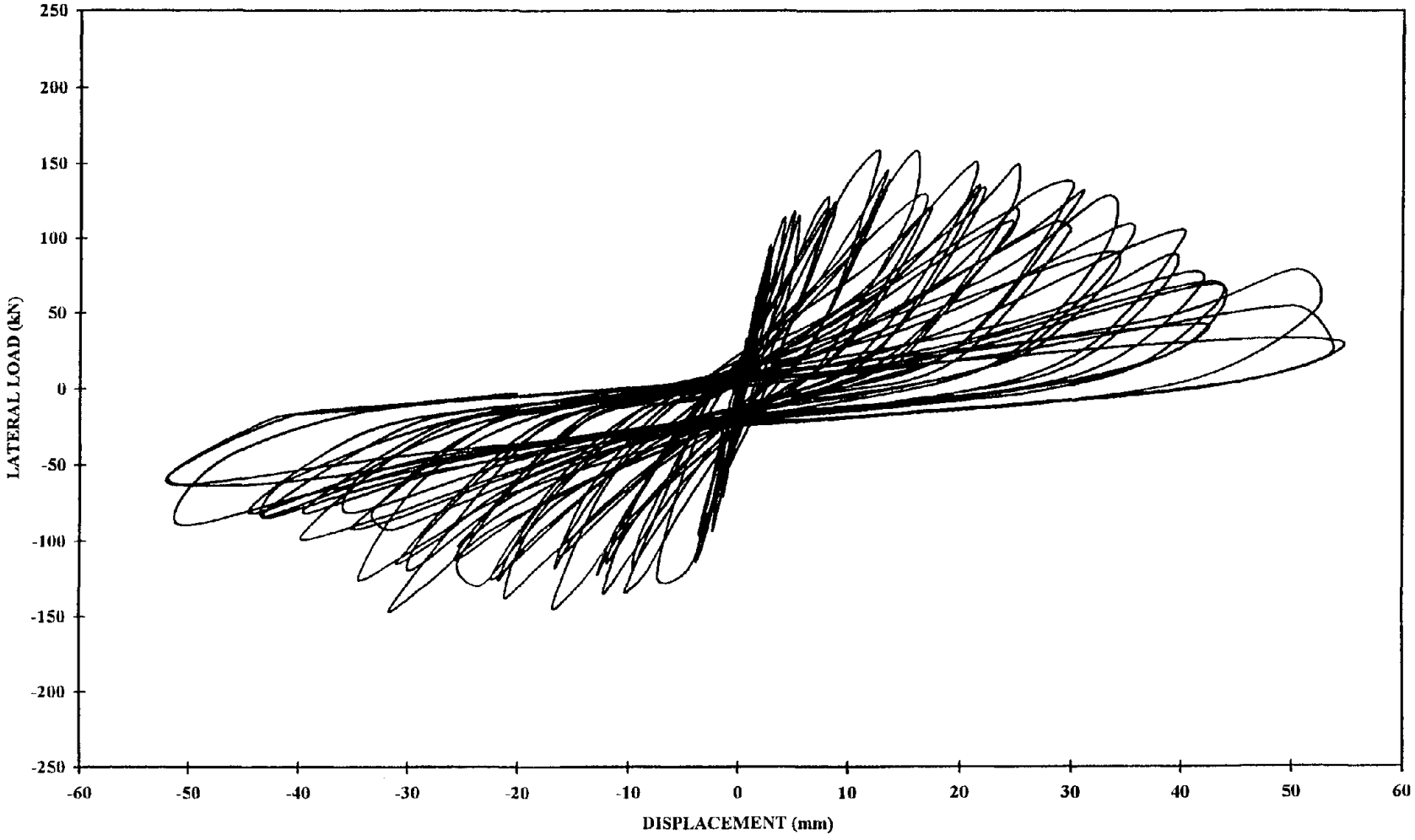

Figure 23. Beam-column joint tests - Load vs. displacement for Specimen 5

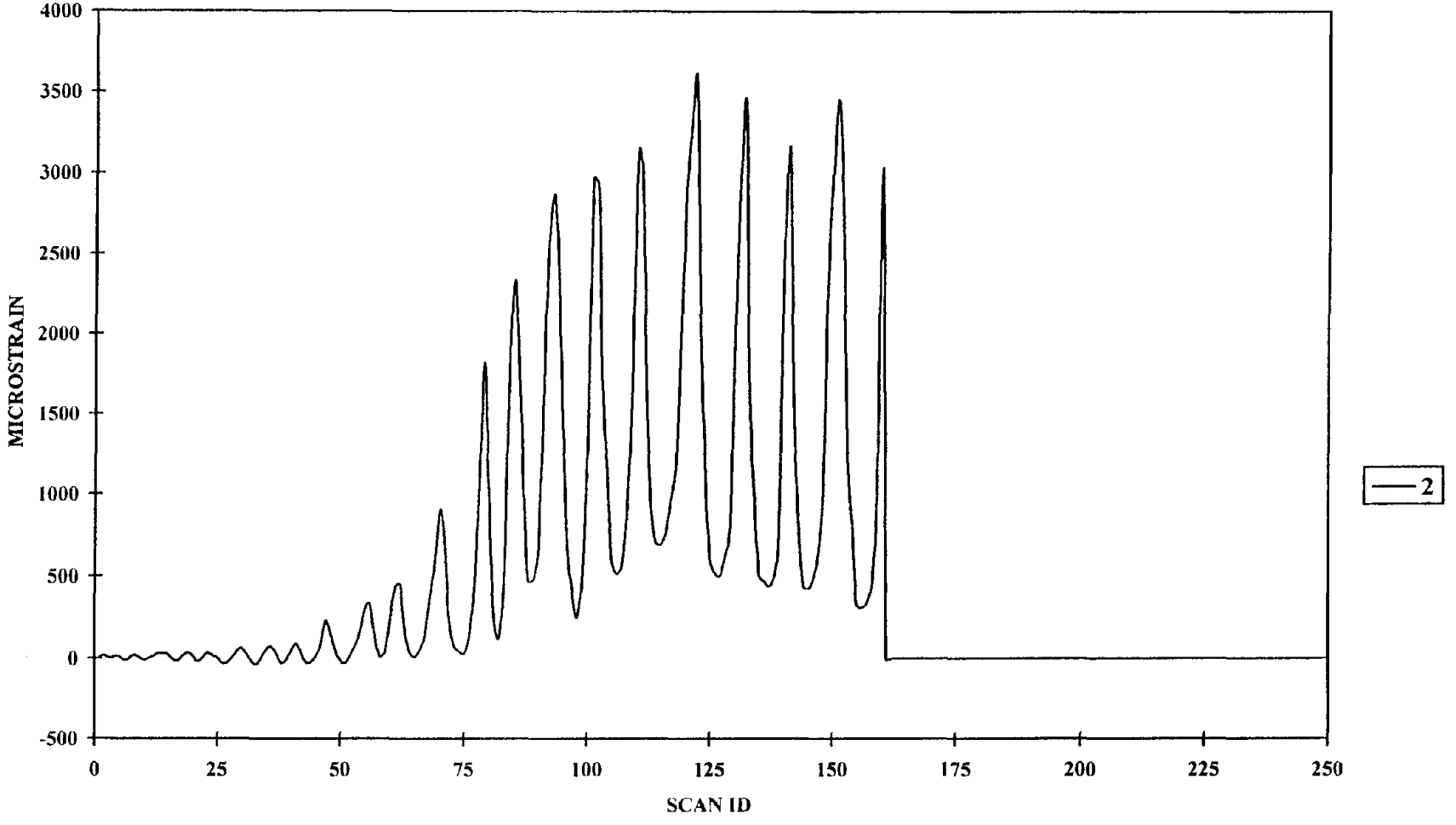

Figure 24. Beam-column joint tests - Strain readings on the composite for Specimen 5

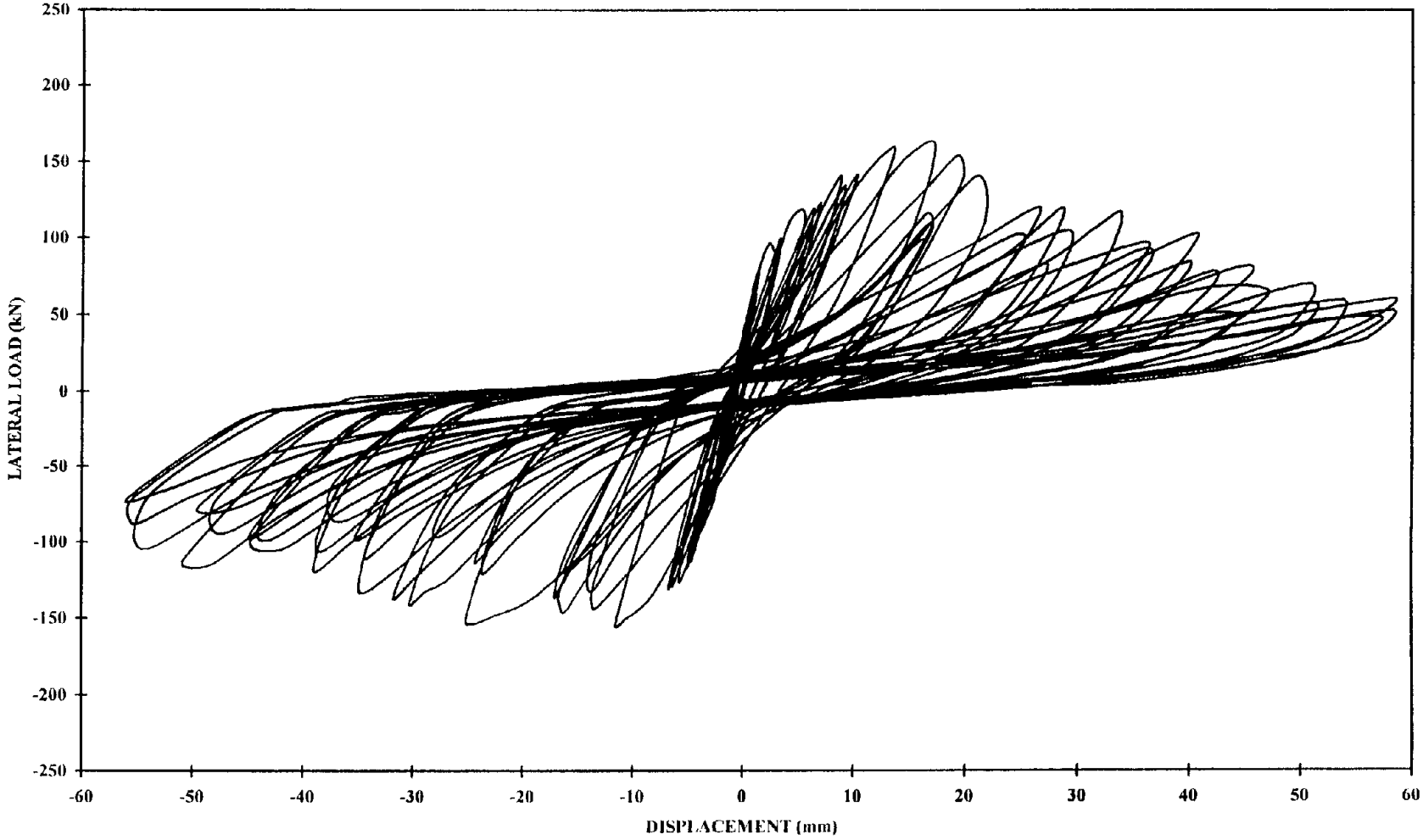

Figure 25. Beam-column joint tests - Load vs. displacement for Specimen 6

confinement in the columns prohibited the formation of flexural cracks, except at the face of the beam (the layer around the column started at a distance of approximately 25 mm).

The additional layers around the beam (next to the joint) contained the damage to the joint region. However, the force level was essentially the same as per Specimen 5. This proves that composite layers are effective in the increase of the joint shear strength (the weakness of the specimens and similar bridge and building joints), only as long as they are bonded to the element's surface. Strain readings on the composite material are given in Figure 26, showing a value of 0.28% at the peak lateral load.

The results for Specimen 6 are:

- The maximum load reached in the push segments is P_{max} = 158 kN, and P_{max} = 140 kN for the pull segments. These values represent no change compared to the results for Specimen 5.
- The ultimate displacement in the push segment was found to be Δ_u = 33.6 mm, and for the pull segment Δ_u = 32.2 mm.

The results for Specimen 7 (identical to Specimen 6 in geometry, and externally bonded reinforcement) are shown in Figure 27. Again, as the load reached its maximum level, the composite delaminated, and after one or two cycles the load dropped. It was observed before testing that on the beam at a location near the joint, the composite had an "air pocket", there was a gap between the composite sheet and the concrete surface. This was due to insufficient adhesive applied to the concrete.

This test showed the repeatability of these experiments, where identical concrete specimens, surface preparation, adhesive and composite layouts produced similar strength results. The following results were obtained for Specimen 7:

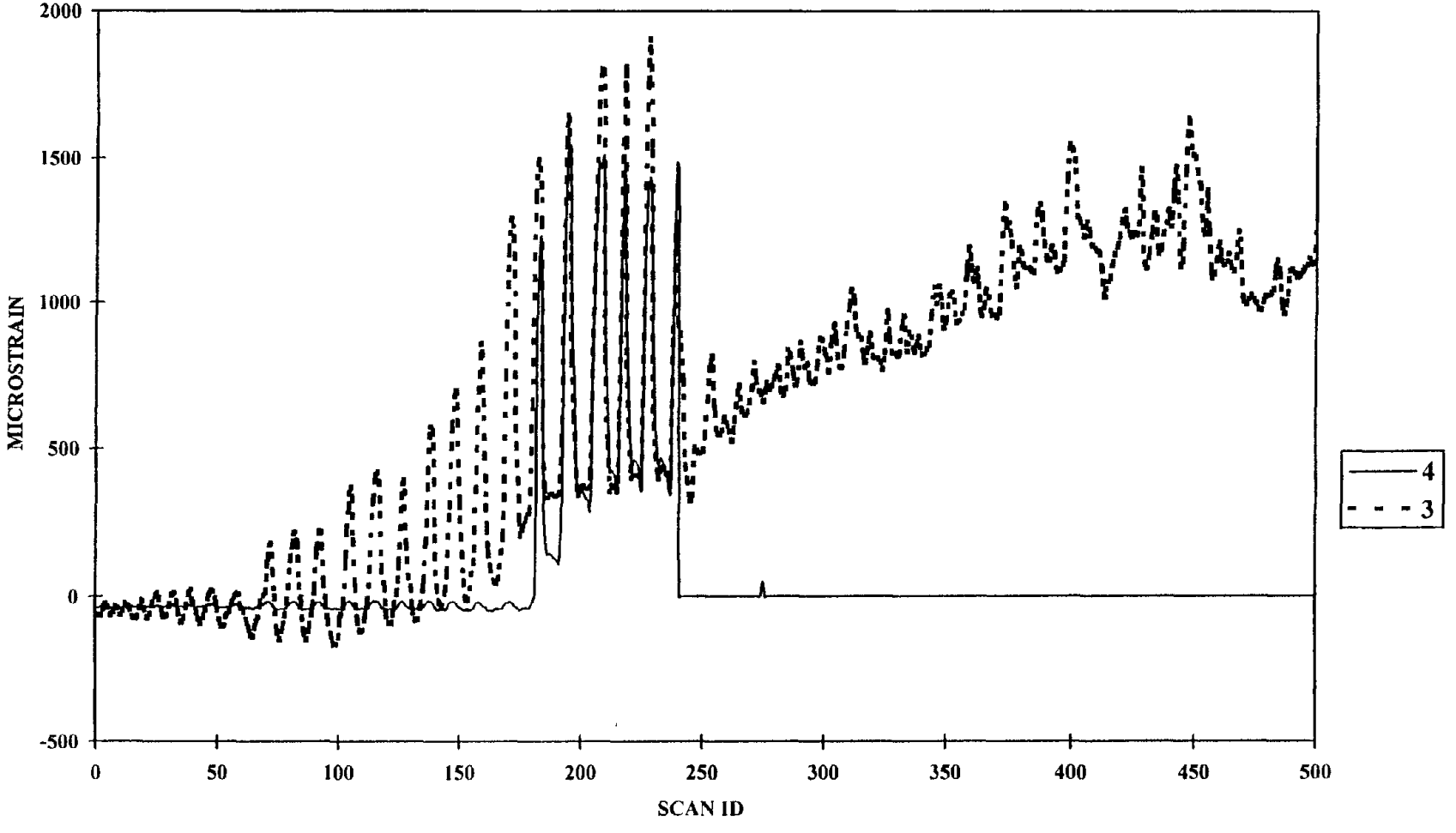

Figure 26. Beam-column joint tests - Strain readings on the composite for Specimen 6

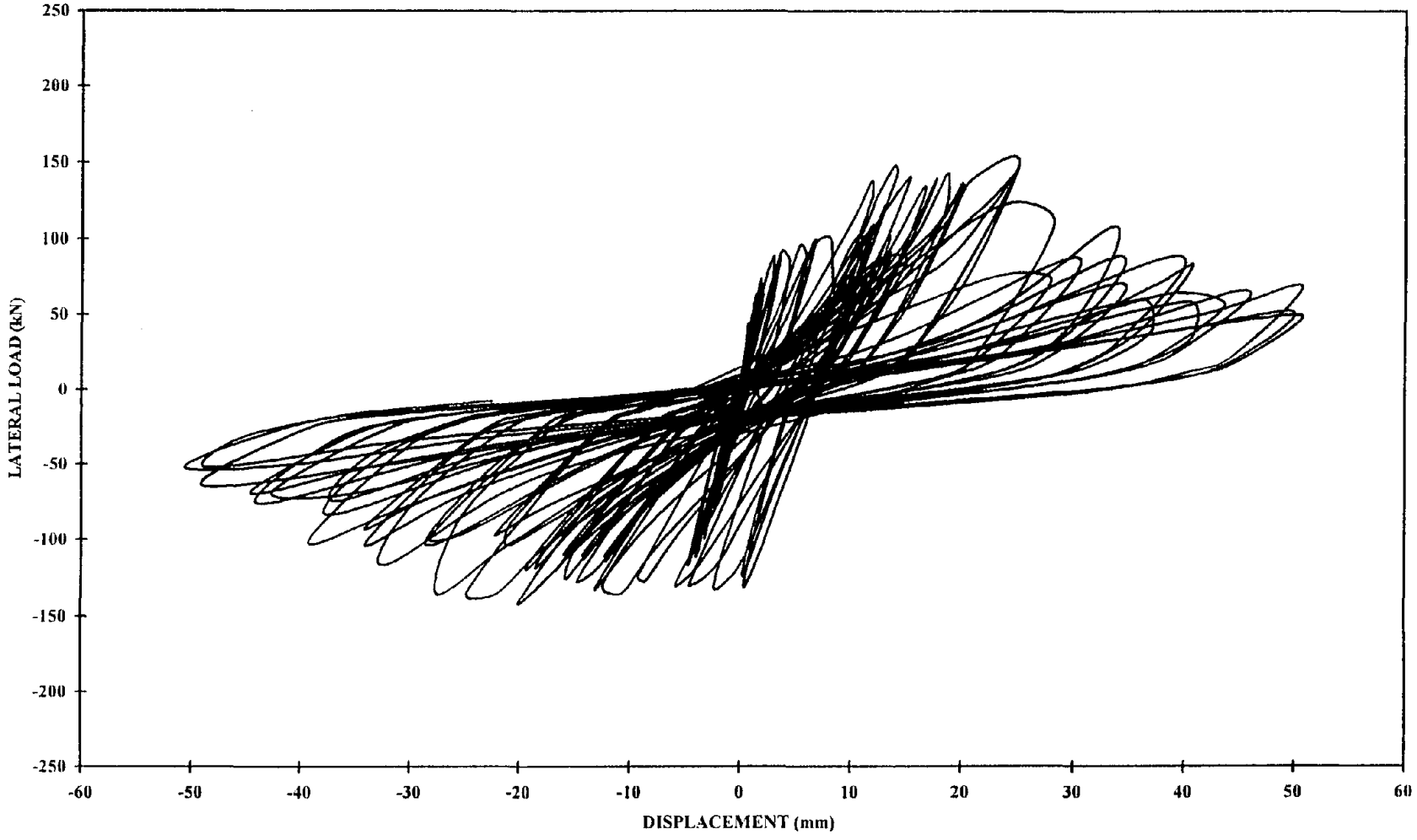

Figure 27. Beam-column joint tests - Load vs. displacement for Specimen 7

- The maximum load reached in the push segment was P_{max} = 156 kN. For the pull segment a value of P_{max} = 143 kN was obtained.
- The ultimate displacement was found to be Δ_u = 35 mm for both segments.

The strain history from the gage attached to the concrete surface (Figure 28) and to the composite material at the same location (Figure 29) shows a similar pattern throughout the test. However, the magnitude of the strain measured on the concrete is significantly higher than the strain on the composite, which is due to a less than perfect bond between the two materials and a subsequent delamination. The shapes of the curves are similar; however, the concrete readings are higher.

4.4 Phase I – Specimens 8 and 9

As it can be seen from Table 5, Specimens 8 has composite layers on both sides of the beam at a $\pm 45^0$ angle and one layer at 90^0 angle at the supports. This composite layout is similar to the one applied to Specimen 4, with the exception of the resin curing system. For Specimen 8, a room temperature cure system was used, as opposed to the elevated temperature cure system of Specimen 4. This change in curing system proved to have no significant effect on the overall specimen behavior.

Figure 30 shows the load-displacement curves for Specimen 8. The only real difference compared to the curves from Figure 21 is the joint's behavior after the peak load. Specimen 8 exhibits higher residual strength at the end of the test. This strength reserve could be very important for a structure after a major event, in order to sustain the gravity load applied to the member.

Once again, a balanced and symmetric composite layout on the beam resulted in

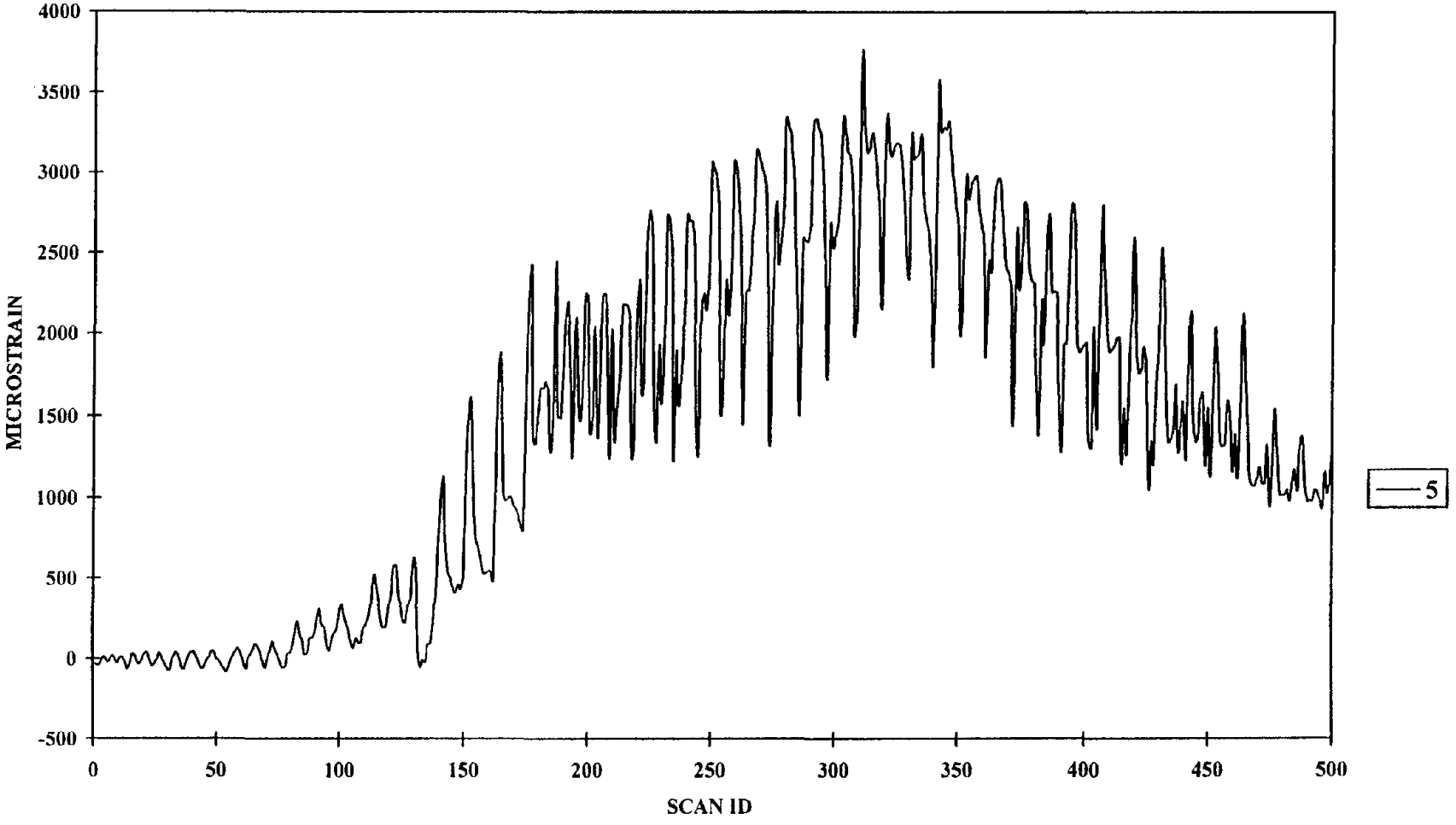

Figure 28. Beam-column joint tests - Strain readings on the rebar for Specimen 7

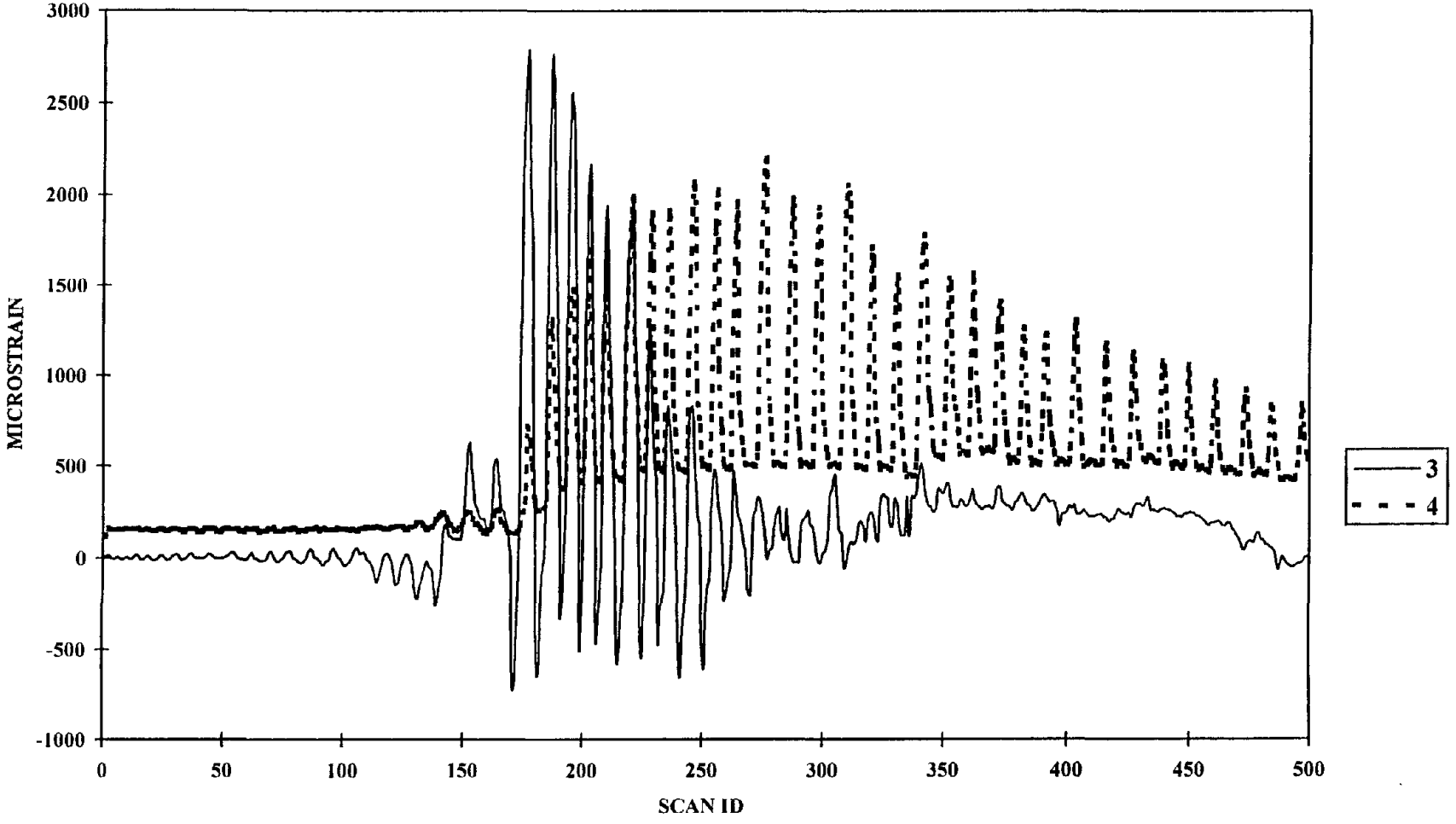

Figure 29. Beam-column joint tests - Strain readings on the composite for Specimen 7

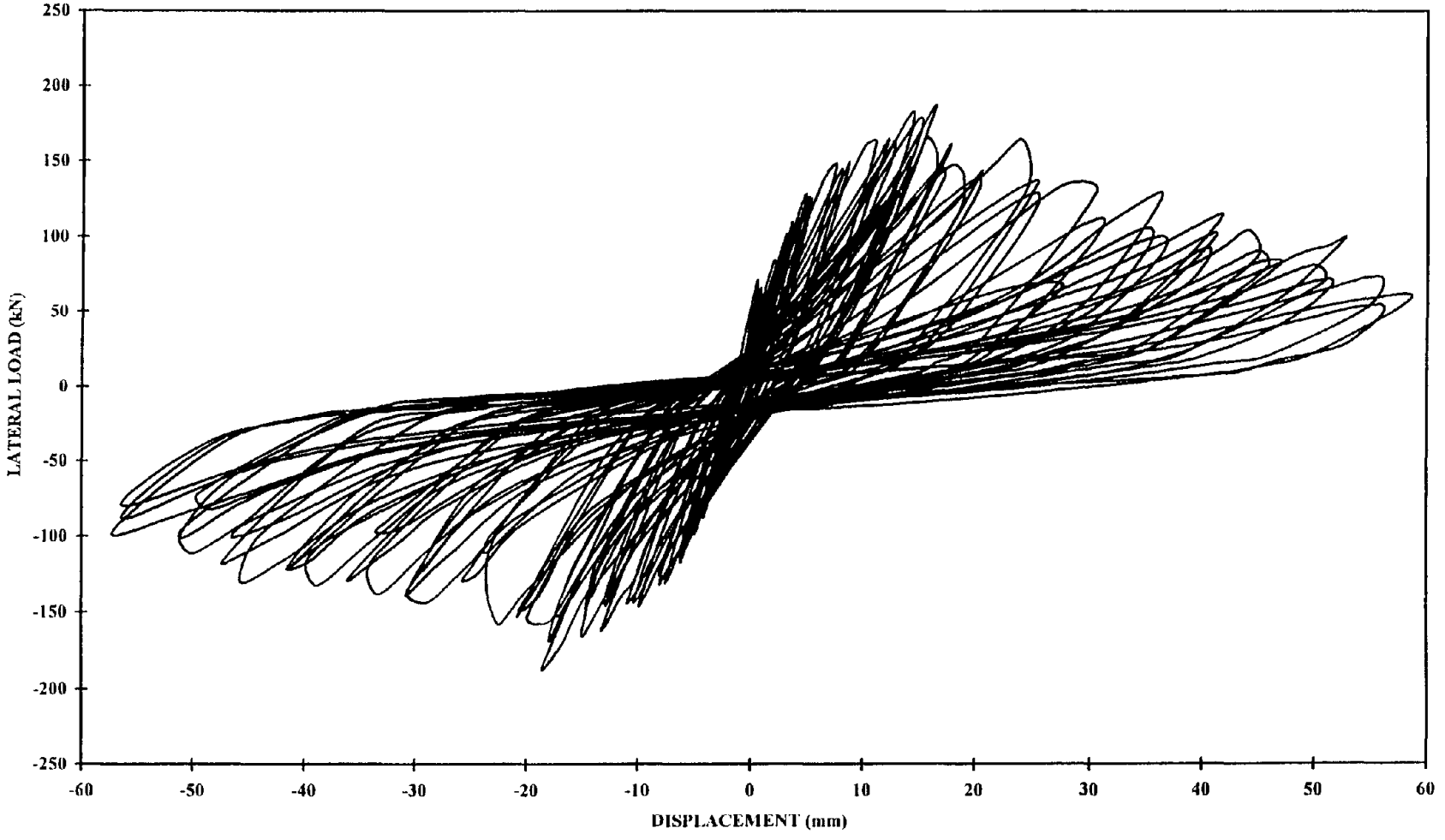

Figure 30. Beam-column joint tests - Load vs. displacement for Specimen 8

symmetric hysteresis curves in the push and pull segments. The recorded displacement and load results for Specimen 8 are:

- The maximum load reached in the push and pull segments was P_{max} = 187 kN. This value represents an identical strength level compared to Specimen 4.
- The ultimate displacement for both segments was found to be Δ_u = 31 mm.

The recorded composite strain at the peak level was close to 0.50% in the joint. After a moderate strain level on the composite material recorded by two strain gages (see Figure 31), toward the end of the test, one of the gages showed a 1.1% strain outside the joint region. This high strain level was close to the tensile capacity of the CFRP sheets, and a tensile failure in the composite next to this strain gage was observed.

In addition to the layout of Specimen 8, Specimens 9 has an additional layer around the column and the beams at a location adjacent to the joints (L_1 and L_3 region shown in Figure 7). The load-displacement curves for Specimen 9 are shown in Figure 32. A 15% increase in strength was observed compared to Specimen 8, which represents the highest level reached during the beam-column joint tests - Phase I.

The extensive concrete and composite damage was contained to the joint region. At approximately the maximum lateral load, the strain level on the composite material suddenly decreased by a factor of three (see Figure 33). After the composite delaminated from the concrete surface, significant shear cracks were developed in the concrete in the joint region. This led to anchorage loss of the column reinforcement, and finally resulted in a drop in the lateral load capacity.

The following results were recorded during the test of Specimen 9:

- The maximum load reached in the push segment was P_{max} = 216 kN, and P_{max} = 200

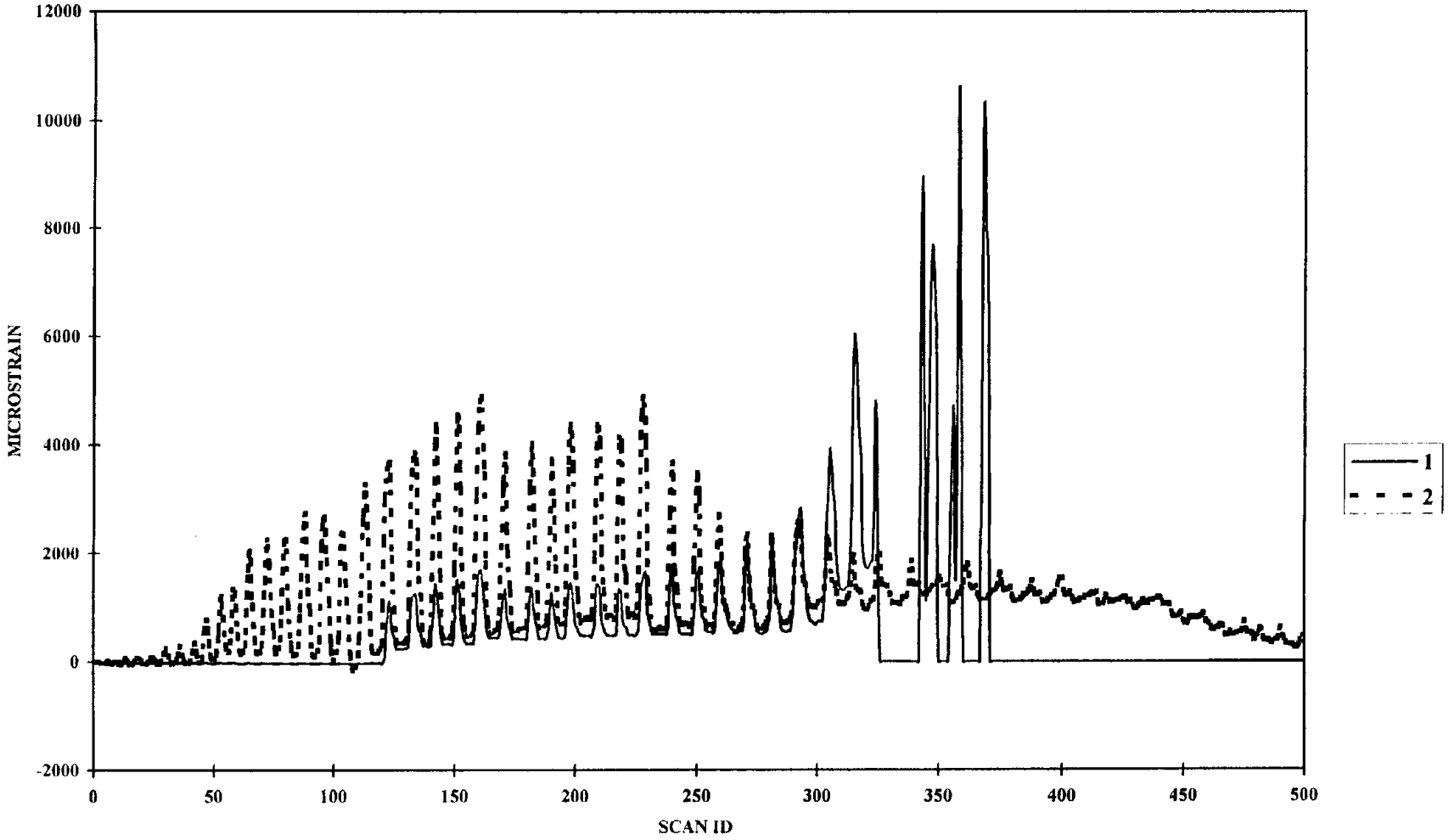

Figure 31. Beam-column joint tests - Strain readings on the composite for Specimen 8

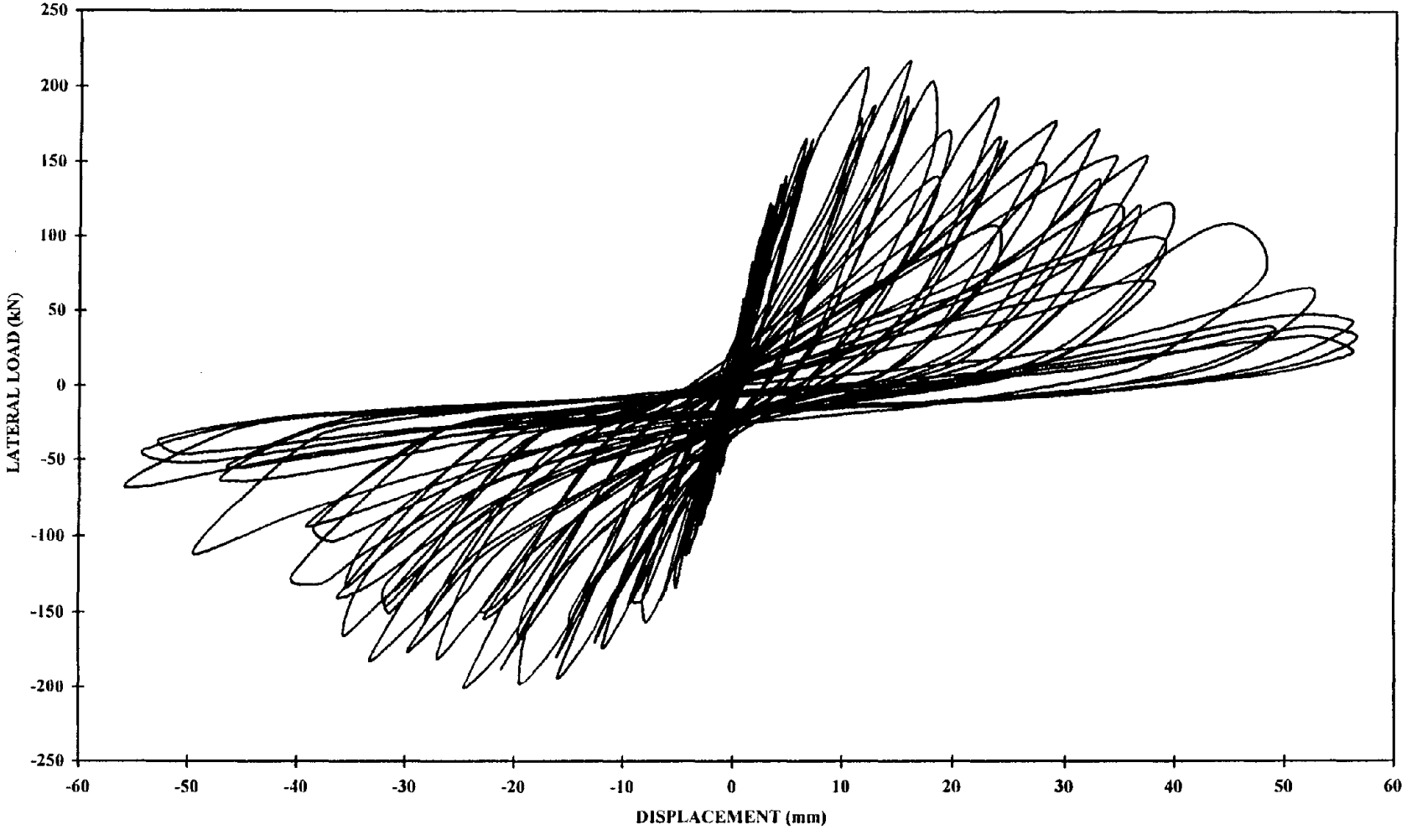

Figure 32. Beam-column joint tests - Load vs. displacement for Specimen 9

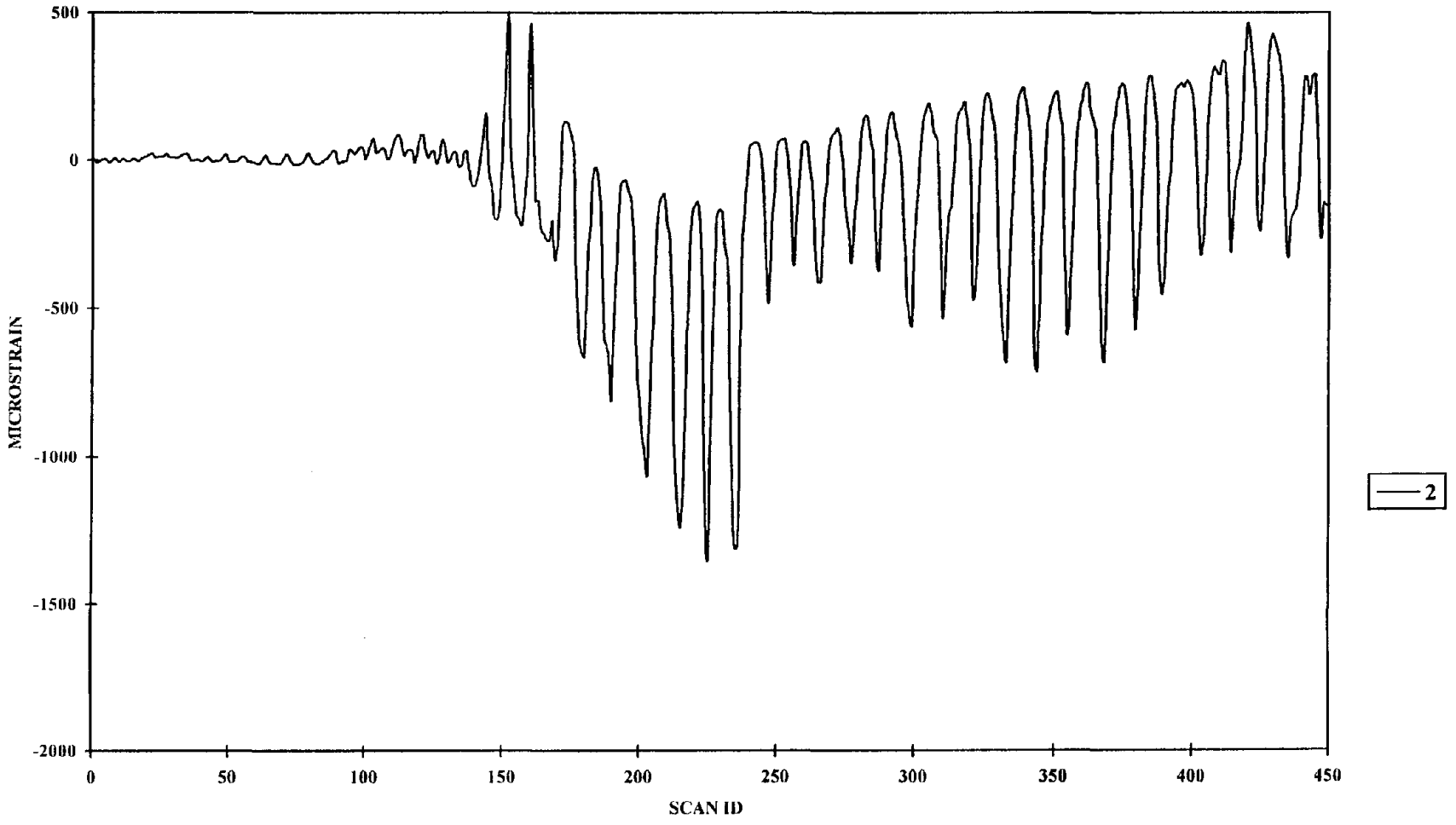

Figure 33. Beam-column joint tests - Strain readings on the composite for Specimen 9

kN for the pull segment.

- The ultimate displacement in the push segment was found to be Δ_u = 32.8 mm, and for the pull segment Δ_u = 25.6 mm.

4.5 Phase II – Specimens 10 and 11

In Phase II the measured concrete compressive strength was higher than the strength for the previous nine specimens (in Phase I). However, these six specimens are identical in every other detail (dimension and reinforcement) to the specimens from Phase I. Specimens 10 and 11 are the baseline specimens, and Specimens 12 to 15 were strengthened using composite sheets.

Figure 34 shows the load-displacement curves for Specimen 10. At the time of testing it was surprising that the lateral load capacity of this specimen was similar to the capacity of Specimen 1 and 2 despite the difference in the concrete compressive strength. However, as the strain recordings from the force link have been analyzed, it was found that a larger torsion was introduced into the system. The magnitude of this torsion was approximately 4 kN-m at the peak load, equivalent to an eccentricity of 32 mm. The load was maintained until the end of the test.

In the second phase an additional displacement transducer was used to measure the rigid body motion of the specimen. In order to find the true flexure of the specimen, all the displacement readings were corrected by this movement. The following results were obtained for Specimen 10:

- The maximum load reached in the push segment was P_{max} = 126 kN, and in the pull segment was P_{max} = 116 kN. These values represent a lower strength level than the

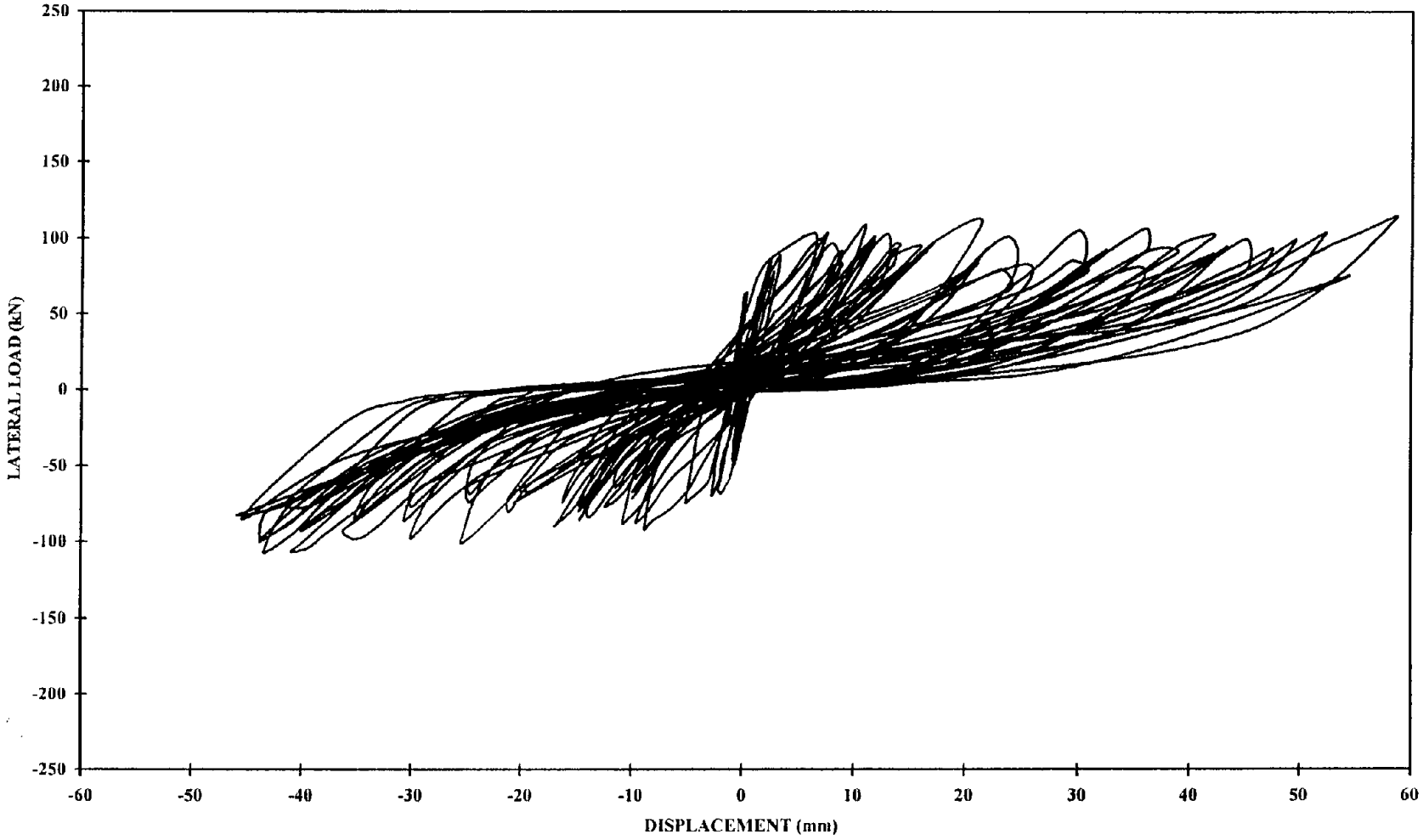

Figure 34. Beam-column joint tests - Load vs. displacement for Specimen 10

capacity of Specimens 1 and 2.

- The ultimate displacement was found to be Δ_u = 58.6 mm in the push segment, and the value for the pull segment was Δ_u = 43.8 mm.

Figure 35 shows the corrected horizontal column displacement throughout the test. Due to a less than perfect transducer calibration, the first three cycles were not symmetric, but this error was corrected at the end of the 44.5 kN load step.

The load-displacement curves for Specimen 11 are shown in Figure 36. This was the last baseline specimen tested in the 15 specimen beam-column joint test series. Although with only a small amount, Specimen 11 had the highest lateral load capacity, which was expected considering the increased concrete compressive strength. The reason for this limited increase in capacity is the extensive cracking in the joint region combined with bar pullout and loss in anchorage for the column longitudinal reinforcement extended into the beam.

At the 100 kN load cycle, a significant joint crack was observed in the pull segment exposing the longitudinal rebar from of column. As shown in Figure 36, after this event, Specimen 11 lost its lateral capacity in the pull segment, and was unable to reach the peak load achieved in the push segment for the same specimen.

The peak load and lateral deflections recorded for this specimen are similar to the values from Specimen 10. The following results were found for Specimen 11:

- The maximum load reached in the push segment was P_{max} = 148 kN, and P_{max} = 98 kN for the pull segment.
- The ultimate displacement in the push segment was found to be Δ_u = 54.6 mm, and for the pull segment Δ_u = 25.6 mm.

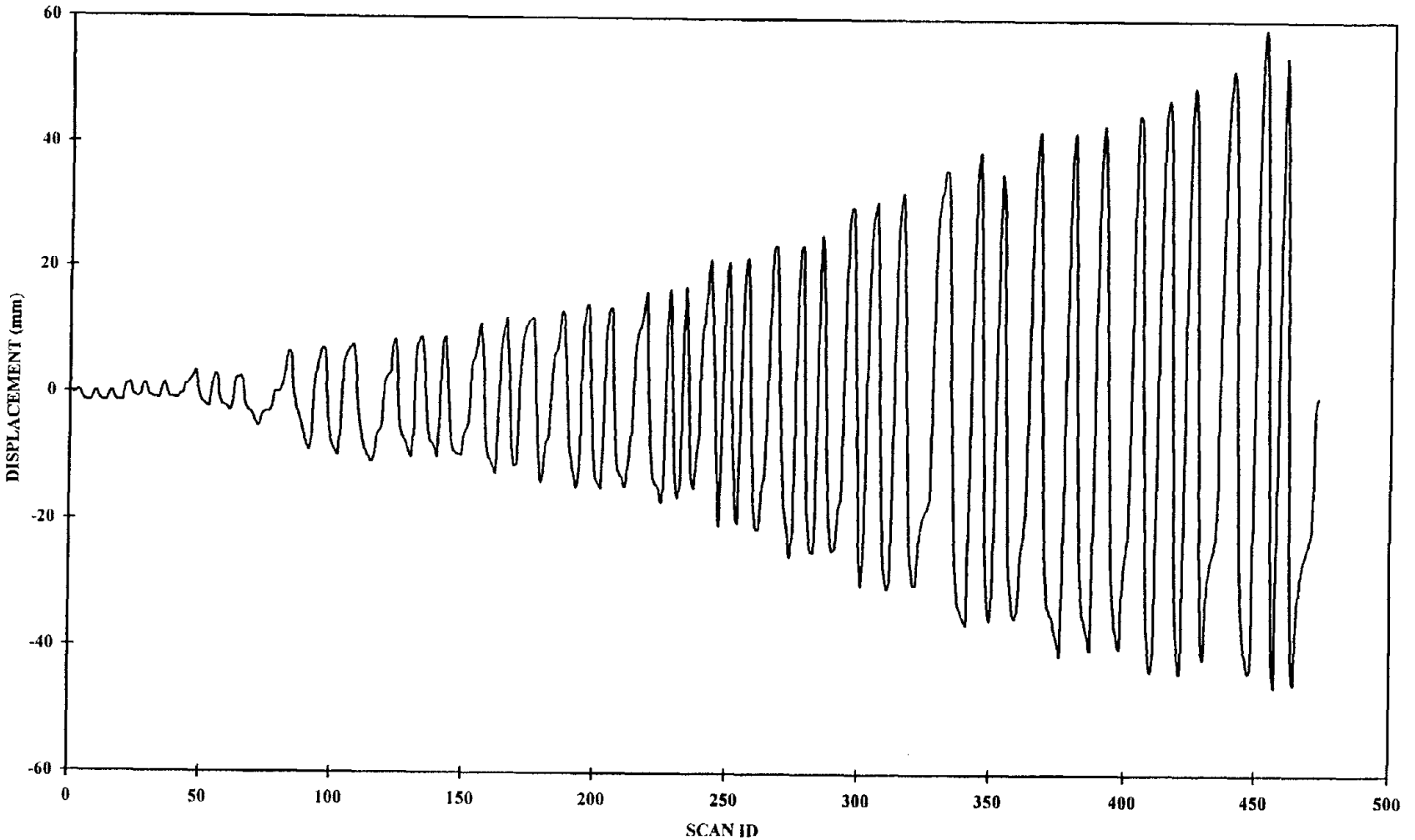

Figure 35. Beam-column joint tests - Horizontal displacement history for Specimen 10

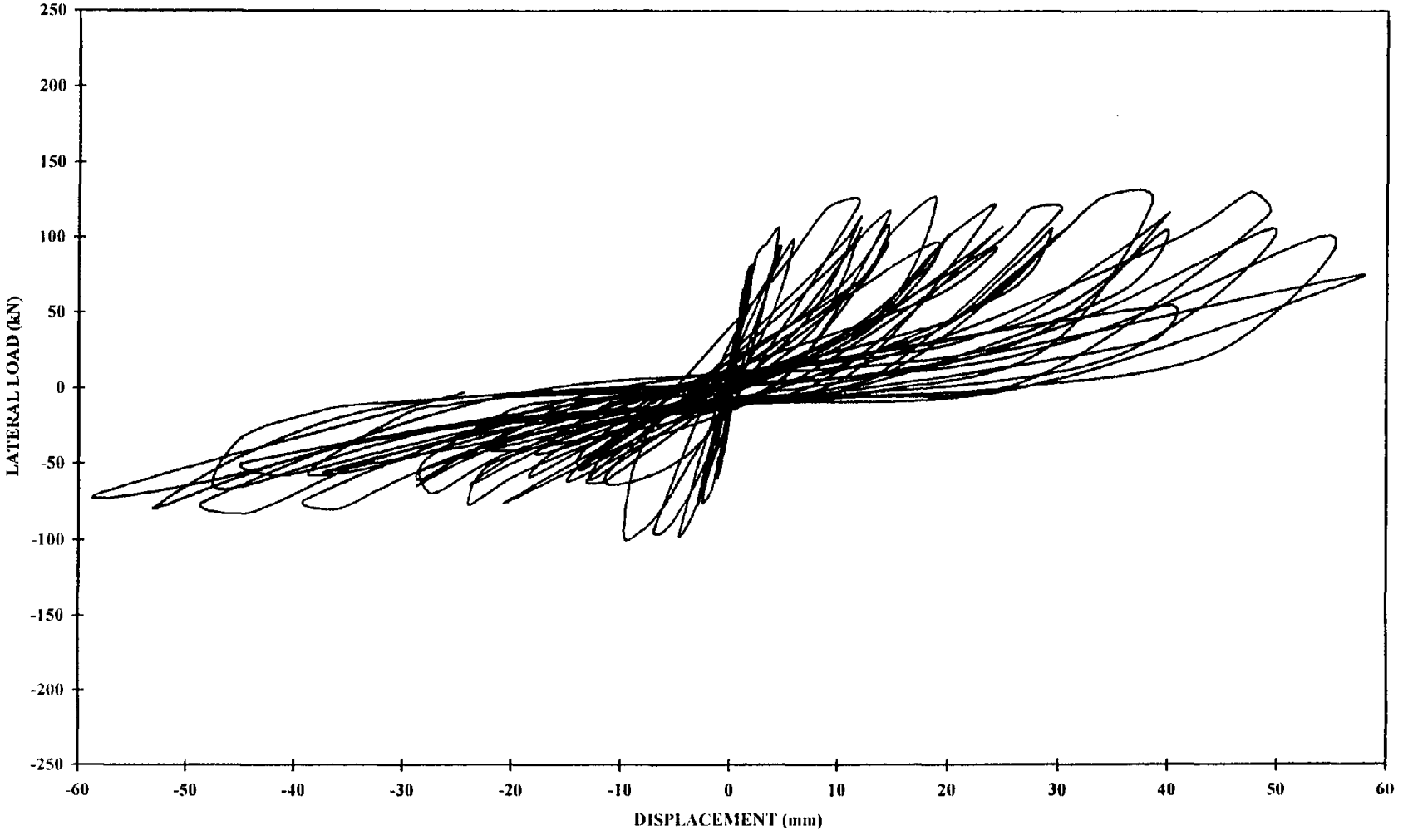

Figure 36. Beam-column joint tests - Load vs. displacement for Specimen 11

Figure 37 shows the recorded stain values from two strain gages attached to the surface of the concrete. The position of these gages (shown in Figure 9) was selected to monitor the strain on the concrete at the location of maximum bending stresses in the beam and the column. The strain gage on the column (Gage 9) shows a very small strain level. Due to an early crack at the beam-column interface, this gage does not show any significant tensile strains (which are positive values in the present work).

The strain gage on the beam (Gage 7) shows tensile values well below 2070 microstrains, the yielding value of the reinforcement. This value was exceeded only in the last part of the test (Scan ID 1200), after the joint had been damaged significantly.

4.6 Phase II – Specimens 12, 13 and 14

Specimens 12, 13 and 14 have a composite layer on both sides of the beam at a 45^0 angle and one layer at 90^0 angle (with respect to the beam's longitudinal axis) at the supports. In addition, they have one layer around the column and the beams at a location adjacent to the joints (areas marked on Figure 6 with dimensions L_1 and L_3). This layout is similar (with minor differences) to the one applied to Specimen 9.

For Specimen 12 the dimension L_3 is 406 mm and it is extended only 51 mm beyond the corner at the bottom of the beam. This layer for Specimen 13 however, is extended to the forth side of the beam with a 51 mm overlap. The layout for Specimen 14 is identical to the layout for Specimen 12. However, instead of wire brushing the concrete surface, a more extensive surface preparation has been used. This consisted of grinding the surface using a powerful water jet (276 MPa), and the application of a thin layer of high strength structural adhesive (Sikadur 31). This method proved to increase

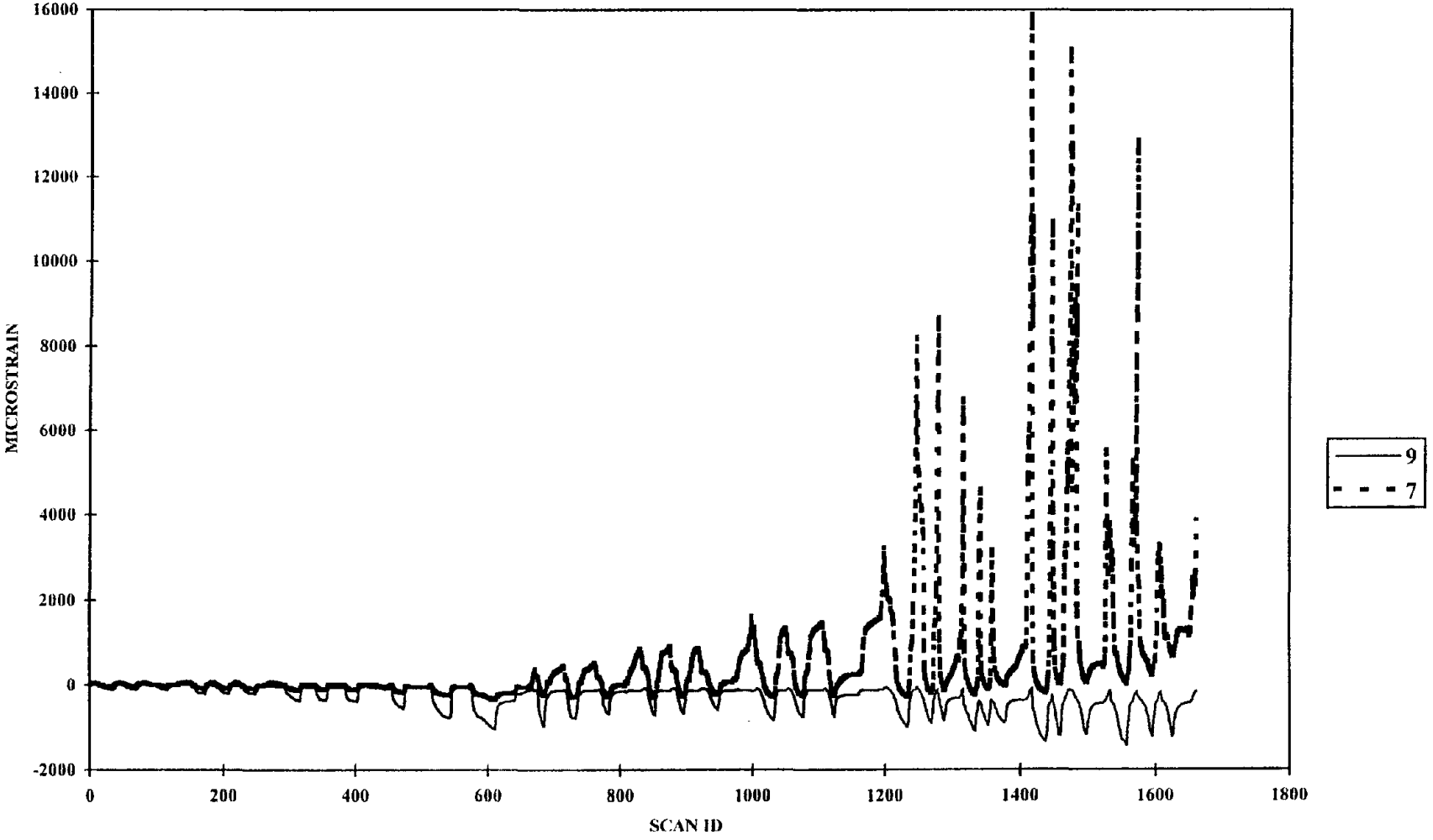

Figure 37. Beam-column joint tests - Strain readings on concrete for Specimen 11

the bond between CFRP sheets and concrete surface.

In a building or a bridge bent, the top of the beam is not accessible for external repair due to the slab or girders at that location. By not extending the layer at 90^0 angle on the beam all around the member, a similar situation was created. Although this layer could not develop significant confinement effect in the beam, it did increase the beam's shear capacity and the anchorage of the inclined layers extended beyond the joint region.

Figure 38 shows the load-displacement curves for Specimen 12. The lateral load values recorded are similar to the results from Specimen 9. In the push segment, after the peak has been reached, a continuous degradation was observed, and resulted in a low displacement level at failure.

The results for Specimen 12 are:

- The maximum load reached in the push segments was P_{max} = 184 kN, and for the pull segment P_{max} = 217 kN.
- The ultimate displacement was found to be Δ_u = 36.1 mm in the push cycle. In the pull cycle the ultimate displacement was Δ_u = 58.7 mm.

The location of strain gages attached to the composite surface is shown in Figure 9. These locations were chosen in order to record the maximum strain level in and around the joint region. The data recorded by Gages 13, 14 and 12 (on the inclined composite) are shown in Figure 39. As it was expected, the highest strain was recorded closer to the perimeter of the joint (by 13 and 12), where due to the vertical layer around the beam, the anchorage was more effective.

The load-displacement curves for Specimen 13 are shown in Figure 40. Despite the fact that the L_3 transverse composite layer on the beam was applied all around the

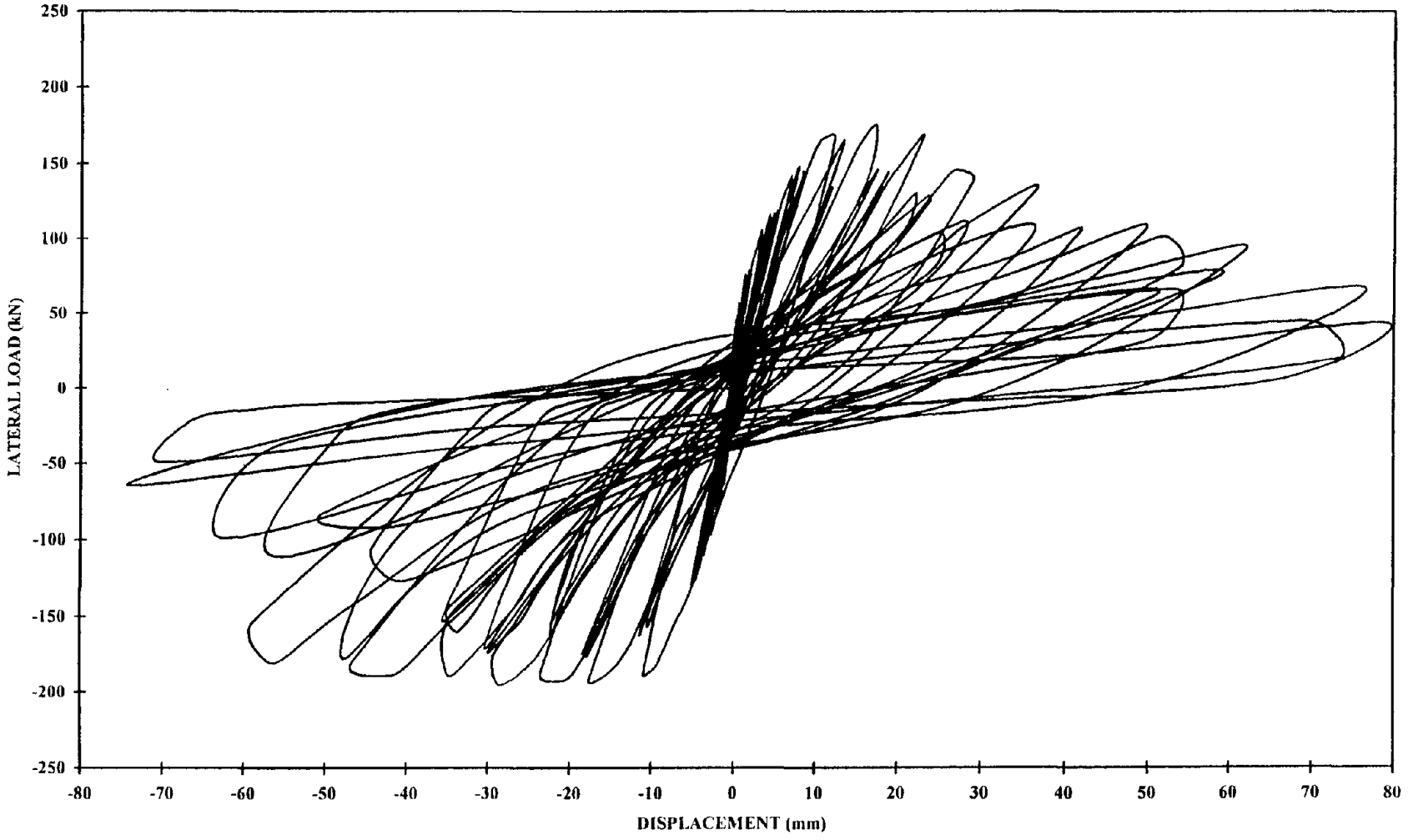

Figure 38. Beam-column joint tests - Load vs. displacement for Specimen 12

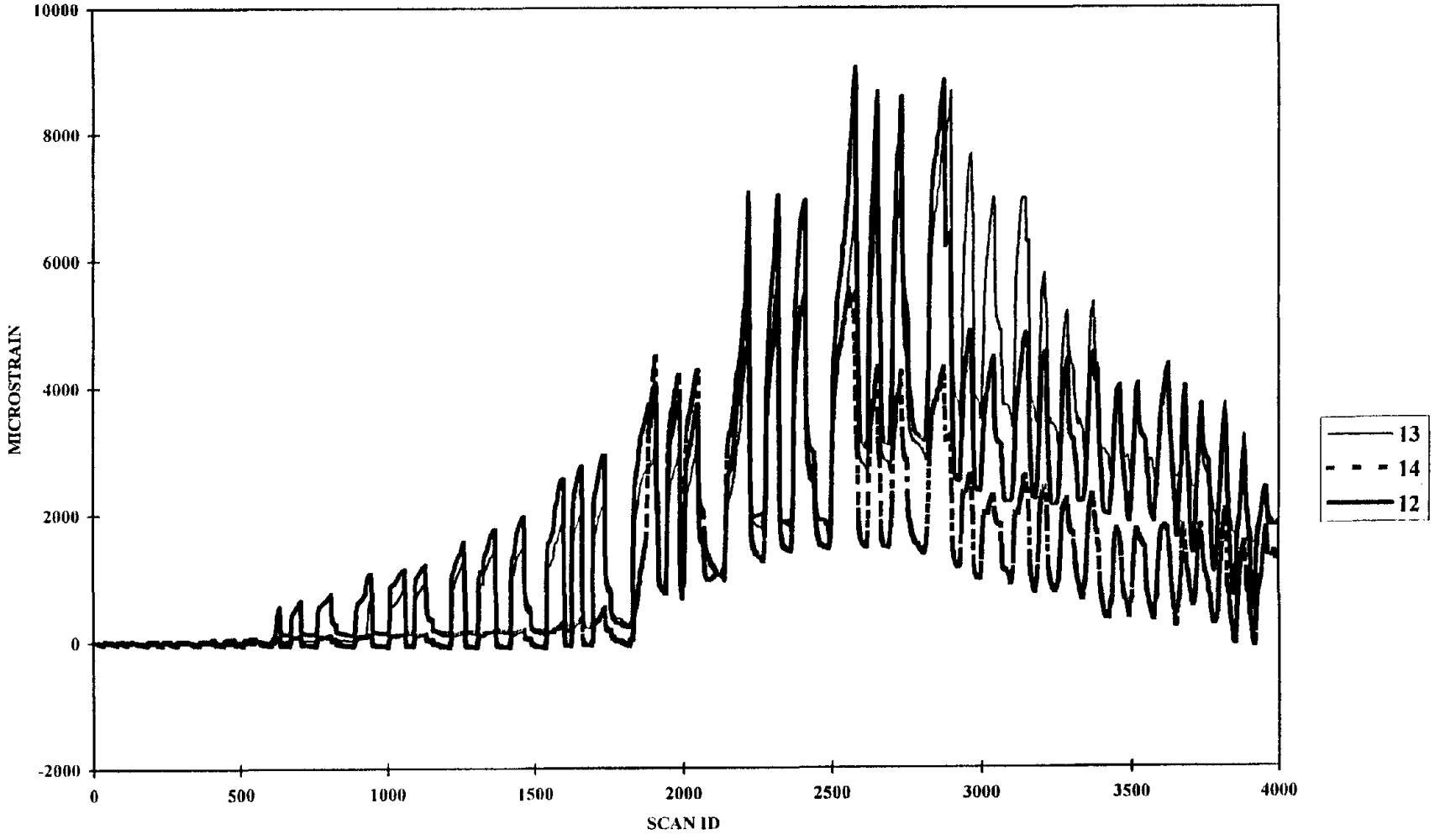

Figure 39. Beam-column joint tests - Strain readings on composite in the joint for Specimen 12

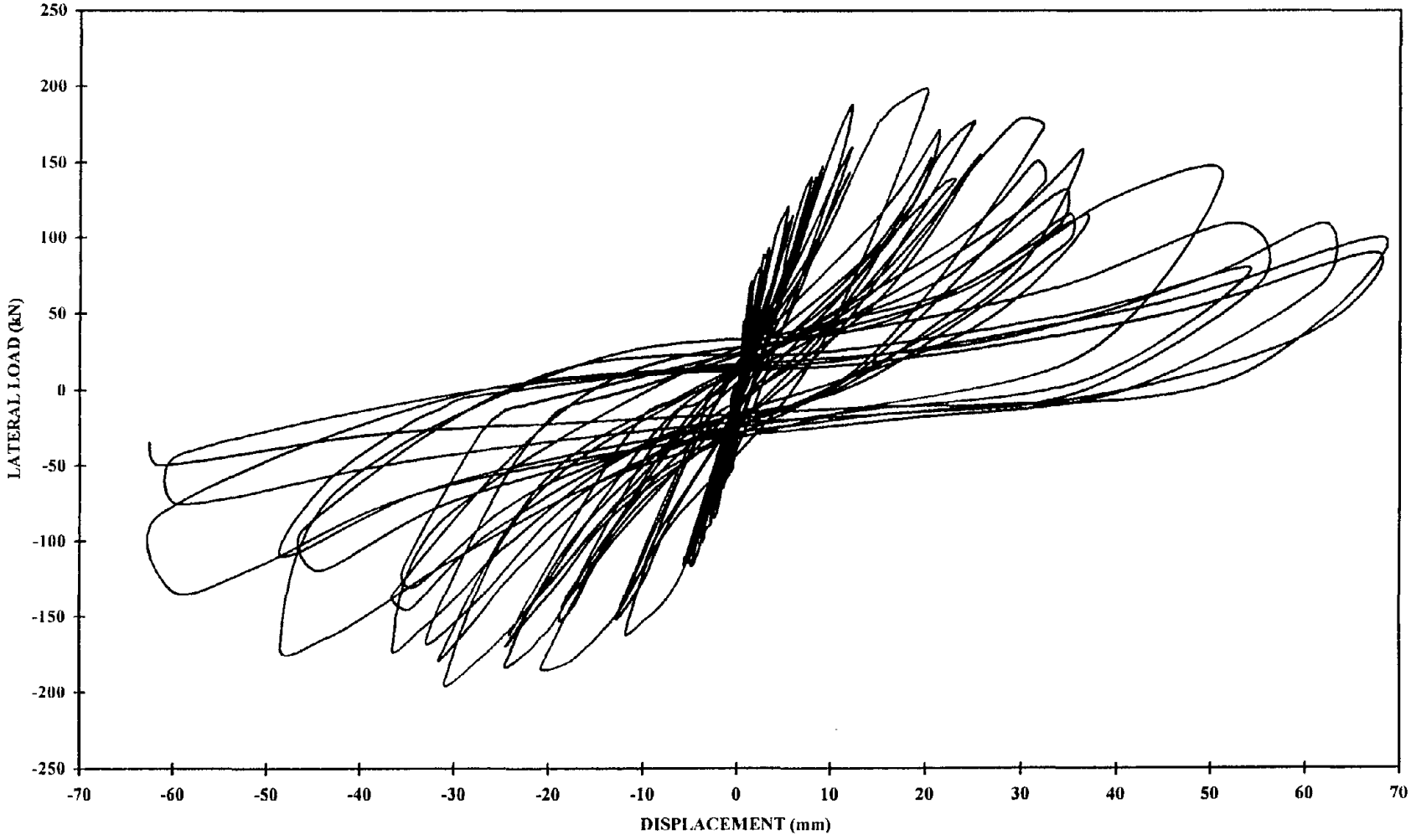

Figure 40. Beam-column joint tests - Load vs. displacement for Specimen 13

beam (as opposed to the layer for Specimen 12), there was no real difference between these two tests. At a displacement level of 20 mm, the entire composite layout debonded from the joint's surface, resulting in no difference in the specimen's behavior.

The force and ductility results for Specimen 13 are:

- The maximum load reached in the push segments was P_{max} = 204 kN, and P_{max} = 196 kN for the pull segments. The average of these values is approximately the same as the average maximum load reached for Specimen 12.
- The ultimate displacement in the push segment was found to be Δ_u = 36.4 mm, and for the pull segment Δ_u = 48.5 mm.

Figure 10 shows the location of strain gages on the composite in the joint region. These gages recorded a moderate strain level throughout the test (see Figure 41), except for Gage 12. After the composite delaminated from the joint region, this gage recorded larger compression values.

Figure 42 shows the load-displacement curves for Specimen 14. As expected, this specimen had a higher lateral load resistance capacity than Specimen 12, the only difference between them being the surface preparation. This surface preparation (grinding using water jet and the application of Sikadur 31) proved to compensate for the deficiency caused by the limited extension of the vertical composite layers at the bottom of the beam.

The results for Specimen 14 are:

- The maximum load reached in the push segments was P_{max} = 229 kN, and for the pull segment P_{max} = 224 kN. These peak lateral load values are higher by approximately 5% than the average loads of Specimen 12 and 13.

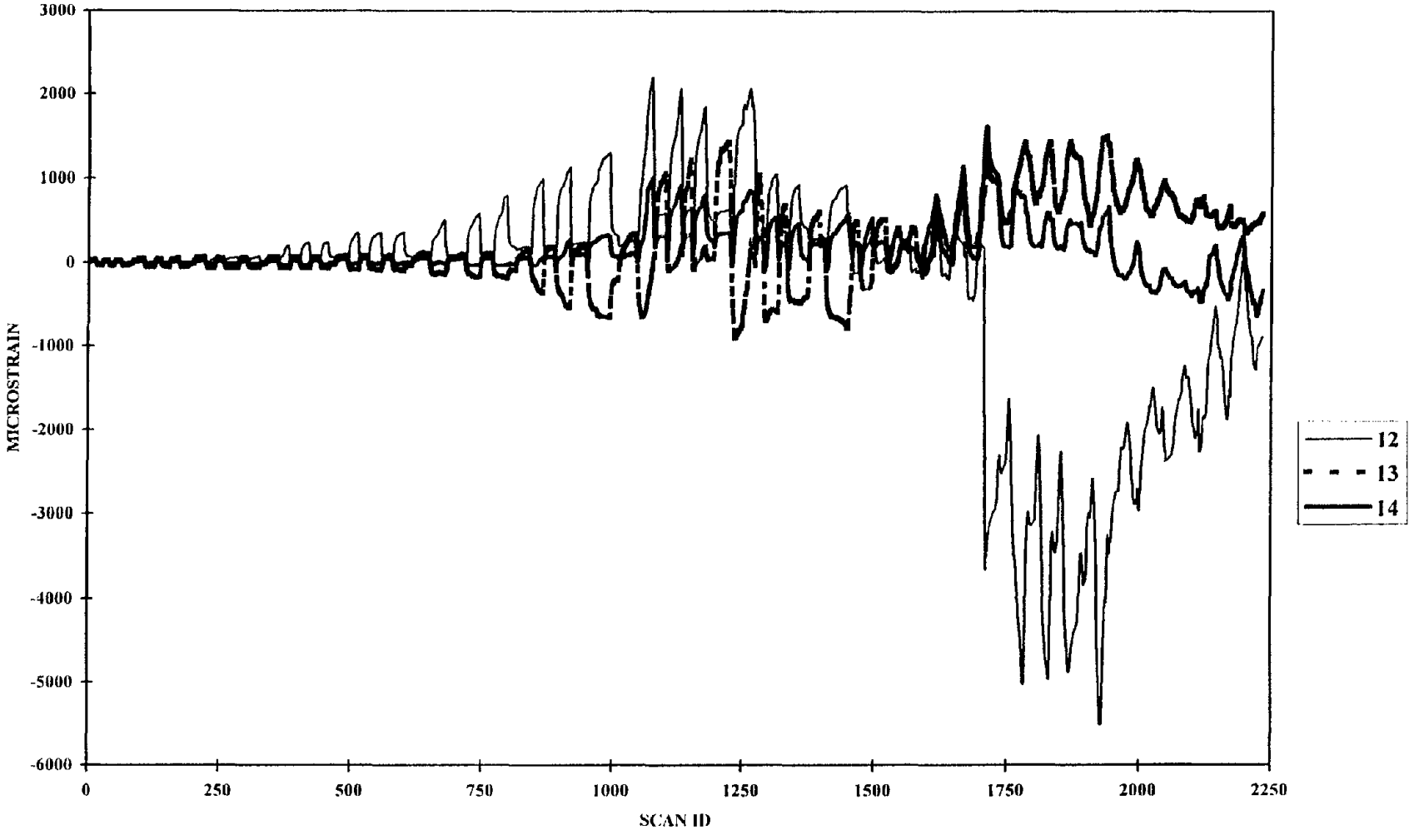

Figure 41. Beam-column joint tests - Strain readings on composite for Specimen 13

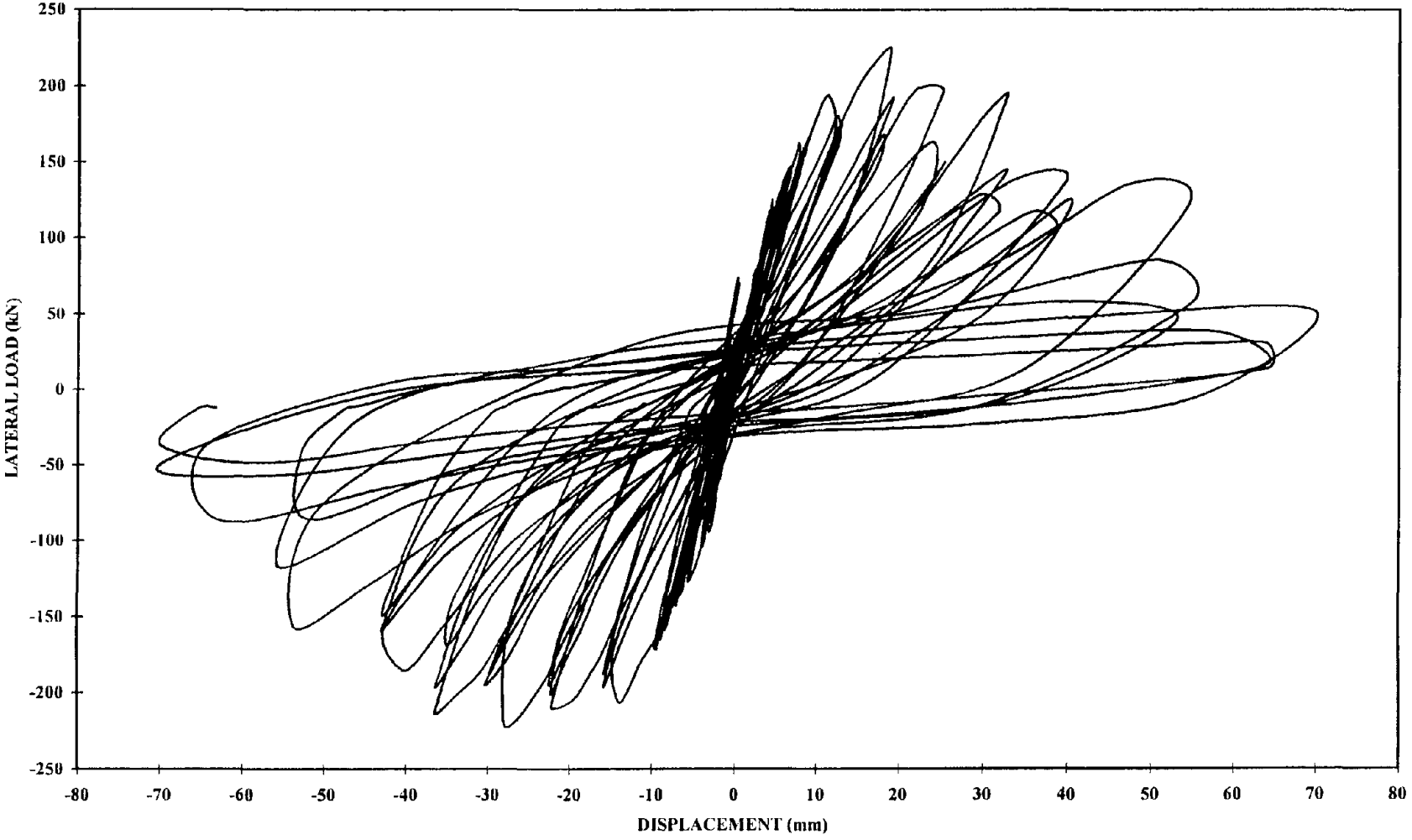

Figure 42. Beam-column joint tests – Load vs. displacement for Specimen 14

- The ultimate displacement in the push segment was found to be $\Delta_u = 32.8$ mm. In the pull segment, the ultimate displacement was $\Delta_u = 42.8$ mm.

It was expected to see higher composite tensile stresses due to higher lateral loads. As it can be seen from Figure 43, Gage 12 reached a very high strain level (over 1.4%) just before the composite failed in tension. Gage 13 recorded a strain level up to 0.65%, and decreased as the composite delamination extended beyond the joint region.

4.7 Phase II – Specimen 15

Specimen 15 has a composite layout similar to Specimen 14, and the additional layers are shown in Figure 8. The additional horizontal layer on both sides of the beam, together with the double U-shaped layers anchored back to the column, provided a significant shear capacity increase for the beam-column joint specimen. The surface preparation was identical to the one applied to Specimen 14.

Compared to Specimen 14, a 50% increase in lateral load capacity was recorded. However, even at a displacement of 50 mm (at the end of the test), the load capacity was similar in magnitude to the peak value of the baseline specimens. The load-displacement curves for this specimen are shown in Figure 44. Significant delamination and composite tensile failure were observed at a displacement level of 25 mm, followed by a gradual loss in load capacity.

The following results were obtained for Specimen 15:

- The maximum load reached in the push segments was $P_{max} = 336$ kN, and for the pull segment $P_{max} = 330$ kN. These values represent an increase over the baseline specimens of approximately 200%.

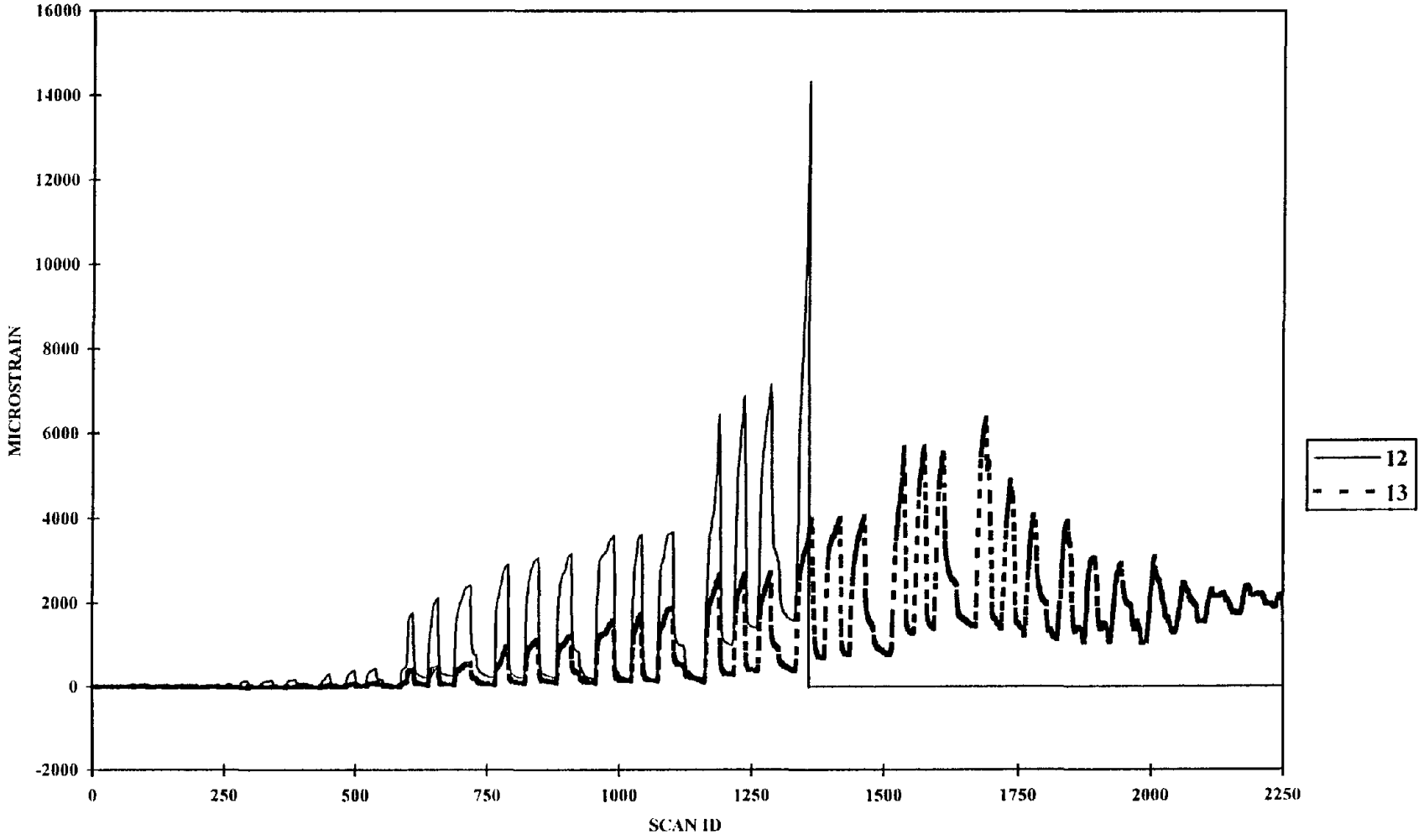

Figure 43. Beam-column joint tests - Strain readings on composite for Specimen 14

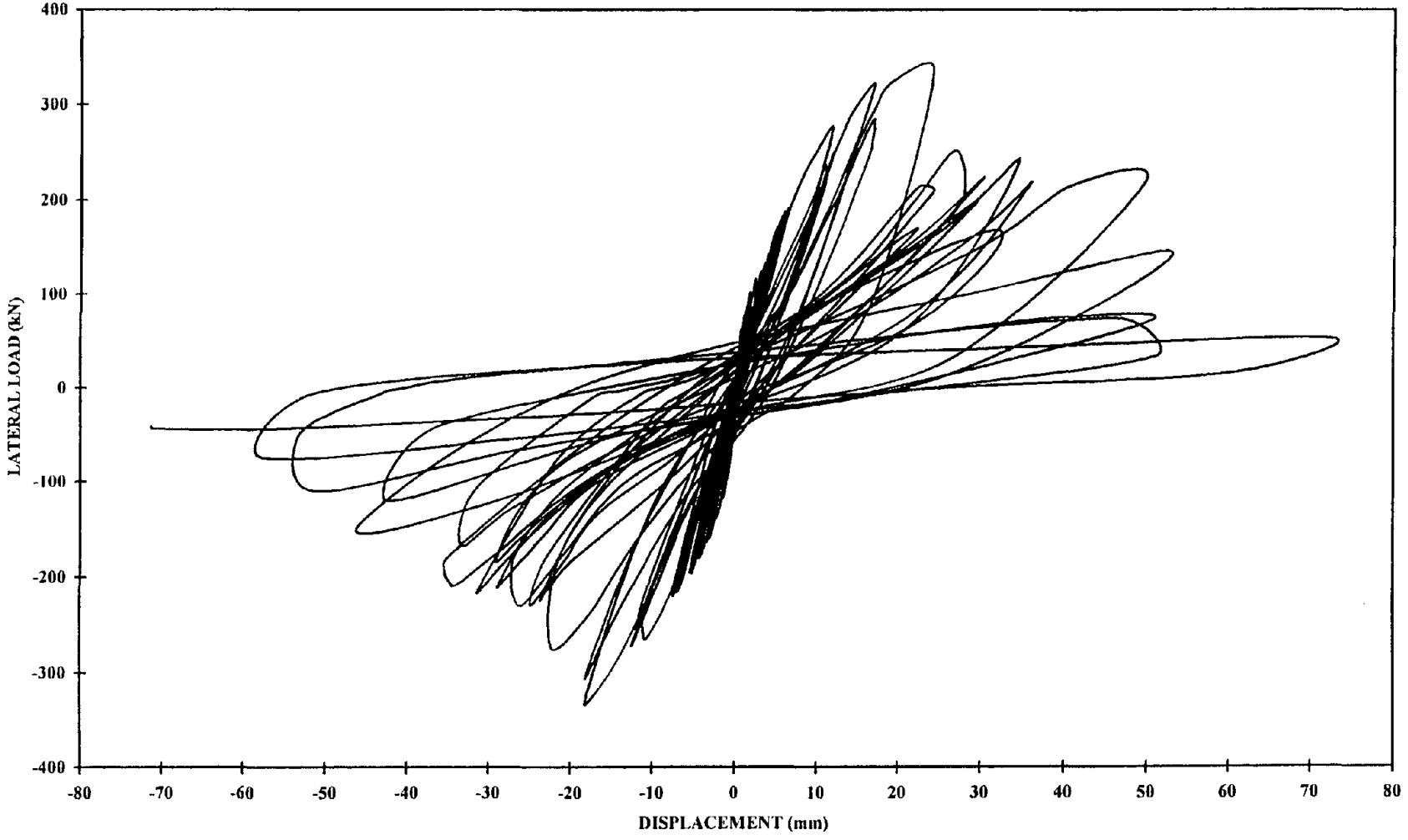

Figure 44. Beam-column joint tests - Load vs. displacement for Specimen 15

- The ultimate displacement was found to be $\Delta_u = 27.0$ mm in the pull segment, and $\Delta_u = 23$ mm in the pull segment.

By having extra composite layers in the joint (compared to Specimen 14), it was normal to find lower stresses in the inclined composite layers. Gages 19, 20 and 21 (shown in Figure 45) were mounted to the horizontal layers. The maximum stresses were recorded by the top gage (see Figure 46). It was expected that the layers on the upper part of the joint would show a higher stress level due to a more effective anchor.

Gages 11 and 18 were located on the vertical layers. The first gage was on the beam, and the second one on the U-shaped double layer extended into the column. After the failure of the U-shaped layers, the stress level in Gage 18 decreased (shown in Figure 47). At the same time, the vertical layers on the beam recorded an increasing strain level.

To compare the results, Table 6 provides the recorded peak lateral load for each specimen.

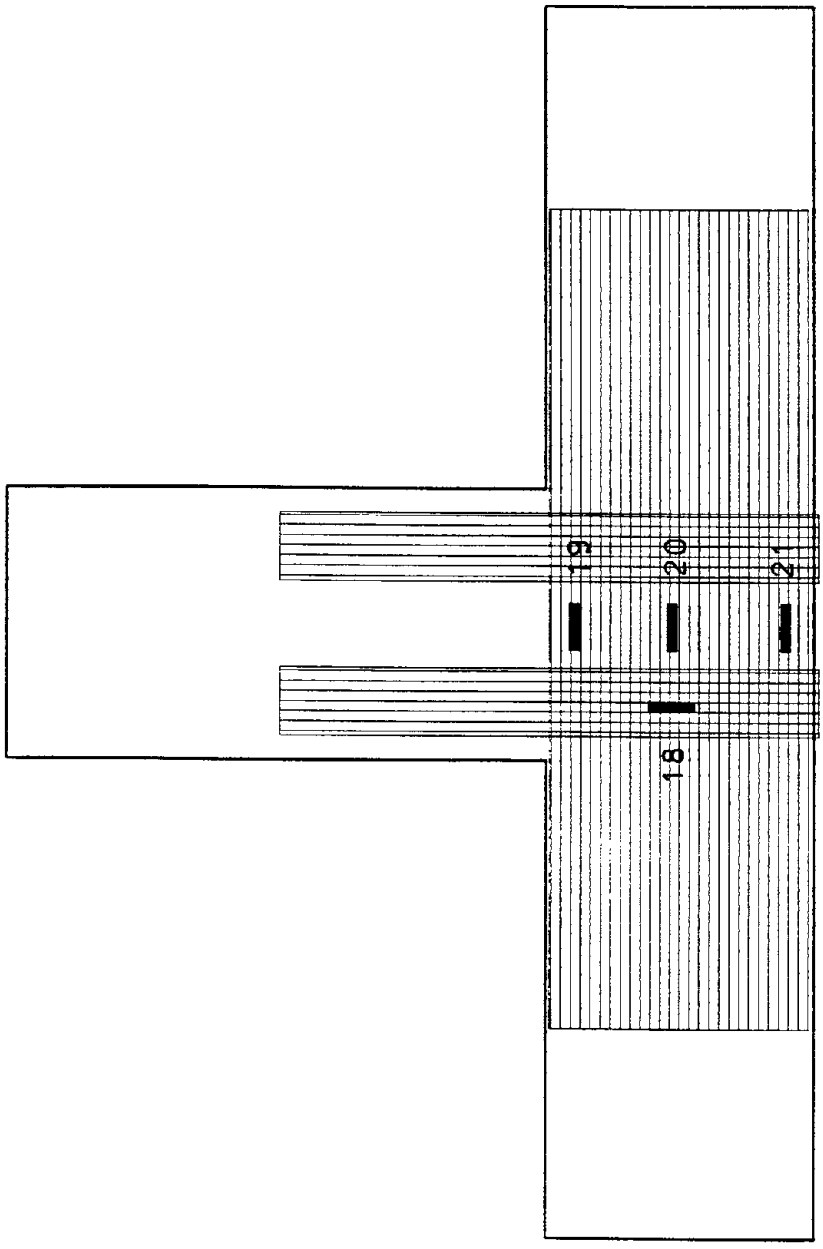

Figure 45. Additional strain gages on Specimen 15

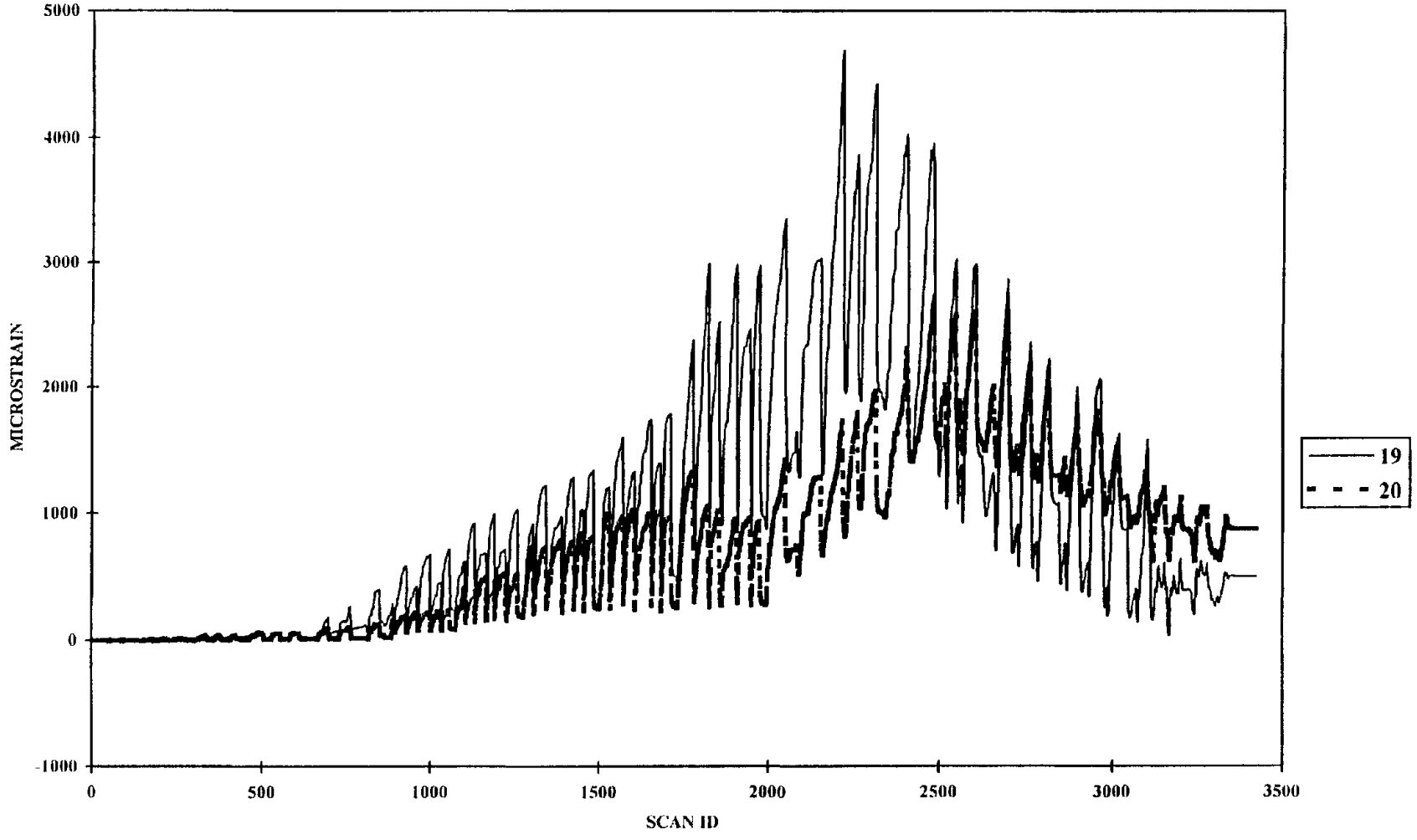

Figure 46. Beam-column joint tests - Strain readings on composite in the joint region for Specimen 15

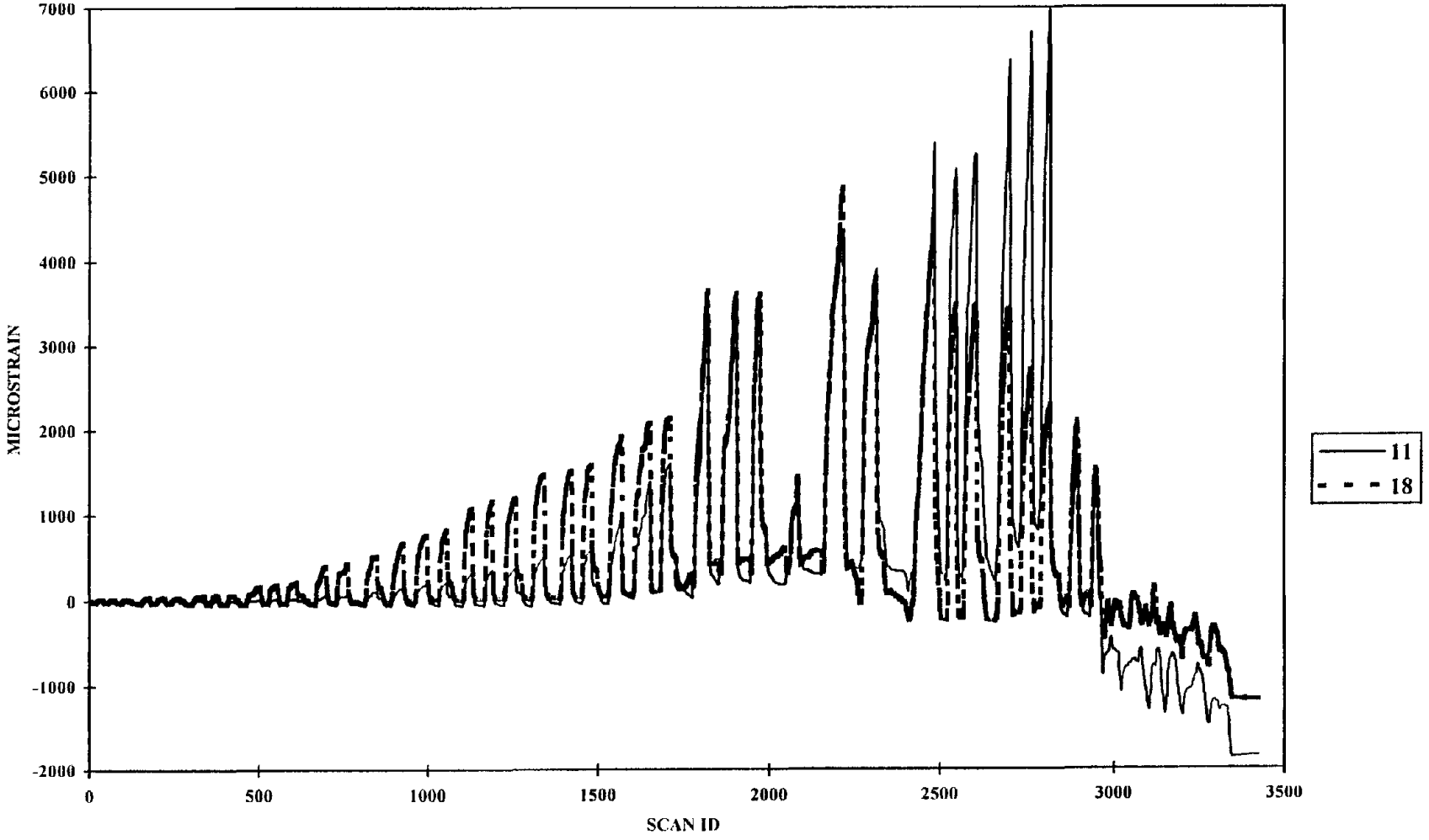

Figure 47. Beam-column joint tests - Strain readings on composite for Specimen 15

Table 6. Beam-column joint test results

Phase (1)	Specimen (2)	Surface Preparation (3)	Curing Temperature (5)	Load (kN) *Push* (6)	Load (kN) *Pull* (7)
I	1[1,2]	N/A	N/A	~129	~129
	2[1]	N/A	N/A	129	142
	3	Wire Brush	Elevated	182	142
	4	Wire Brush	Elevated	187	187
	5	Wire Brush	Room	161	154
	6	Wire Brush	Room	158	140
	7	Wire Brush	Room	156	143
	8	Wire Brush	Room	187	187
	9	Wire Brush	Room	216	200
II	10[1]	N/A	N/A	126	116
	11[1]	N/A	N/A	148	98
	12	Wire Brush	Room	184	217
	13	Wire Brush	Room	204	196
	14	Water Jet	Room	229	224
	15	Water Jet	Room	336	330

Note: [1] Baseline specimens
[2] Approximate values

CHAPTER 5

BEAM-COLUMN JOINTS – ANALYTICAL RESULTS

The experimental results presented in the previous chapter were checked using different analytical methods. First, a finite element program was used to perform a pushover analysis of the beam column assembly. The same program was used to calculate the forces in the beam-column joint region. Then using the joint forces from the baseline specimens and from the FRP reinforced specimens, a design aid has been developed for the increase in the shear capacity of reinforced concrete joints.

5.1 Pushover analysis

5.1.1 Analytical model

To perform the finite element analysis, the DRAIN-2DX program has been used. Considering the planar nature of the specimens and the test setup, and by neglecting any torsional effects resulting from test fixture misalignment, a two-dimensional model was found to be adequate. The model is shown in Figure 48a with the specimen dimensions, the boundary conditions and the loading conditions.

From Figure 11 it is clear, that the fixtures at the beam-ends allow rotation, but prohibit any vertical movement, and in addition, the end stops create a horizontal reaction. This reaction generates a compression force in the beam's right hand side (in

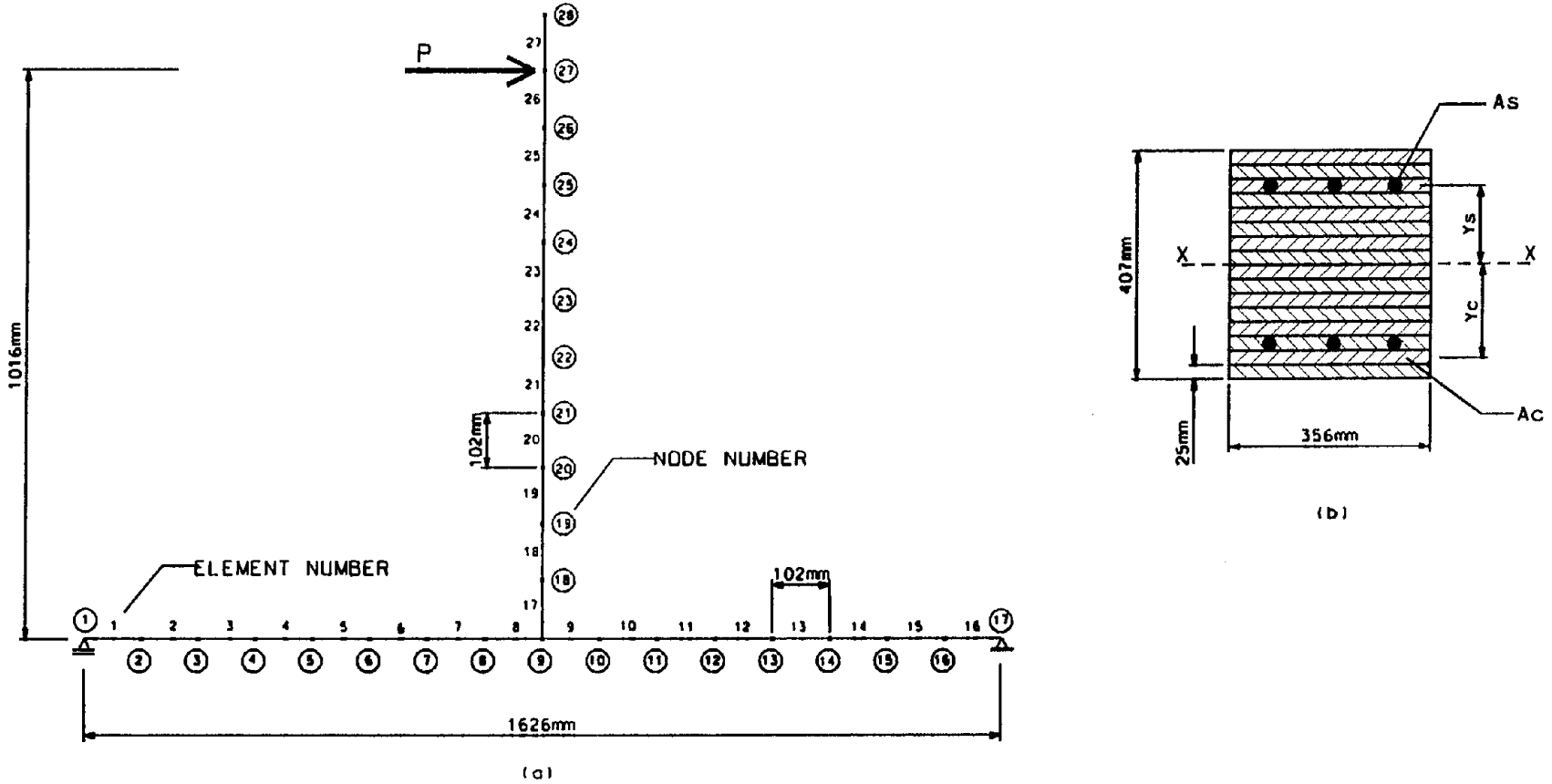

Figure 48. Two-dimensional model of beam-column specimens (a), using the fiber element meshing (b)

the push segment). However, it is important to notice that there was no tension developed at the left-hand side of the beam (for the loading condition shown in Figure 48), and resulted in different beam forces at the two sides of the joint.

The beam and the column are divided into 102 mm long elements, a total of 27 elements. The joint region was modeled as beam and column elements, because the only other option in the program, a rigid joint model, did not represent the softness of the joint. However, all the joint forces have been evaluated at the face of the joint; specifically at nodes 7 and 11 for the beam, and node 19 for the column. The program does not take into account any shear failure (in the elements or in the joint region). These values had to be checked manually.

The beam and the column are represented by the program's fiber element option. In the 2-D version, this option allows the input of different horizontal slices for concrete and steel materials, which are located at a certain distance from the section's geometric center (see Figure 48b). Thus, each horizontal slice (25 mm thick for the concrete sections) is represented by its cross-sectional area (A_i) and the distance (y_i) to the geometric center.

The input file for the DRAIN-2DX model is presented in the Appendix A. It can be seen, that each material is modeled by its stress-strain curve. The behavior of the concrete is represented by a five-point compression curve, without taking into account the concrete's tensile capacity. The reinforcing steel is modeled as an elastic-perfectly plastic material. Due to the fact that the specimens showed an elastic joint behavior, the effect of steel hardening was neglected.

The only difference in the input file for the Phase II baseline specimen is in the

concrete stress-strain curve. Every other detail is identical to the one presented in Appendix A.

5.1.2 Pushover analysis

A horizontal static load has been applied at node 27 by controlling the displacement at the top of the column. Load-displacement couples were recorded during the pushover analysis.

To compare the analytical results with the test data, the findings from Specimen 2 were used. As it was mentioned earlier, Specimen 2 (Phase I) during the first push segment in the first cycle was subjected to an unintentional monotonic load. This unscheduled loading provided a unique opportunity to calibrate the analytical model described in the previous section.

The load-displacement curves for three cases are presented in Figure 49. These three cases are: the test data from Specimen 2, the analytical results for the baseline specimens in Phase I and Phase II. There has been no yielding observed for any of the above-mentioned cases, which correlates well with the recorded peak lateral loads and the capacity values presented in Table 4. The specimen lost its strength at approximately the lateral load level corresponding to the beam's shear capacity (144 kN).

As it was mentioned earlier, the analytical results given by DRAIN-2DX did not include any shear calculation, so this shear failure could not be captured. Furthermore, it was observed that the analytical results depend greatly by the behavior of the beam elements 8 and 9, adjacent to node 9. For the same lateral load, the moment at these locations was higher than at the face of the column, where all the forces were evaluated.

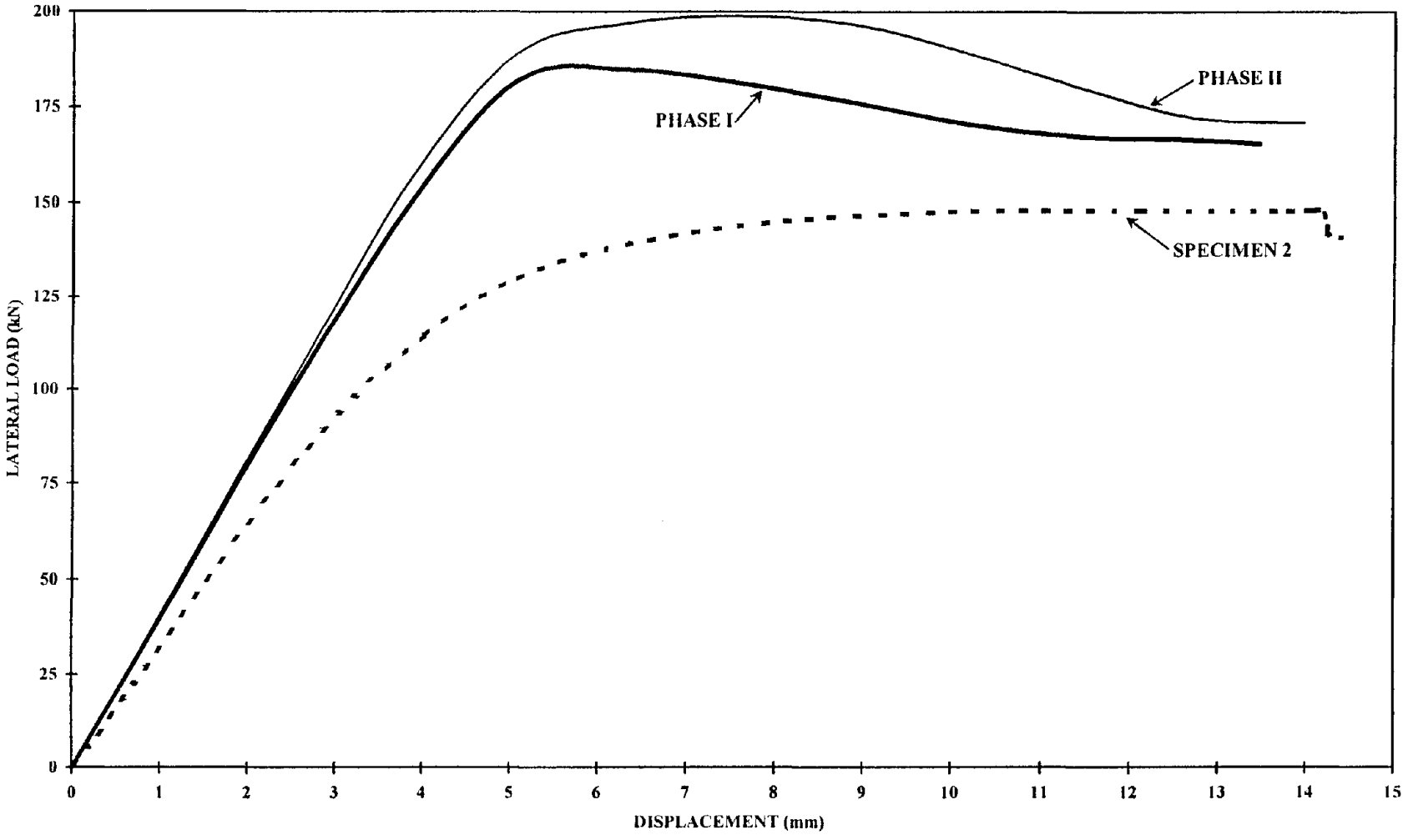

Figure 49. Beam-column specimen - pushover curves

The stiffness degradation seen in Figure 49 for Phase I and II was due to the yielding of the reinforcement in these elements. Even though the concrete compressive strength was higher for the latter case, these curves prove again (also see Table 6) that the stronger concrete had relatively small influence in the specimen's overall behavior.

5.2 Calculated joint shear forces and stresses

To calculate the horizontal and vertical shear forces in the joint region, the forces acting at the face of the column and the beam are reduced to tension-compression couples. This is illustrated in Figure 50a with all the forces at the joint. Figure 50b shows the resulting force couples. It can be seen that due to the horizontal reaction H_b acting on the beam, the forces T_b and C_b will not be identical.

In order to find these forces, the output from DRAIN-2DX was used. This output provided the strain at the outside faces, and the curvature for any given cross-section. Given these data, the strain values were found at the longitudinal reinforcement level in the beam and the column.

By multiplying the strain values with the elastic modulus and the area of the rebars, the forces could be calculated. The readings were taken at a lateral load level experienced during the tests for both phases, thus eliminating the influence of a stiff joint model. These values were also checked by hand-calculation, which required an iterative procedure.

Table 7 summarizes the bending moment, the shear and the axial compression values at the sections shown in Figure 50a. For each phase, the average maximum lateral load was taken into account for the baseline specimens. As the best representation of the

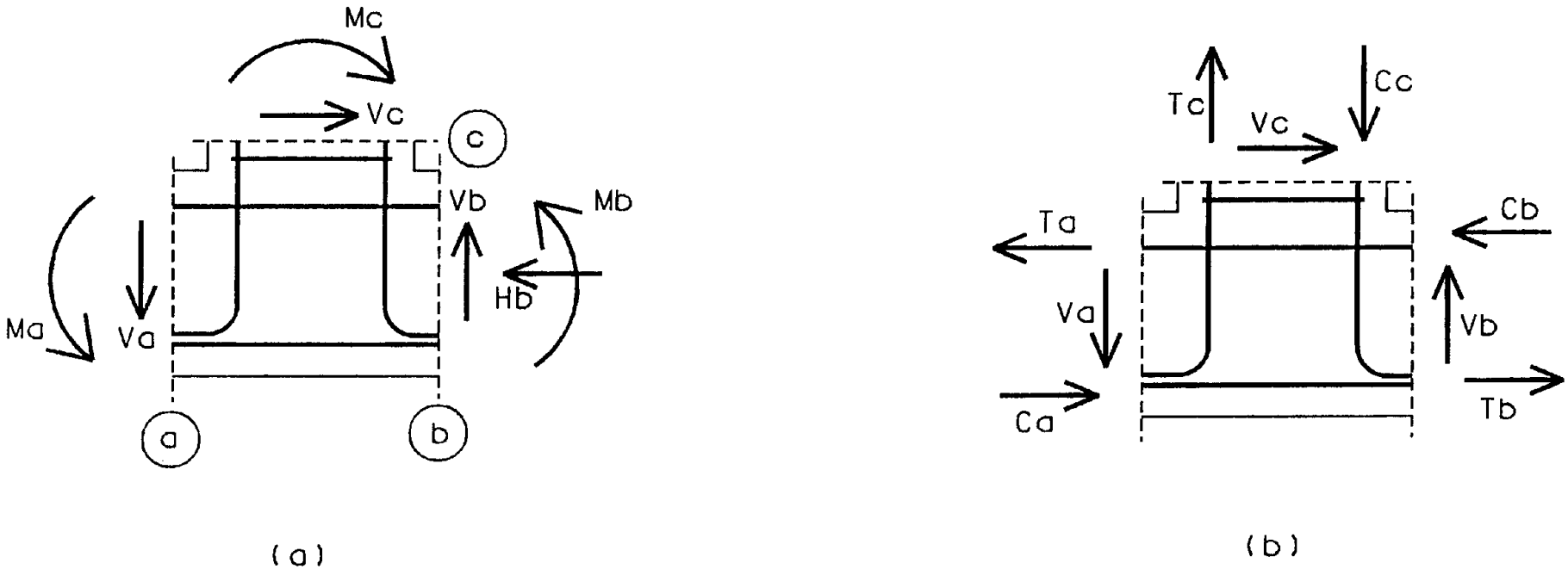

Figure 50. Bending, shear and axial forces at the joint (a), and the corresponding tension – compression couples (b)

Table 7. Bending moment, shear and axial load values for selected specimens

Phase (1)	Specimen Number (2)	Section a (Beam)		Section b (Beam)			Section c (Column)	
		M_a (kN-m) (3)	V_a (kN) (4)	M_b (kN-m) (5)	V_b (kN) (6)	H_b (kN) (7)	M_c (kN-m) (8)	V_c (kN) (9)
I	1 & 2 [1]	53	87	53	88	139	113	139
	9 [2]	79	129	79	129	206	168	206
II	10 & 11 [1]	51	84	51	84	134	109	134
	14 [2]	87	142	86	141	227	185	227

Notes: [1] Baseline specimens
[2] FRP reinforced specimens

FRP reinforced specimens, Specimen 9 was selected from Phase I, and Specimen 14 for the Phase II test series.

To calculate the compression forces C_i (see Figure 50b), the contribution of the reinforcement in the compression zone was also included with the concrete section. This was necessary due to the scale of the specimens, and the amount of reinforcement provided for the elements. In a larger section with several layers of intermediate rebars, this contribution could have been neglected (for example in the case of a bridge beam or a column).

The tension-compression couples calculated from the element forces are given in Table 8. To calculate the horizontal and vertical joint shear forces (given in columns 9 and 10 in Table 8), the following equations (derived from the force equilibrium relations shown in Figure 51) have been used:

$$V_{j,vert} = T_c - V_a \tag{5}$$

$$V_{j,horz} = C_a + T_b \tag{6}$$

where:

$V_{j,vert}$ – the joint vertical shear force;

T_c and V_a – the forces given in Tables 7 and 8;

$V_{j,horz}$ – the joint horizontal shear force;

C_a and T_b – the forces given in Tables 7 and 8.

Due to the low strain level in the concrete throughout the compression zone (the

Table 8. Calculated beam-column joint forces for selected specimens

Phase (1)	Specimen Number (2)	T_a (kN) (3)	C_a (kN) (4)	T_b (kN) (5)	C_b (kN) (6)	T_c (kN) (7)	C_c (kN) (8)	$V_{j,vert}$ (kN) (9)	$V_{j,horz}$ (kN) (10)
I	1 & 2 [1]	162	162	93	232	327	327	240	255
	9 [2]	243	243	140	346	487	487	358	382
II	10 & 11 [1]	154	154	87	221	347	347	263	241
	14 [2]	261	261	147	375	589	589	447	408

Notes: [1] Baseline specimens
[2] FRP reinforced specimens

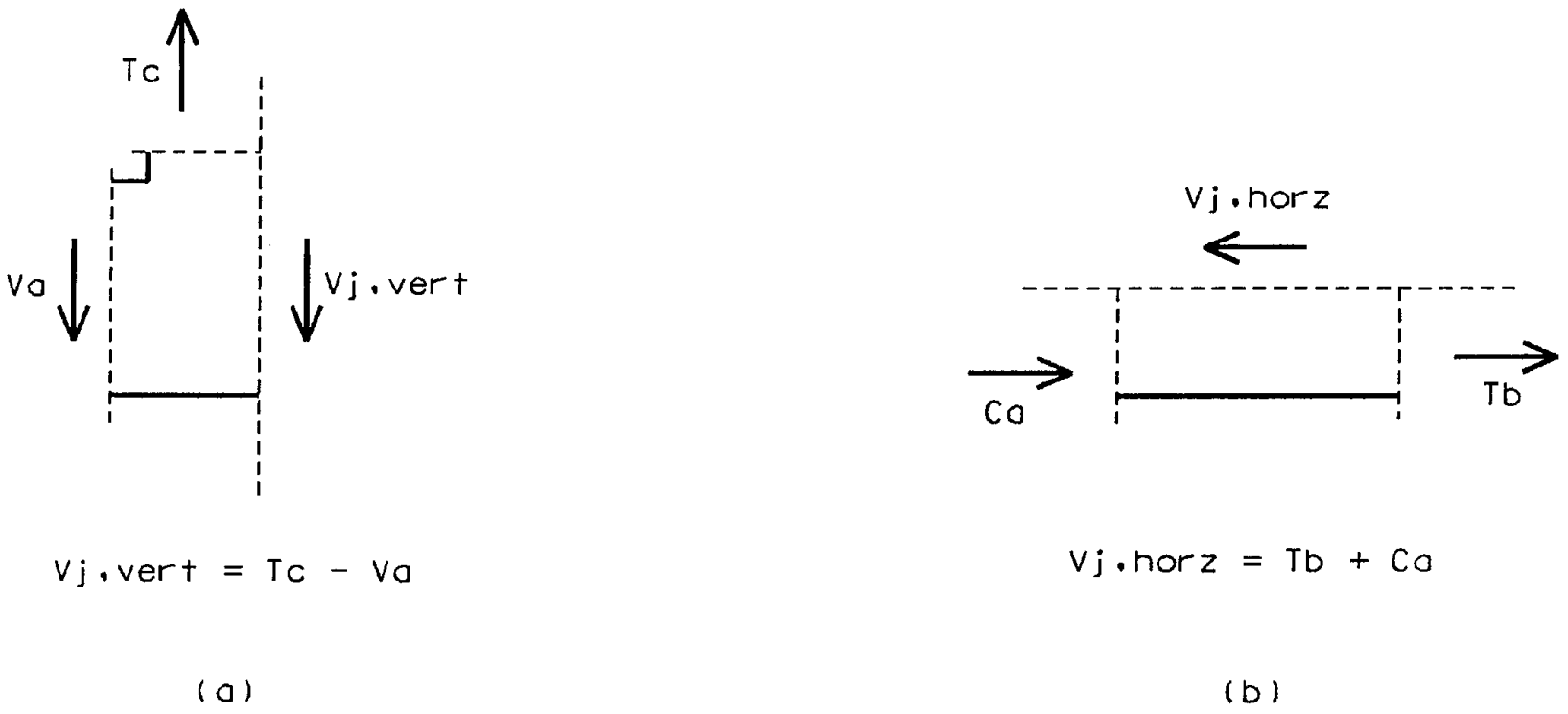

Figure 51. Calculation of joint vertical (a), and horizontal (b) shear forces

highest value was $\varepsilon_{c.max}$ = 834 με), the concrete can be estimated as a linear material. Thus, it can be assumed that the joint vertical and horizontal shear forces (within a certain phase) are proportional to the applied load, given the fact that there are no plastic hinges formed in the beams or the columns.

The shear stresses in the joint region can be calculated using the following formulas:

$$v_{j,vert} = \frac{V_{j,vert}}{h_b \times b_b} \tag{7}$$

$$v_{j,horz} = \frac{V_{j,horz}}{h_c \times b_c} \tag{8}$$

where:

$v_{j,vert}$ – the joint vertical shear stress;

$V_{j,vert}$ – the calculated vertical shear forces (using Equation (5));

h_b – the effective depth of the beam;

b_b – the effective width of the beam;

$v_{j,horz}$ – the joint horizontal shear stress;

$V_{j,horz}$ – the calculated horizontal shear forces (using Equation (6));

h_c – the effective depth of the column;

b_c – the effective width of the column.

In the case of the tested beam-column joint specimens, the effective width of the beam is the same as the effective width of the column (356 mm); and the effective depth of the beam is equal to the effective depth of the column (406 mm). But this is only true

for these specimens. If the dimensions of the columns are not identical to the dimensions of the beams, which is the case in most reinforced concrete structures (buildings or bridges), the effective dimensions used in Equations (7) and (8) should be evaluated according to the ACI 352 R-91 specifications.

The calculated joint shear stresses are given in Table 9 (columns 3 and 4). These stresses are only a fraction of the joint shear strength given in the ACI 352 R-91. The recommended values are calculated by Equation (9).

$$v_j = 0.083 \times \gamma \times \sqrt{f_c'} \tag{9}$$

where:

v_j – the nominal joint shear strength;

γ – the configuration parameter. The specimens tested classify as corner joint Type 1, for which no significant inelastic deformations are anticipated, and this parameter is given as 15.

f'_c – the concrete compressive strength (19.65 MPa and 33.92 MPa respectively).

The nominal joint shear strength calculated using Equation (9) is 5.52 MPa for the baseline specimens in Phase I and 7.25 MPa in Phase II. It is important to note that the recommended values do not include any external shear strengthening, they apply to newly designed and properly confined concrete joints.

Nilsson and Losberg (1976) performed several tests on typical beam-column joints subjected to bending moments. They found out that the performance of the T-joints tested was only 24 to 40% of what was expected. The reinforcement and the

Table 9. Calculated joint shear and diagonal tensile stresses for selected specimens

Phase (1)	Specimen Number (2)	Vertical Shear Stress - $v_{j,vert}$ (MPa) (3)	Horizontal Shear Stress - $v_{j,horz}$ (MPa) (4)	Diagonal Tensile Stress - σ_t (MPa) (5)	Ratio $\frac{\sigma_t}{\sqrt{f_c'}}$ (6)
I	1 & 2 [1]	1.66	1.76	1.71	0.39
	9 [2]	2.48	2.64	2.56	0.58
II	10 & 11 [1]	1.82	1.67	1.75	0.30
	14 [2]	3.09	2.82	2.96	0.51

Notes: [1] Baseline specimens
[2] FRP reinforced specimens

loading conditions were similar to the one in the present study, and the specimens in the present research showed a similar behavior. Lowes and Moehle (1995) came to the same conclusion for tests performed on reinforced concrete bridge T-joints.

So, why did the baseline specimens fail at approximately the third of the suggested design strength values? There are several reasons for this:

- Beam-column joints lacking horizontal shear reinforcement do not develop their full capacity. This is true if one assumes that the joint horizontal shear forces are taken by the column reinforcement passing through or properly anchored in the joint region.
- When the joint nominal principal tension stress reaches the tensile stress of the concrete, diagonal cracks will cause extensive damage in the joint region.
- T-joints having the column reinforcement bent away from the joint, do not provide adequate confinement for the concrete in the joint core. In addition, the tensile stresses in these bars and hooks, generate an inclined force pointing outward from the hooks and overload the beam at the tension zone. This effect created an unreasonably high stress in the beam longitudinal reinforcement.
- If the diameter of the reinforcement passing through the joint is high compared to the overall size of the beams and columns, the potential for bar slippage and reduction in bond stresses is very high.

Based on test results, Priestley et al. (1996) found that joint cracking can be expected when the joint nominal principal tension stress (σ_t) exceeds $0.29*\sqrt{f'_c}$. The nominal principal tension stress (or diagonal tensile stress) developed in the beam-column joint region can be evaluated by:

$$\sigma_t = \frac{\sigma_p}{2} + \sqrt{\frac{\sigma_p^2}{4} + v_j^2} \tag{10}$$

where:

σ_t – the calculated nominal principal tension stress or diagonal tensile stress;

σ_p – the axial compression stress in the joint (from axial load or prestress); for the specimens studied, this stress was negligible;

v_j – the equivalent joint shear stress, taken as the average of the joint horizontal and vertical shear stresses.

The calculated diagonal tensile stresses are summarized in Table 9 (column 5). The ratio of the diagonal tensile stress with respect to the concrete compressive strength is given (column 6 in the same table) to provide direct comparison with the tensile strength of the concrete.

For both phases, the baseline specimens failed at a tensile stress level slightly higher than the given strength values, even though the shear stresses were much lower than the expected values. This proves again, that the specimens failed due to excessive diagonal cracks caused by high diagonal tensile joint stresses.

5.3 Shear strengthening of beam-column joints

It is clear from Table 9 that the specimens reinforced by externally bonded CFRP sheets showed an improved shear capacity of the beam-column joints. In the majority of the repaired test specimens, a substantial strength loss was observed immediately after the composite sheets delaminated from the face of the joints. This delamination took

place within one load cycle, which suggests a rather brittle failure.

Table 10 provides a summary of the diagonal tensile stresses for all the beam-column joint specimens (see column 5). To identify the improvement made by applying the composite sheets, the increase over the baseline specimens (for each phase) is also included (column 6); and finally, the contribution of CFRP sheets is included as well (column 7). This contribution is calculated by multiplying the increase in diagonal tensile stress by the thickness of the composite sheets inclined in the same direction (1.32 mm per ply).

It can be seen from Table 4e that the contribution of one single layer on each beam face (Specimens 3, 5, 6 and 7) was rather inconsistent. It was not possible to compensate for any construction problems for these specimens. The poor redundancy for this setup was improved by applying the sheets based on a balanced and symmetrical pattern, when each beam face contained sheets in both directions.

By grouping the remaining specimens, a good correlation was observed for similar layouts and surface preparations. These groups are:

- Group A: Specimens 4 and 8 (no transverse layers around the column and the beam).
- Group B: Specimens 9, 12 and 13 (with transverse layers and wire brushed surfaces).
- Group C: Specimen 14 (with transverse layers and water jetted surfaces).

As it was expected, the third group showed the highest improvement, and the first group provided the least increase in the joint shear/diagonal tensile stresses. Furthermore, the measured average strains in the composite layers were very small (in the range of 0.1% to 0.3%), and represent only a fraction of the ultimate tensile strain (1.0%). This implies that these layers loose effectiveness by early delamination from the

Table 10. Beam-column joint performance

Phase (1)	Specimen (2)	CRFP Layout[3] (3)	Surface Preparation (4)	Diagonal Tensile Stress (MPa) (5)	Increase in σ_t (MPa) (6)	Contribution of CFRP (MPa × mm) (7)
I	1 & 2[1]	N/A	N/A	1.71	0	N/A
	3	[45]	Wire Brush	2.04	0.33	0.44
	4	[±45]	Wire Brush	2.36	0.65	1.72
	5	[45]	Wire Brush	1.99	0.28	0.37
	6	[45]	Wire Brush	1.88	0.17	0.22
	7	[45]	Wire Brush	1.89	0.18	0.24
	8	[±45]	Wire Brush	2.36	0.62	1.64
	9	[±45]	Wire Brush	2.56	0.85	2.25
II	10 & 11[1]	N/A	N/A	1.75	0	N/A
	12	[±45]	Wire Brush	2.59	0.84	2.22
	13	[±45]	Wire Brush	2.58	0.83	2.19
	14	[±45]	Water Jet[2]	2.96	1.21	3.20

Note: [1] Baseline specimens
[2] Water jet and Sykadur 31
[3] CFRP layout on each vertical face of the beam (see Chapter 3 for more details)

concrete surface, rather than by reaching their tensile capacity.

By looking at the results from Table 10, one recommendation for the design of the CFRP sheets used to increase the joint shear capacity, is to include the transverse layers around the beams, and to specify a minimum surface preparation. Therefore, only the results from the Group B (Specimens 4 and 8) and the Group C (Specimens 9, 12 and 13) will be used to develop a design equation for the external composite application in the joint region. It is clear from the results that by water jetting the concrete specimens and by using a high strength adhesive (e.g., Sikadur 31), a 50% increase in strength was observed from the present study.

Because the axial loads in the joint region are negligible, the diagonal tensile stresses are approximately equal to the joint horizontal and vertical shear stresses. The diagonal tensile stresses however, are proportional to the axial strains developed in the CFRP sheets. So the relationship between the increase in the joint shear forces/stresses and composite properties can be expressed as:

$$V_f = n \times t \times \varepsilon_f \times E_f \times d_c \times (\sin\beta / \cos\beta) \qquad (11)$$

where:

V_f – the increase in the joint shear force provided by the CFRP sheets, in kN;

n – the total number of composite layers inclined by the same angle β with respect to the member's longitudinal axis;

t – the calculated thickness of the composite sheets, in m (see Equation (1);

ε_f – the average axial strain in the fiber direction at the peak horizontal load

calculated for each group, in mm/mm;

E_f – the elastic modulus of the composite material, in kPa (see Table 3);

d_e – the effective joint depth, in m (see Figure 52). From previous studies it has been found that the development length of the composite sheets bonded to concrete is approximately 51 mm. Thus, the effective joint depth represents the height of the joint minus twice the development length.

β - the angle between the orientation of fibers and the member's longitudinal axis.

For the two groups considered, the shear force provided by the CFRP sheets are:

$$V_f^{II} = 2 \times 0.00132 \times 0.0021 \times 64{,}730{,}000 \times 0.305 \times (\sin 45^0 / \cos 45^0) = 109kN \qquad (12)$$

for the Group B, and for Group C:

$$V_f^{III} = 2 \times 0.00132 \times 0.0033 \times 64{,}730{,}000 \times 0.305 \times (\sin 45^0 / \cos 45^0) = 172kN \qquad (13)$$

The shear forces calculated using Equations (12) and (13) however, represent an increase in the joint shear stress of 0.76 MPa for Group B, and 1.18 MPa for Group C. These shear stresses are slightly lower then the observed values given in Table 10, which might be due to an overestimated development length. The most effective composite inclination in the joint region for these T-joints is a $\pm 45^0$, parallel to the principal planes.

So far only the diagonal tension was considered in the previous analysis. Although the diagonal compression had the same magnitude as the diagonal tension, Equation (11) did not include any composite layer in compression. The reason is, that the

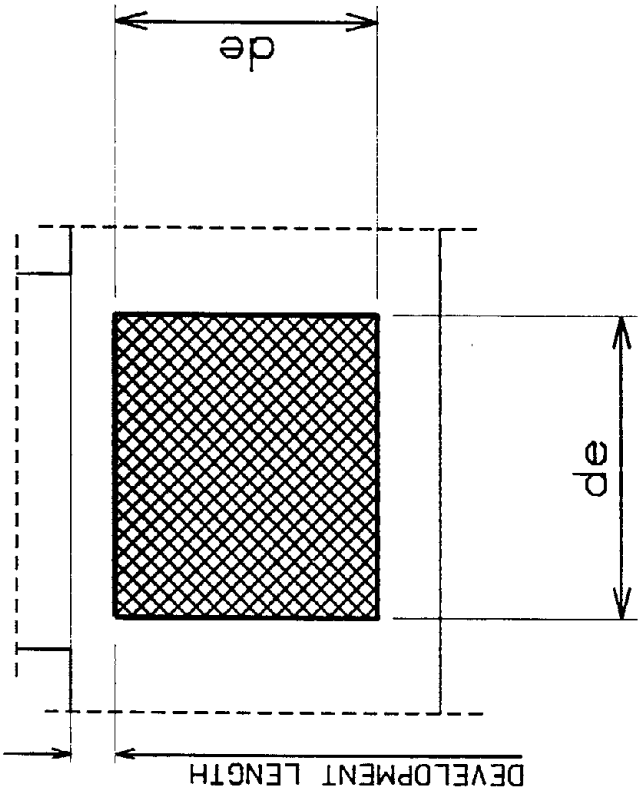

Figure 52. Definition of effective depth for a square joint

concrete compressive strength is substantially higher than its tensile strength, so the concrete was capable of taking the compressive forces. Therefore, the composite compressive stresses were negligible. This was also observed by looking at the compressive strain values recorded during the tests. In general, there were no negative strains (for compression) observed on the composite sheets.

CHAPTER 6

REPAIR OF BRIDGE PIER WITH CFRP

In addition to the beam-column joint tests, the application of carbon fiber reinforced plastics for a bridge bent was also performed. The application included the analysis and testing of a bent in the existing condition (Bent #5), design and application of composite for a similar bent, and the testing of the repaired bent (Bent #6).

The bridge was designed and built in the early 1960s. As part of the Interstate-15 reconstruction project, the I-15 bridges along the Wasatch front were demolished and replaced with a new freeway system. This provided an opportunity to test two bridge bents of the old system. These reinforced concrete bents presented several deficiencies, among those, the seismic and corrosion related problems were the most serious. Designed over 30 years ago, the structure was missing the basic reinforcement necessary to provide adequate lateral load capacity.

6.1 Analysis and testing of Bent #5

6.1.1 Pushover analysis of the bent

By providing analytical results for the bent, an estimate of the peak lateral load and the maximum horizontal displacement were identified. It was found that the existing pile anchorage would not provide adequate uplift capacity for the foundation system.

The yielding sequence of the structural members was observed, and post-yield member forces were calculated. All of the information is necessary for the design of the repair, and these are the only data available for an everyday retrofit project.

The same program as for the T-joint specimens was used to perform the pushover analysis. To construct the 2-D model of the structure, the existing conditions had to evaluated and compared with the original design plans. The bent general dimensions are shown in Figure 53, including the reinforcement details. The important sections of the columns and the cap beam are shown in Figure 54. It can be seen from these plans that the column transverse reinforcement is inadequate in the lap-splice region, and the anchorage of the longitudinal rebars is insufficient.

The design plans specified an embedment of 305 mm for the piles into the pile cap. However, from the experience of other bridges built at the same time and already demolished, it was decided to improve the tensile capacity of the piles. This was achieved be coring a 38 mm hole through the pile cap and 1524 mm into the piles, and by inserting a dywidag anchored with epoxy.

It was assumed that this support condition is not fixed and is not pinned either. So the tension-compression resistance of the piles was modeled using axial spring elements. The location of these elements corresponded with the piles, and the spring constant values were estimated based on the axial stiffness of the dwydag bar-pile system.

After running the program with several stiffness values (ranging from pinned to fixed support conditions), it was obvious, that these values have a great influence in the outcome of the analysis. After testing Bent #5, based on the maximum observed pile cap

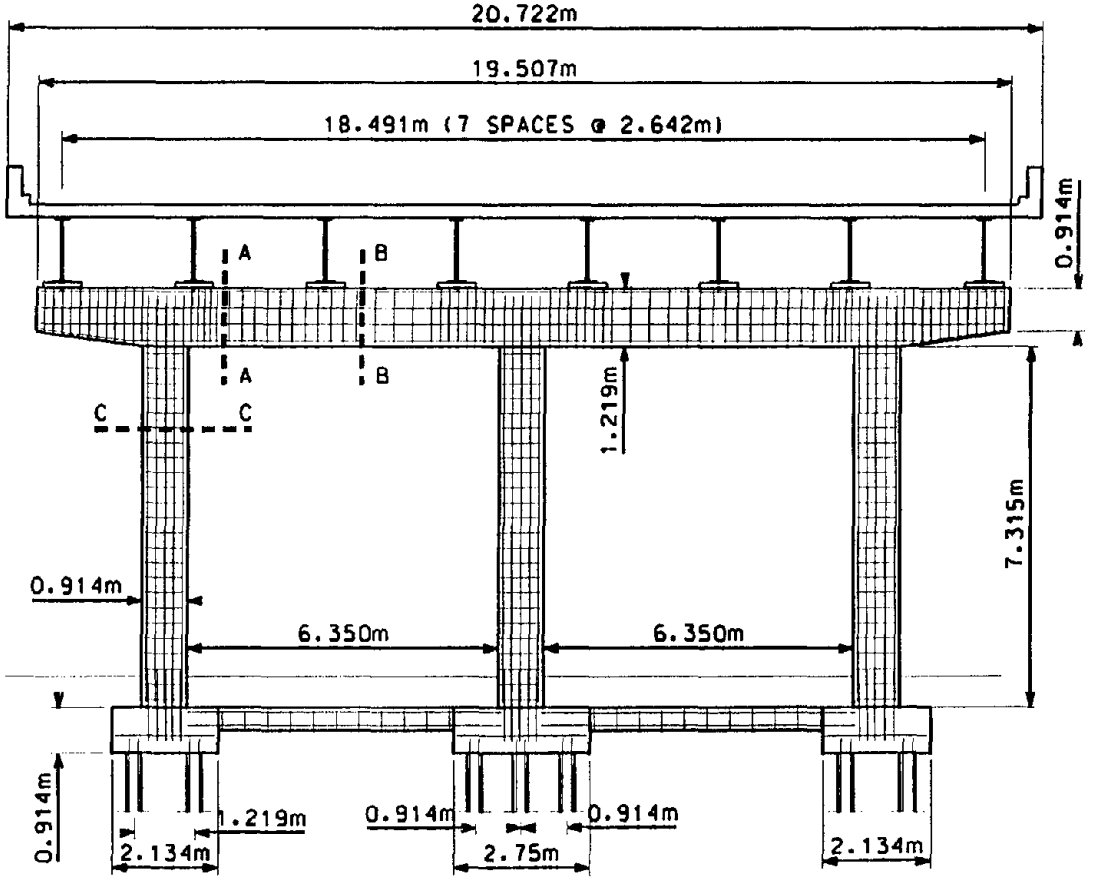

Figure 53. I-15 Bridge bent dimensions and reinforcement

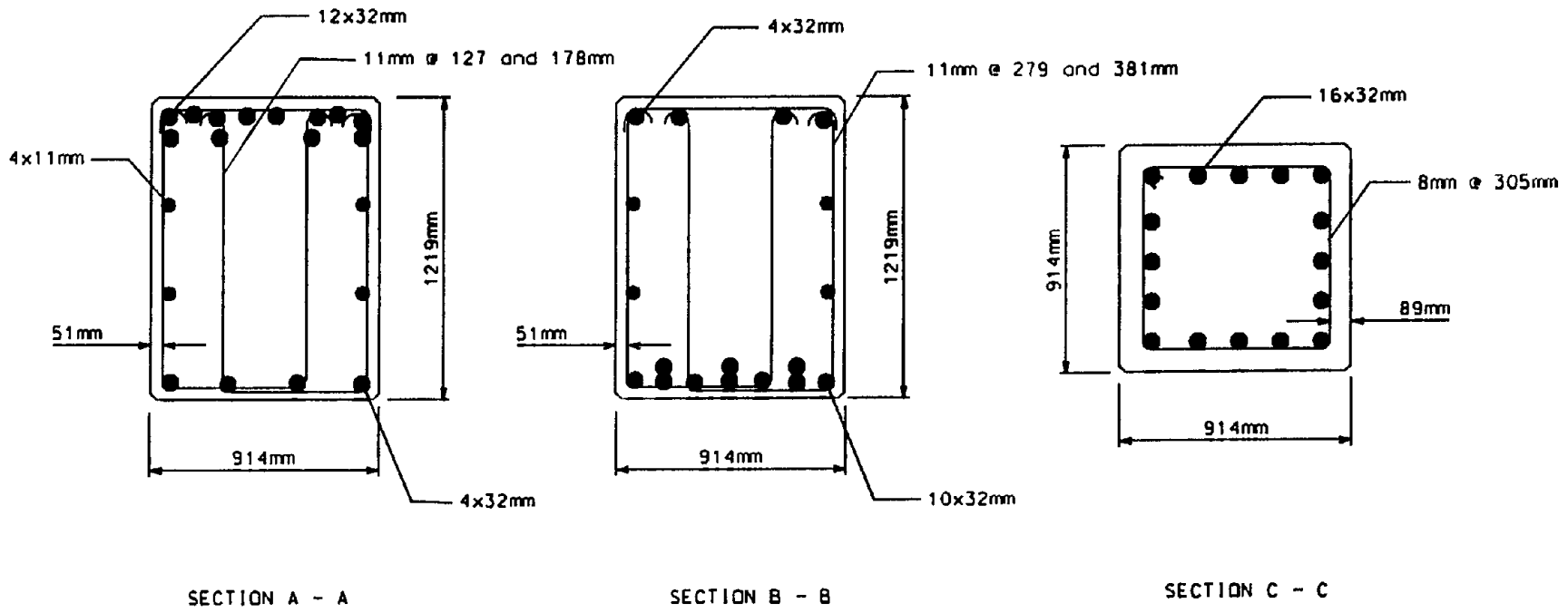

Figure 54. Beam cap and column sections from Figure 53

movement (3.8 mm), the input stiffness values (K_1 and K_2) have been calibrated to provide a more realistic model.

The loading conditions are shown in Figure 55. The reaction frame was positioned between the south-bound (still in use) and the north-bound bridges. The horizontal load was applied at the cap beam level. To pull on the bent, the load was transferred to the other end of the bent by twenty prestress tendons. The lateral load capacity of the piles was smaller than the anticipated value, so dywidag bars were run between the footing of the reaction frame, and the outside pile cap. Thus, the horizontal load was kept in the bent-frame system, and the horizontal movement at the pile cap level was prevented.

To simulate the existing conditions as much as possible, the deck system between the two tested bents was kept in place. Therefore, half of the original dead load was acting on each bent. This dead load is transmitted to the cap beam by welded plate girders, sitting on eight reinforced concrete pedestals. The weight of the deck including the cap beam distributed to eight nodes was 240 kN per node. The weight of the columns (144 kN each) was included as concentrated loads at the bottom of the columns.

The majority of the concrete cover on the cap beam was loose and was removed; therefore, in the model, the outside 50 mm concrete was not included. The specified concrete strength was 20.68 MPa, and the yield strength of the longitudinal and the transverse reinforcement was given as 275.79 MPa.

Figure 56 shows the model of the bridge bent, including the location of the elements, the gravity and horizontal loads, and the boundary conditions. The basic procedure to build this model was similar to the one followed for the joint specimens. As

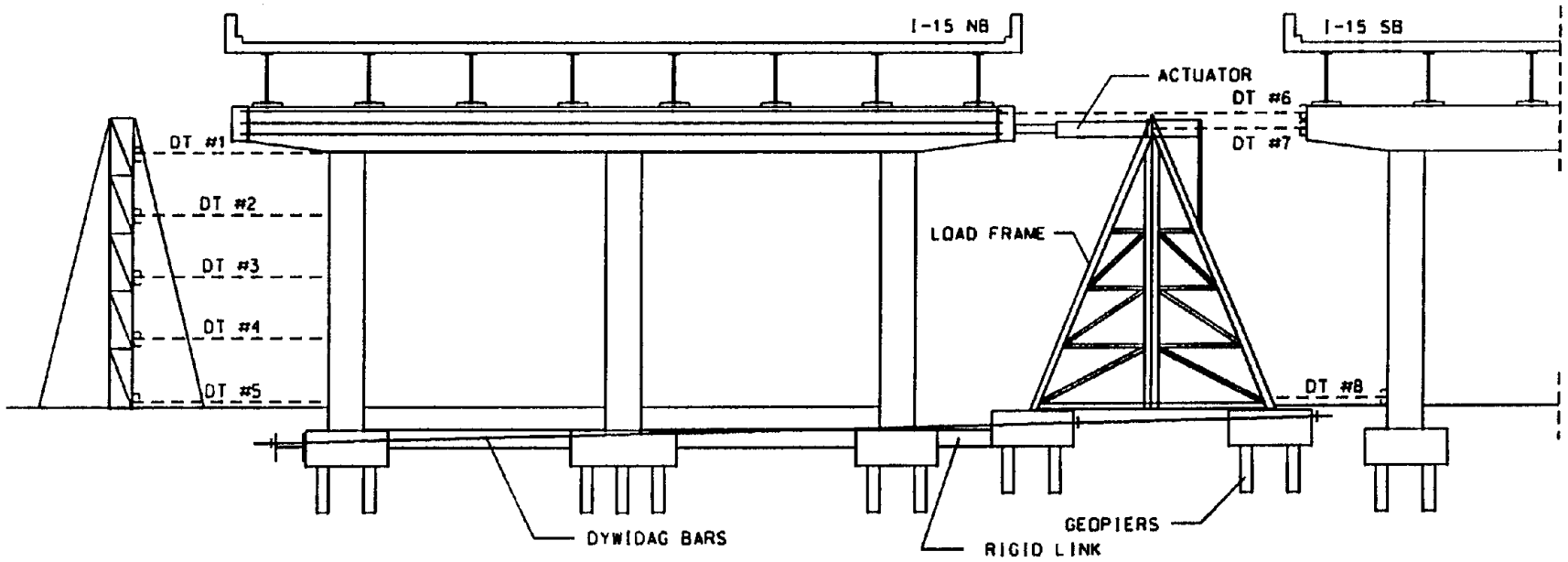

Figure 55. Loading conditions and locations of displacement transducers

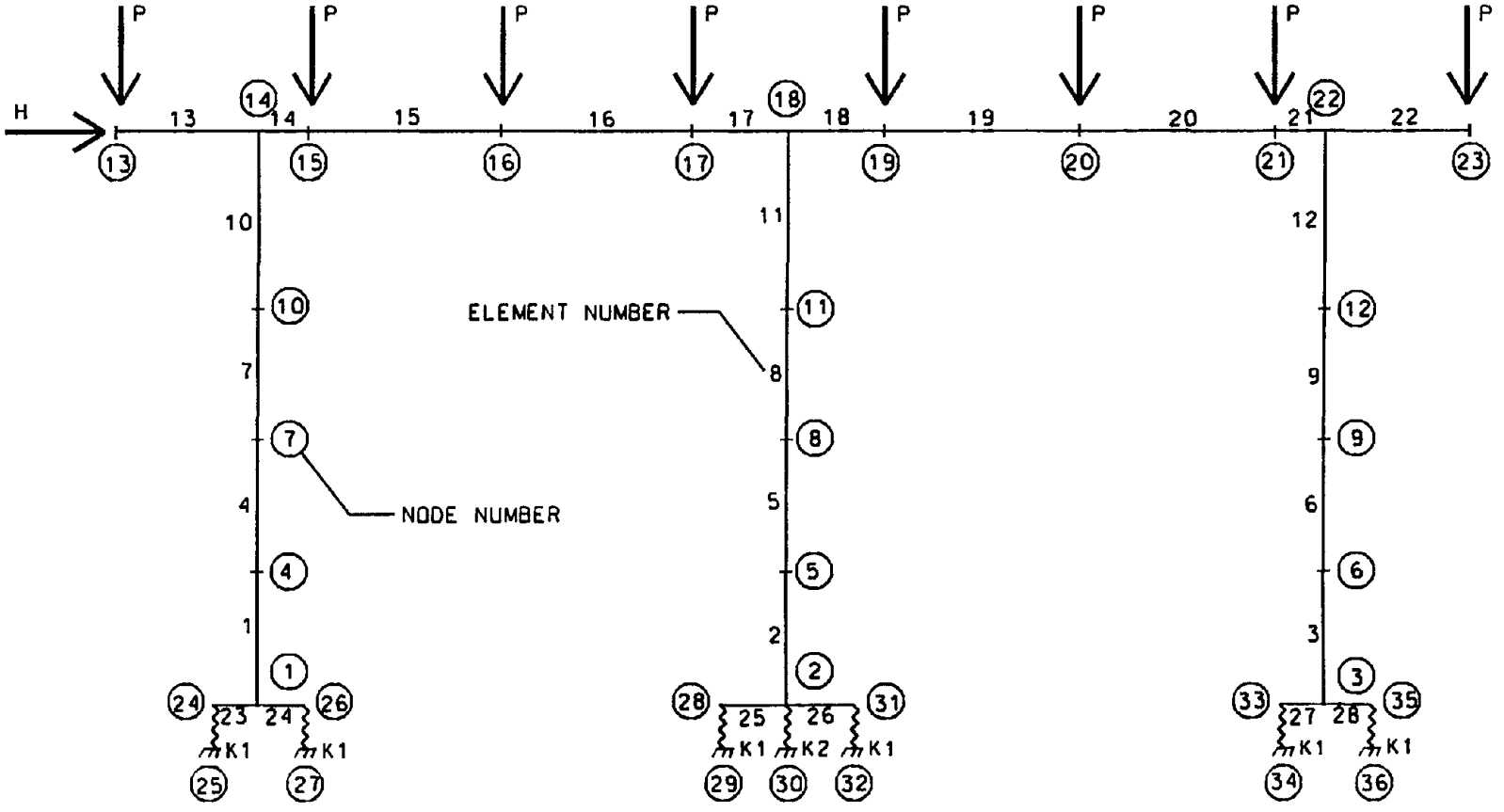

Figure 56. Two-dimensional model of I-15 bridge bent

it was mentioned earlier, the lateral movement was prevented at the level of the pile caps (nodes 1, 2 and 3), and the supports were modeled as springs with axial stiffness only. The input file for the DRAIN-2DX program is listed in Appendix B for further reference.

After performing the test it was observed that the analytical model overestimated the peak lateral capacity. Calibrating the spring constants solved the first problem, as it was described earlier (see Figure 57 for the effect of the support conditions). The early models of the bent had only one single element for the entire column section. This coarse meshing provided an unreasonably stiff column. Dividing the column into four elements solved the second problem.

The pushover curve for the bridge bent in the as-is condition is shown in Figure 58. The magnitude of the peak lateral force was 1552 kN, after which, the load decreased gradually. The first yielding occurred at the top section of the middle column at a displacement of 30 mm, and a horizontal load of 876 kN. A total of seven elements yielded in the sequence shown in Figure 59. It is clear from this figure that a mechanism has been formed, and with the extension of the plastic hinge region, the structure could not take additional horizontal load.

As it was mentioned earlier, the procedure outlined in Section 5.2 is valid for joints with small axial stresses. However, in the present case, by applying the horizontal load, larger axial loads are generated in the joints. To illustrate the solution in these cases, one bridge bent joint will be analyzed.

Figure 60a shows the interior joint of the bent with the member forces at the peak lateral load. Only the values for the horizontal axial forces are shown, which are 1074 kN at the left face of the joint, and 553 kN at the right face. This condition is equivalent

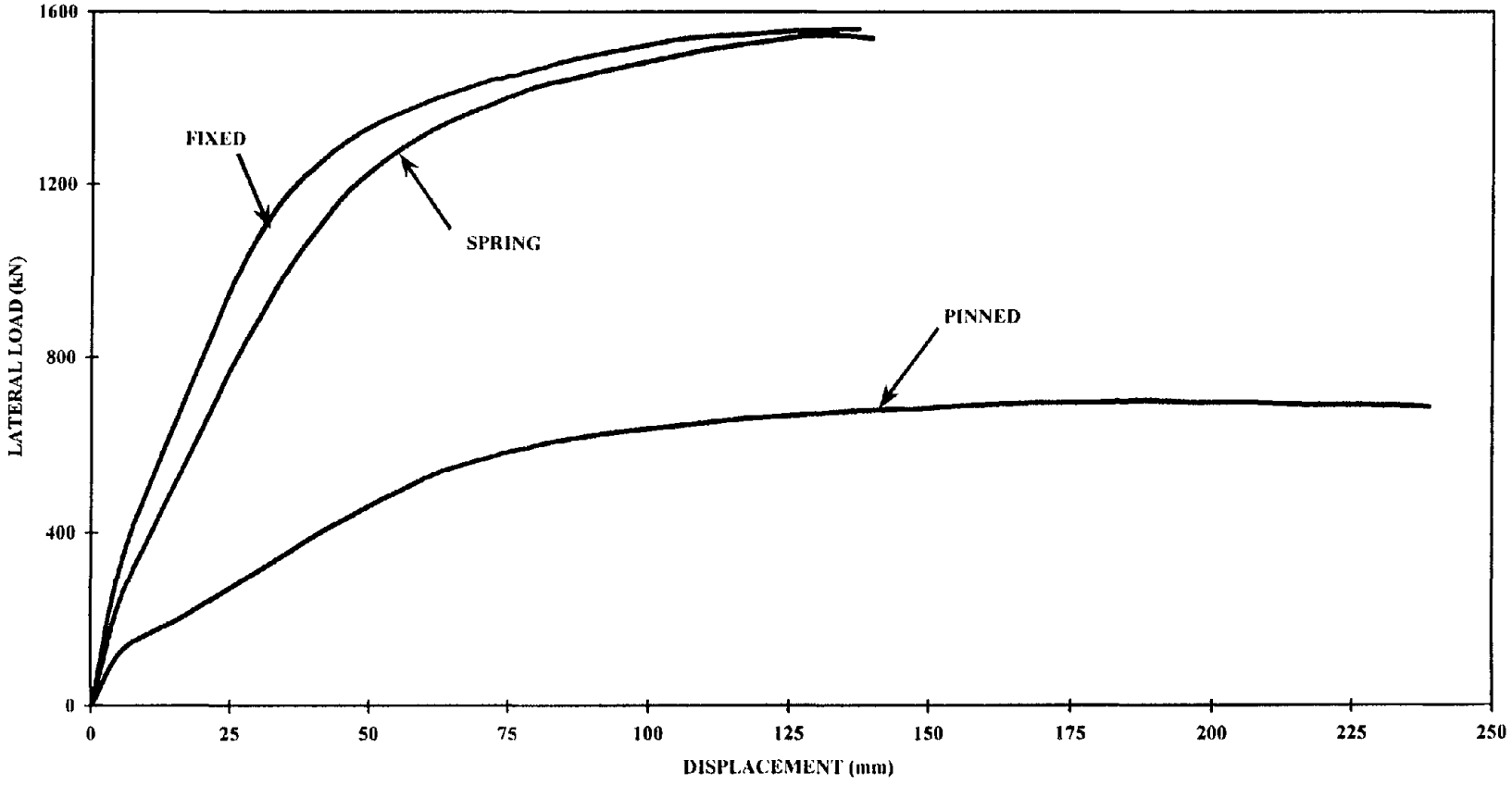

Figure 57. Load vs. displacement for Bent #5 for different support conditions

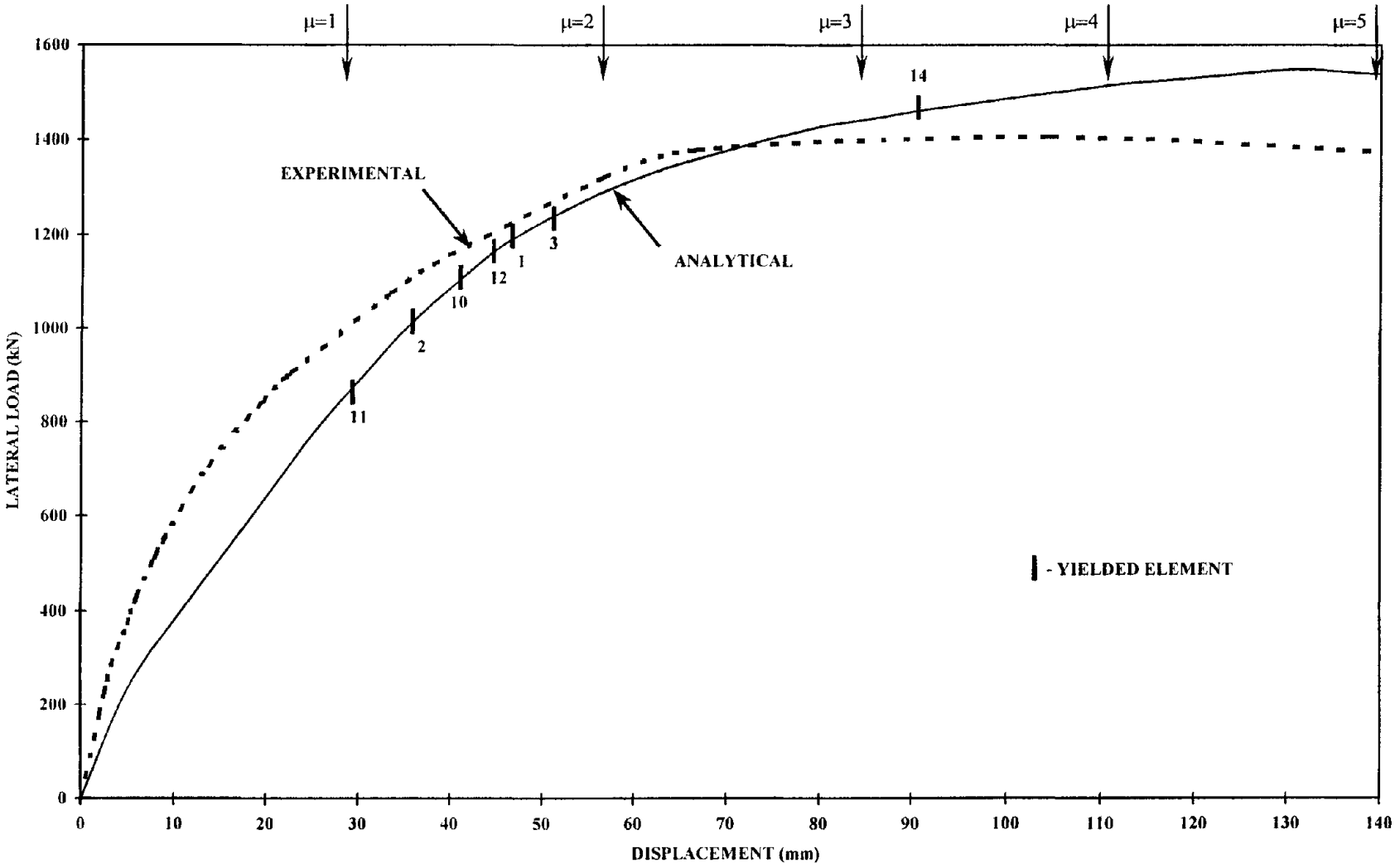

Figure 58. I-15 Bent #5 pushover curves

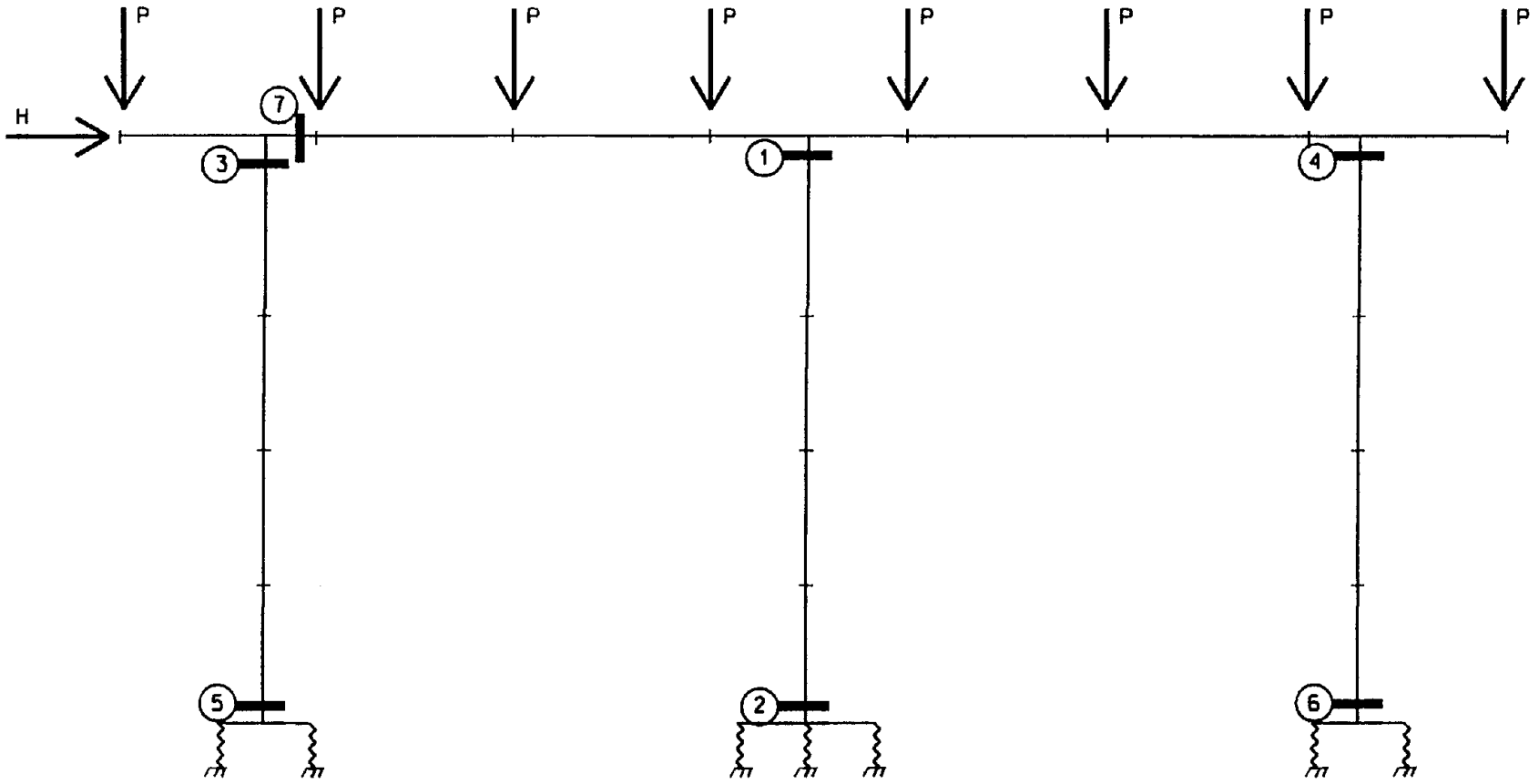

Figure 59. Yielding sequence of the I-15 Bridge bent in the as - is condition

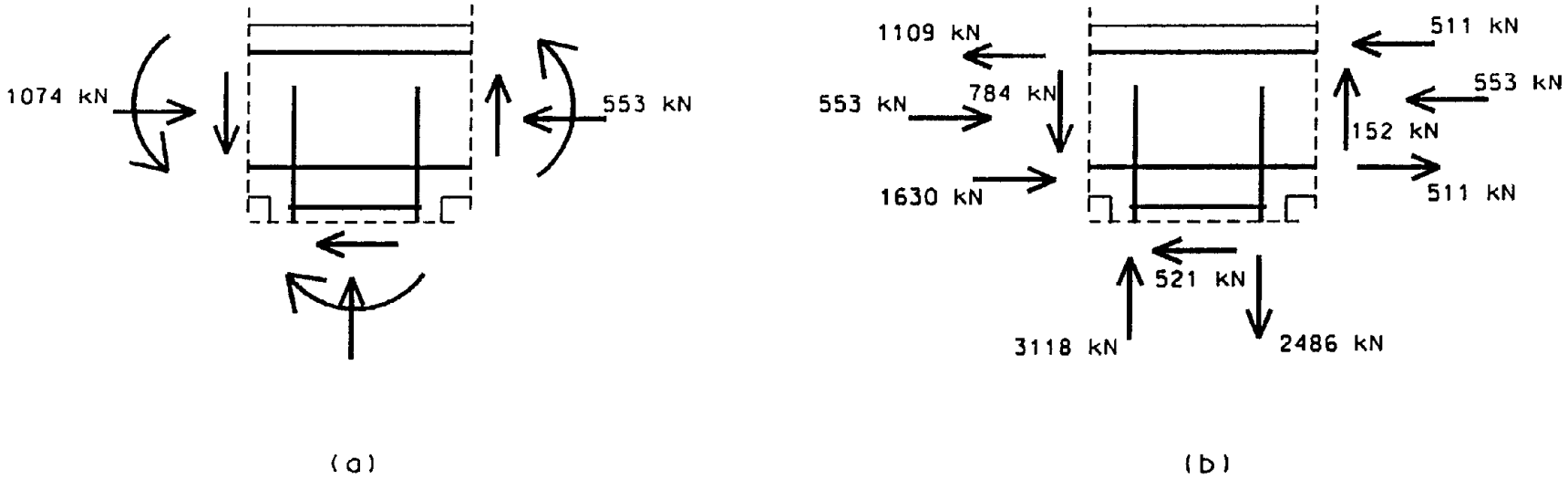

Figure 60. Member forces at the I-15 Bridge bent interior joint (a), and the corresponding tension-compression couples (b)

to a 553 kN force applied to both sides (as a posttensioning force) and an additional 521 kN applied to the left side. The procedure from here is the same as it was described in Chapter 5. The resulting tension-compression couples are shown in Figure 60b.

To calculate the joint shear stresses, the depth of the member minus the concrete cover to the tensile reinforcement was used. The calculated shear forces and stresses in the middle joint are:

- the horizontal joint shear force is $V_{j,horz}$ = 1620 kN, and the horizontal joint shear stress is $v_{j,horz}$ = 2.22 MPa ;
- the vertical joint shear force is $V_{j,vert}$ = 2334 kN, and the corresponding vertical joint shear stress is $v_{j,vert}$ = 2.24 MPa;
- the joint compression stress resulted from the 553 kN axial force is σ_p = - 0.53 MPa (negative for compression).

The joint shear stresses are approximately a third of the nominal joint shear strength recommended by ACI 352 R-91 (5.66 MPa), and given by Equation (9). To calculate the principal tension and compression stresses, Equation (10) was used.

$$\sigma_t = \frac{-0.53}{2} + \sqrt{\frac{(-0.53)^2}{4} + 2.23^2} = 1.98MPa \tag{14}$$

$$\sigma_c = \frac{-0.53}{2} - \sqrt{\frac{(-0.53)^2}{4} + 2.23^2} = -2.51MPa \tag{15}$$

It can be seen from these values that the principal planes will not be at 45^0 from the horizontal plane. Due to the introduced axial compression stresses, the angle of the

principal planes will be 41.6^0. So the orientation of the principal tensile stresses is at 48.4^0, measured clockwise from the horizontal axis.

6.1.2 Testing of the bent in the as-is condition

In order to monitor the behavior of the structure during the test, strain gages, displacement transducers, LVDT-s, and a load cell was used. The location of the most important instruments is shown in Figures 55 and 61. The data acquisition system and the description of these instruments are given in Chapter 3.

To test the bent, a horizontal cyclic load was applied at the cap beam level. In the first part of the test, a force-controlled test was performed with increasing load steps (starting at 180 kN). In each load step, the load was applied for three cycles, and each cycle had a push and a pull segment. After the first yielding had occurred, the test was performed by controlling the lateral displacement. The displacement was increased by a fraction of the yield displacement. The displacement ductility of the beam-column joint specimen was calculated using Equation (16):

$$\mu_\Delta = \frac{\Delta_u}{\Delta_y} \tag{16}$$

where:

μ_Δ - displacement ductility;

Δ_u - ultimate displacement;

Δ_y - yield displacement.

The load-displacement curve for Bent #5 is given in Figure 62. Yielding of the

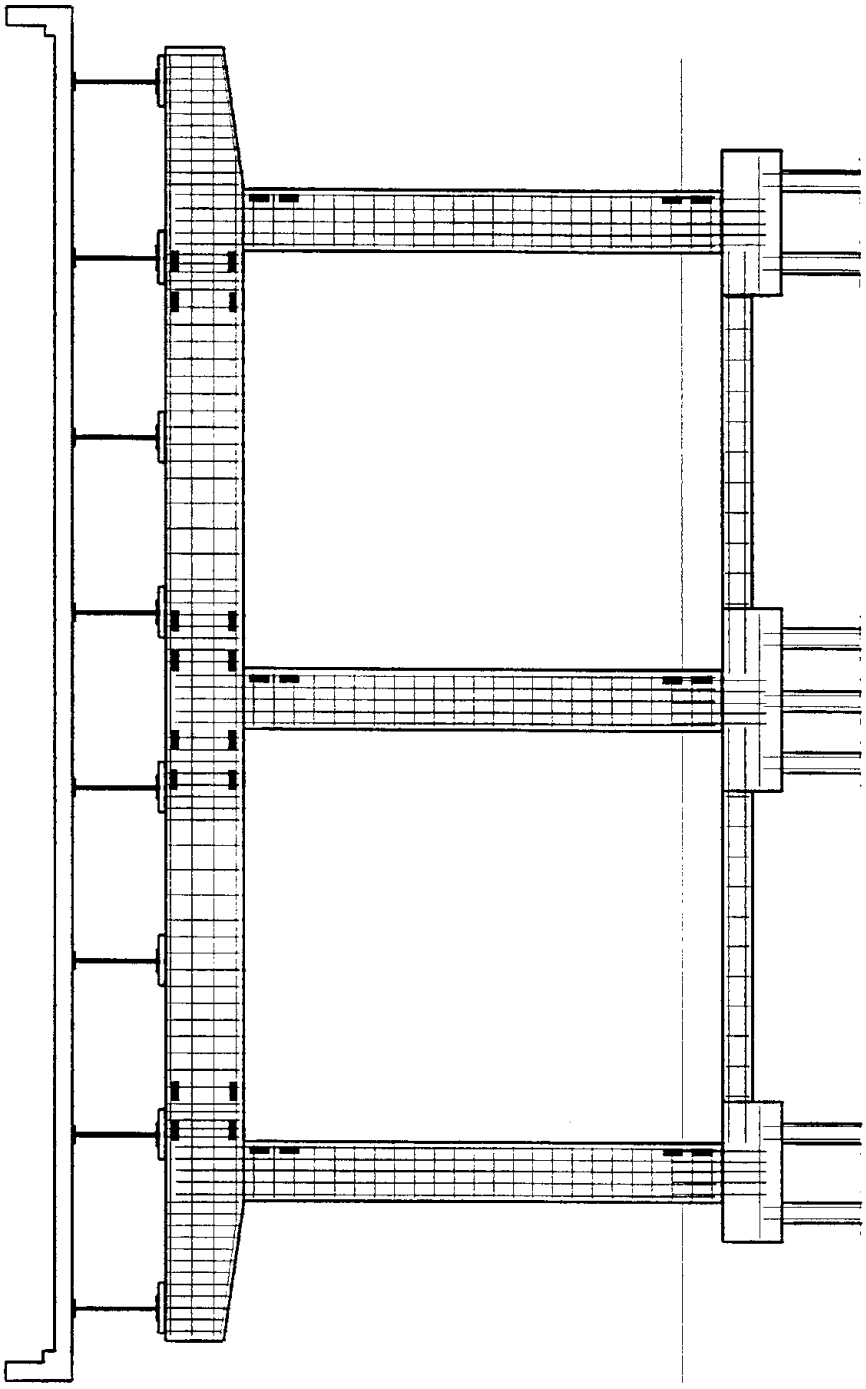

Figure 61. Location of strain gages for I-15 Bridge bent

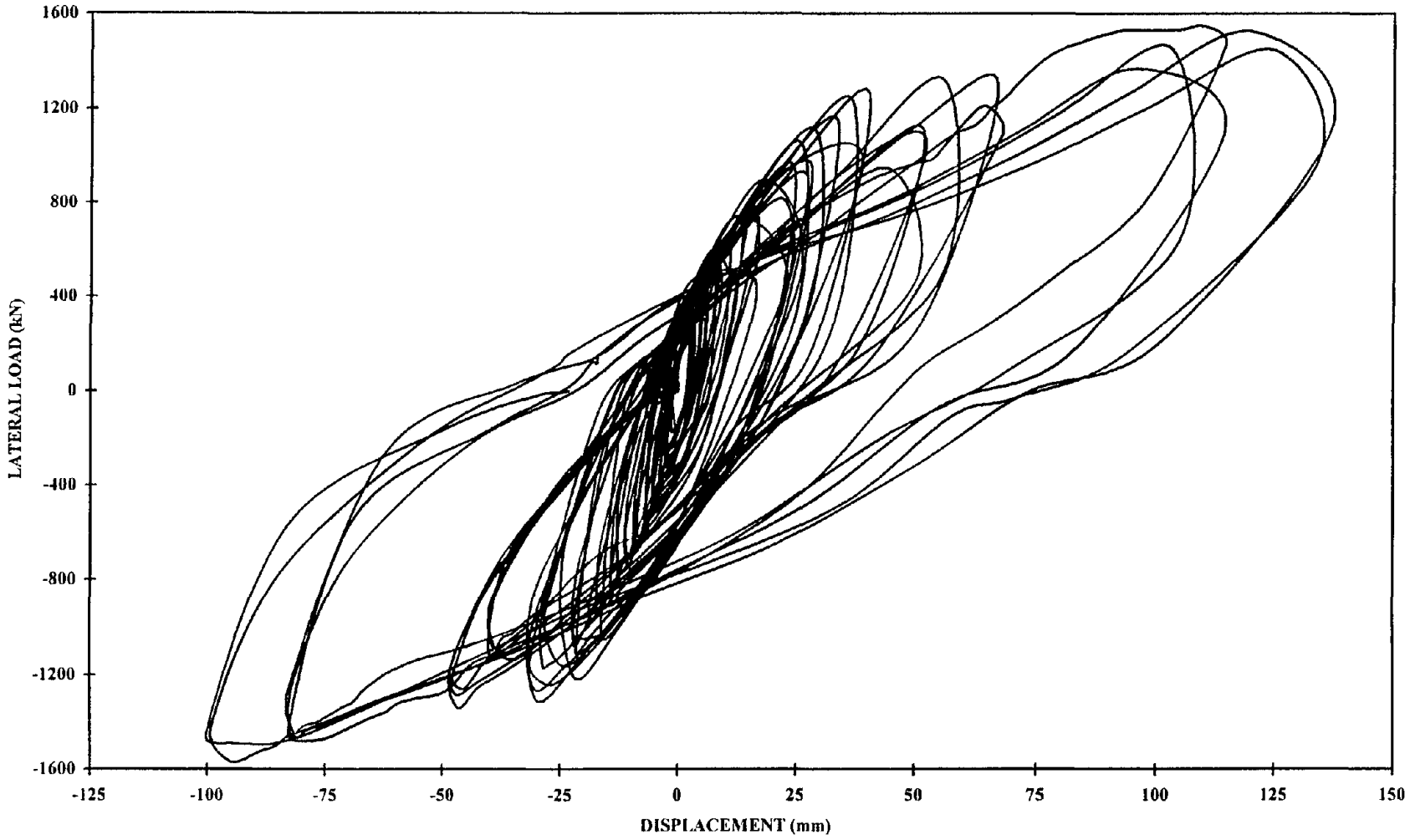

Figure 62. I-15 Bent #5 test - load vs. displacement

structure occurred at a lateral displacement of 29 mm, corresponding to a lateral load of 801 kN. These values are close to the analytical results described in the previous section. Using Equation (16), the ductility of the system at the end of the test was found to be 5.0.

To draw the "backbone curve," the FEMA 273 (1997) guidelines were followed, which specifies data reduction for experimental data: "A smooth backbone curve should be drawn through the intersection of the first cycle curve for the (i)th deformation step with the second cycle curve of the (i-1)th deformation step, for all i steps."

The envelope of the load-displacement curve with the analytical pushover curve is drawn in Figure 58. There is a good similarity between these results. The experimental backbone curve shows a higher initial stiffness, but the peak loads are within 10%.

The location of the plastic hinges was identical to the analytical results given in Figure 58. The similarity between analysis and experiment in the load-displacement curves and in the location of plastic hinges proves that with a well-defined member stiffness and boundary conditions, a reliable model can be built. Based on this model, a performance based design for the retrofit could be performed.

Plastic hinges formed at the base and the top of the column, and in the cap beam at one location. This behavior was different from the one desired by current practice. Due to the difficulties presented by the repair of the column base after a major earthquake, today's design allows for development of plastic hinges only at the top of the column. This fact prompts the designer of a bridge retrofit to pay special attention to the condition of the column base, and to the connection of pile cap with the pile system.

Flexural cracks developed at the top of the columns, and these cracks opened as

the bending capacity of these elements was reached. Significant diagonal tension cracks formed in the column-cap beam joint region, showing a gradual joint degradation. After the test, the loose concrete was removed from the joint, and it was apparent that there was not much left from the outside 100 to 150 mm layer. Even the first layer of the column longitudinal reinforcement extended into the joint was exposed, suggesting bar slippage and the loss of reinforcement anchorage.

6.2 Design of CFRP application for Bent #6

From the analytical results it was concluded that the bridge bent has deficiencies in the following areas: the confinement of the column lap splice region, the confinement of the plastic hinges, the shear in the joint region, and the anchorage of the column longitudinal reinforcement into the cap beam. To address all these problems, each element was analyzed, and the structural retrofit using CFRP was specified.

The design of the composite layout followed the equations for beam-column joints developed in the present study and modified to account for the presence of axial stresses in the joint, and the guidelines developed by Seible et al. (1995) for rectangular sections.

6.2.1 Flexural plastic hinge confinement for the columns

To confine the plastic hinge region, the composite layout was designed as a square jacket with twice the CFRP thickness required for the equivalent circular jacket with the effective diameter D_e calculated using Equation (17):

$$D_e = R_1 + R_3 = 646 + 646 = 1292mm \tag{17}$$

where R_1 and R_3 are evaluated using the following expressions:

$$R_1 = \frac{b^2}{a} = \frac{646^2}{646} = 646mm \tag{18}$$

$$R_3 = \frac{a^2}{b} = \frac{646^2}{646} = 646mm \tag{19}$$

with a and b defined using the dimensions of the column:

$$k = \left(\frac{A}{B}\right)^{2/3} = \left(\frac{914}{914}\right)^{2/3} = 1.00 \tag{20}$$

$$b = \sqrt{\left(\frac{A}{2k}\right)^2 + \left(\frac{B}{2}\right)^2} = \sqrt{\left(\frac{914}{2\times 1.00}\right)^2 + \left(\frac{914}{2}\right)^2} = 646mm \tag{21}$$

$$a = kb = 1.00 \times 646 = 646mm \tag{22}$$

The thickness of the composite layers is calculated using Equation (23):

$$t_j = 2\times 0.1\frac{D_e(\varepsilon_{cu} - 0.004)f_{cc}'}{f_{ju}\varepsilon_{ju}} = 2\times 0.1\frac{1292\times(0.0065 - 0.004)\times 24.13}{628\times 0.01} = 2.48mm \tag{23}$$

where:

D_e – the effective diameter calculated by Equation (17);

ε_{cu} – the required ultimate concrete strain;

f'_{cc} – the compressive strength of confined concrete;

f_{ju} – the ultimate composite strength evaluated in Chapter 2;

ε_{ju} – the ultimate composite strain evaluated in Chapter 2.

6.2.2 Lap splice clamping for the columns

Similar to the design of the confining layers, the thickness of the composite required for clamping the lap splice region will be determined based on an equivalent circular jacket and multiplied by two. The lateral clamping pressure can be defined as:

$$f_l = \frac{A_s f_y}{\left[\frac{p}{2n} + 2(d_b + cc)\right] L_c} = \frac{819 \times 275}{\left[\frac{2 \times (648 + 648)}{2 \times 16} + 2 \times (32 + 102)\right] \times 762} = 0.85 MPa \qquad (24)$$

where:

A_s – the area of one longitudinal rebar;

f_y – the yield strength of the longitudinal rebar;

p – the inside crack perimeter along the longitudinal rebars;

n – the number of rebars;

d_b – the diameter of longitudinal rebars;

cc – the concrete cover to the longitudinal rebars;

L_c – the lap splice length.

The contribution of ties to the clamping force is calculated by Equation (25):

$$f_h = \frac{0.002 A_h E_h}{D_e s} = \frac{0.002 \times 200 \times 199949}{1292 \times 305} = 0.20 MPa \quad (25)$$

where:

A_h – the area of the transverse reinforcement (ties);

E_h – the elastic modulus of ties;

D_e – the effective column diameter from Equation (17);

s – the spacing of the ties.

Based on the values calculated using Equations (24) and (25), the thickness of the composite application to clamp the lap splice region is:

$$t_j = 2\frac{500 D_e (f_l - f_h)}{E_j} = 2 \times \frac{500 \times 1292 \times (0.85 - 0.20)}{64730} = 12.97 mm \quad (26)$$

where the only unknown is E_j, the modulus of the composite jacket found in Chapter 2.

6.2.3 Shear strengthening for the columns

To design the composite jacket for shear, first, each of the shear resisting components were evaluated and then subtracted from the design shear. The design shear was estimated as 1.5 times the column shear at yielding. The thickness of the composite jacket inside the plastic hinge region is calculated using Equation (27) (there was no shear strengthening necessary outside the plastic region):

$$t_j = \frac{125}{E_j D}\left[\frac{V_0}{\phi} - (V_c + V_s + V_p)\right] = \frac{125}{64730 \times 0.914} \times \left[\frac{743}{0.85} - (68 + 186 + 46)\right] = 1.28 mm \quad (27)$$

where:

V_0 – the design shear;

V_c – the shear contribution of concrete;

V_s – the shear contribution of ties;

V_p – the effect of axial load;

D – the width of the column;

ϕ – the shear strength reduction factor.

6.2.4 Flexural plastic hinge confinement for the cap beam

Since the shear capacity of the cap beam was found to be adequate (outside the joint region), only the confinement of the plastic hinge was considered. The design of the composite application followed the procedure presented in Section 6.2.1. Due to the different geometry and dimensions of the beam, the effective diameter D_e of the equivalent oval jacket was found as 2079 mm, and the thickness of the jacket was calculated using Equation (28):

$$t_j = 2 \times 0.1 \frac{2079 \times (0.0065 - 0.004) \times 20.68}{628 \times 0.01} = 3.42mm \tag{28}$$

The composite layout for Bent #6 is shown in Figures 63 and 64. The additional six layers of 152 mm wide composite sheets (tapes) are provided in order to decrease the level of stresses in the column longitudinal reinforcement extended into the joint. In addition, these layers in combination with the confining sheets in the plastic hinge region, increased the flexural capacity at the top of the columns.

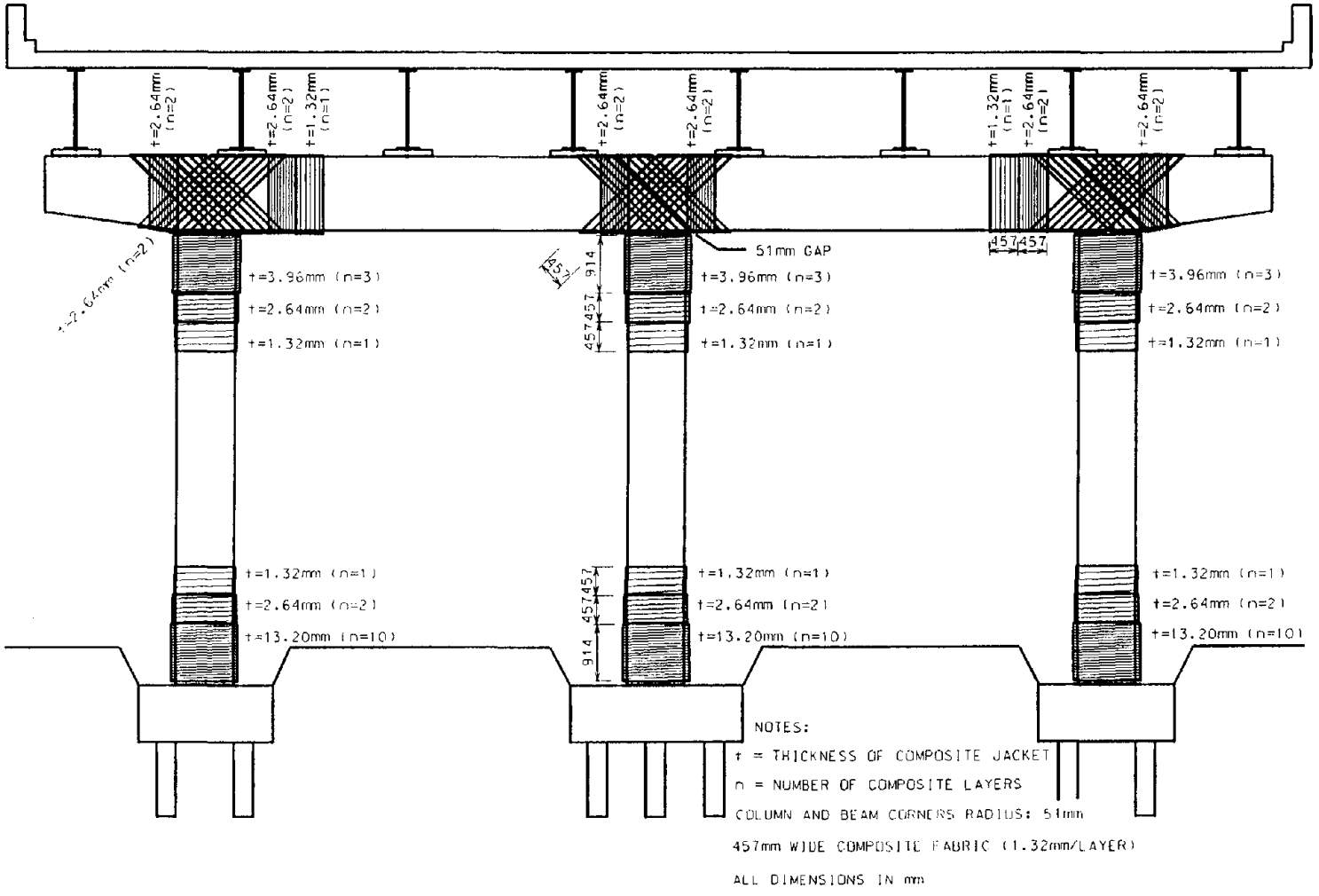

Figure 63. Composite layout for Bent #6

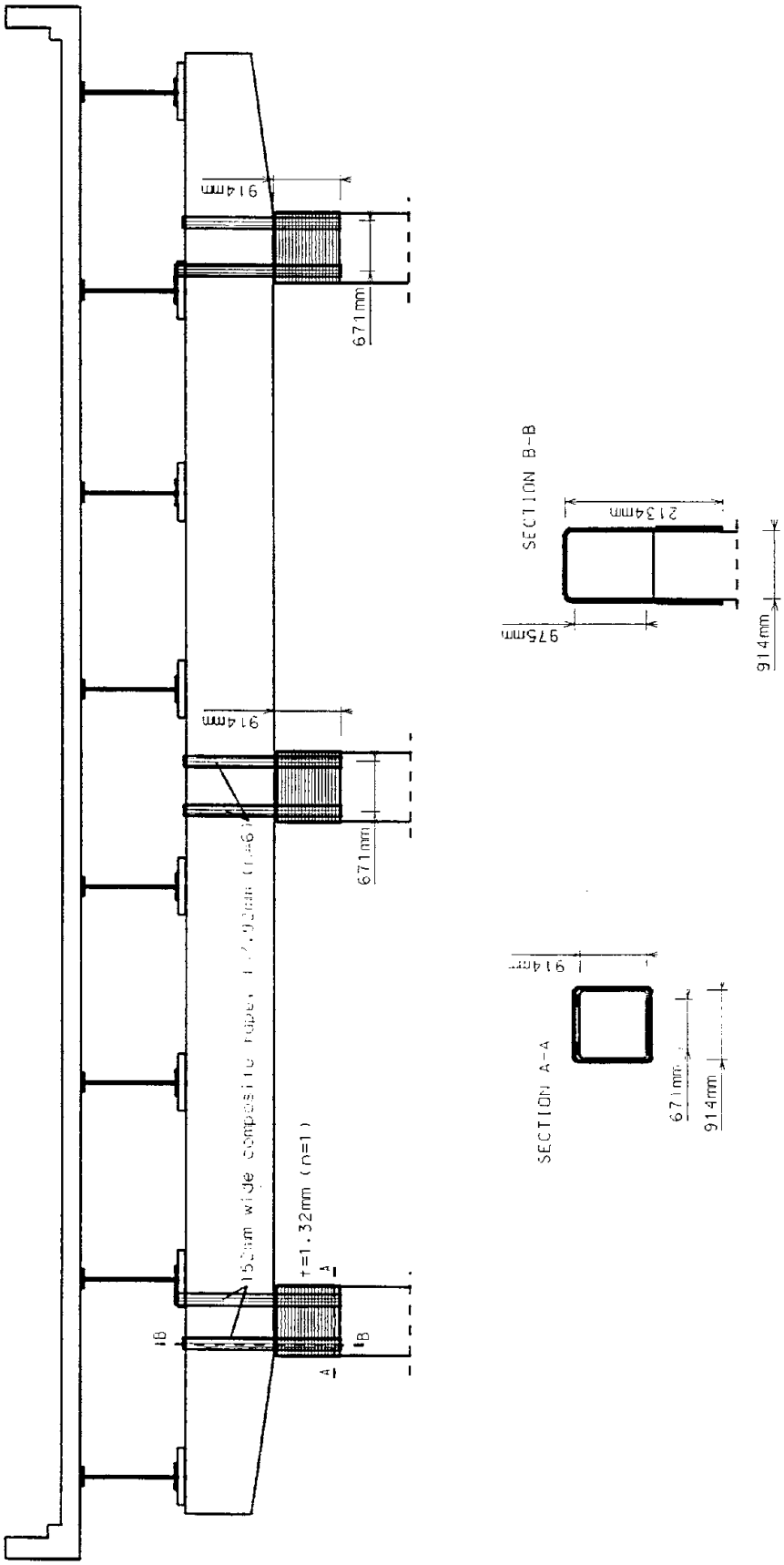

Figure 64. Additional composite layers for Bent #6

6.2.5 Shear strengthening of the column-cap beam joint

In order to design the thickness of the composite in the joint region, the joint shear forces had to be evaluated. This was done by modeling the strengthened bridge bent, using the DRAIN-2DX program, following the procedures described in the previous sections. For further reference, the input file is included in Appendix C.

Figure 65 shows the pushover curve for the bridge bent with the composite retrofit, and Figure 66 gives the experimental and analytical curves for the two bents. As it can be seen, the peak lateral load was increased compared to the results from the test in the as-is condition. which resulted in higher joint shear forces. The calculated shear forces and stresses at the ultimate displacement, in the middle joint, are:

- the horizontal joint shear force is $V_{j,horz}$ = 2176 kN, and the horizontal joint shear stress is $v_{j,horz}$ = 2.99 MPa ;
- the vertical joint shear force is $V_{j,vert}$ = 3139 kN, and the corresponding vertical joint shear stress is $v_{j,vert}$ = 3.02 MPa;
- the joint compression stress resulted from the axial force is σ_p = - 0.63 MPa.

To calculate the principal tension and compression stresses. Equation (10) was used.

$$\sigma_t = \frac{-0.63}{2} + \sqrt{\frac{(-0.63)^2}{4} + 3.00^2} = 2.70 MPa \qquad (29)$$

$$\sigma_c = \frac{-0.63}{2} - \sqrt{\frac{(-0.63)^2}{4} + 3.00^2} = -3.33 MPa \qquad (30)$$

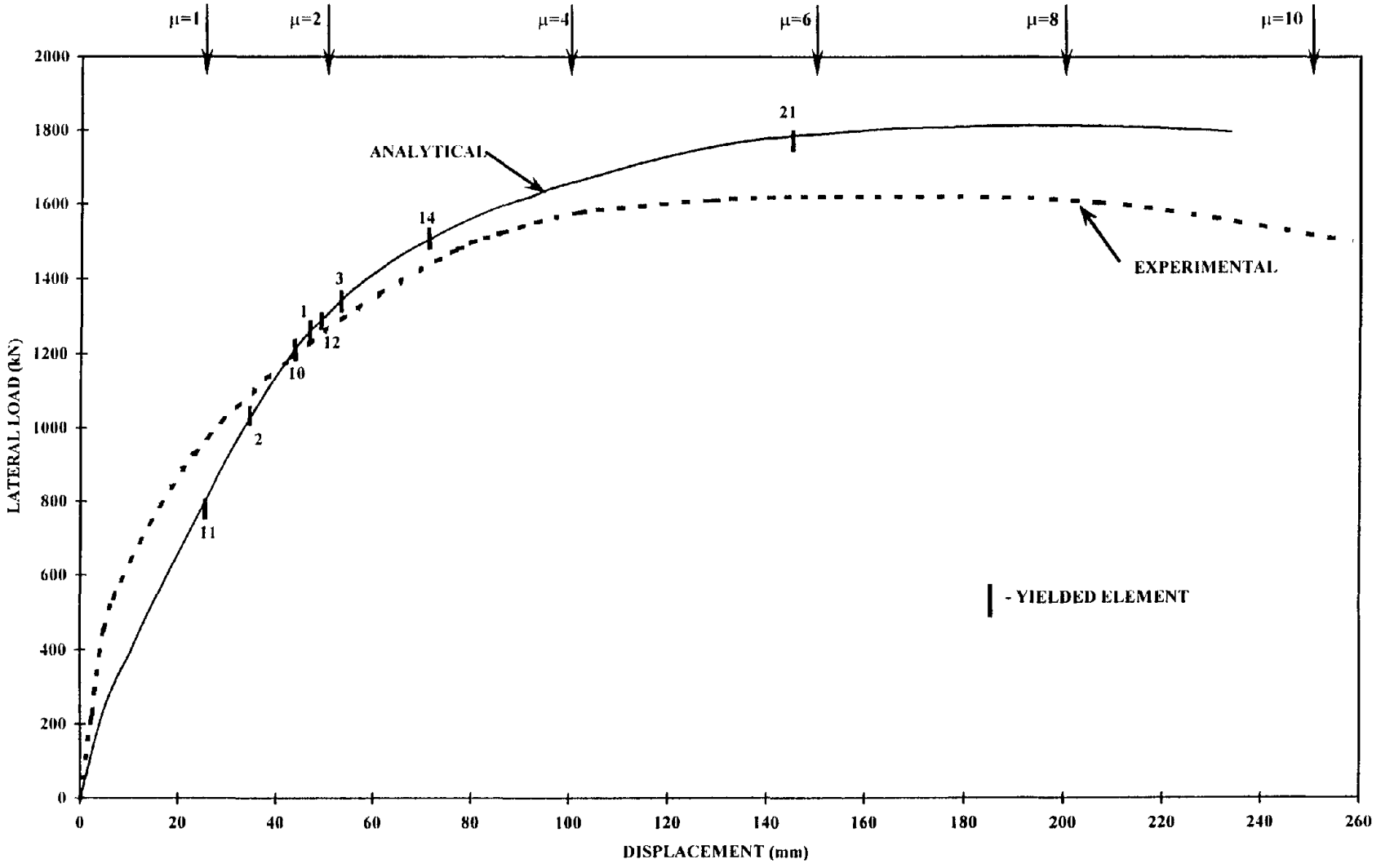

Figure 65. I-15 Bent #6 pushover curves

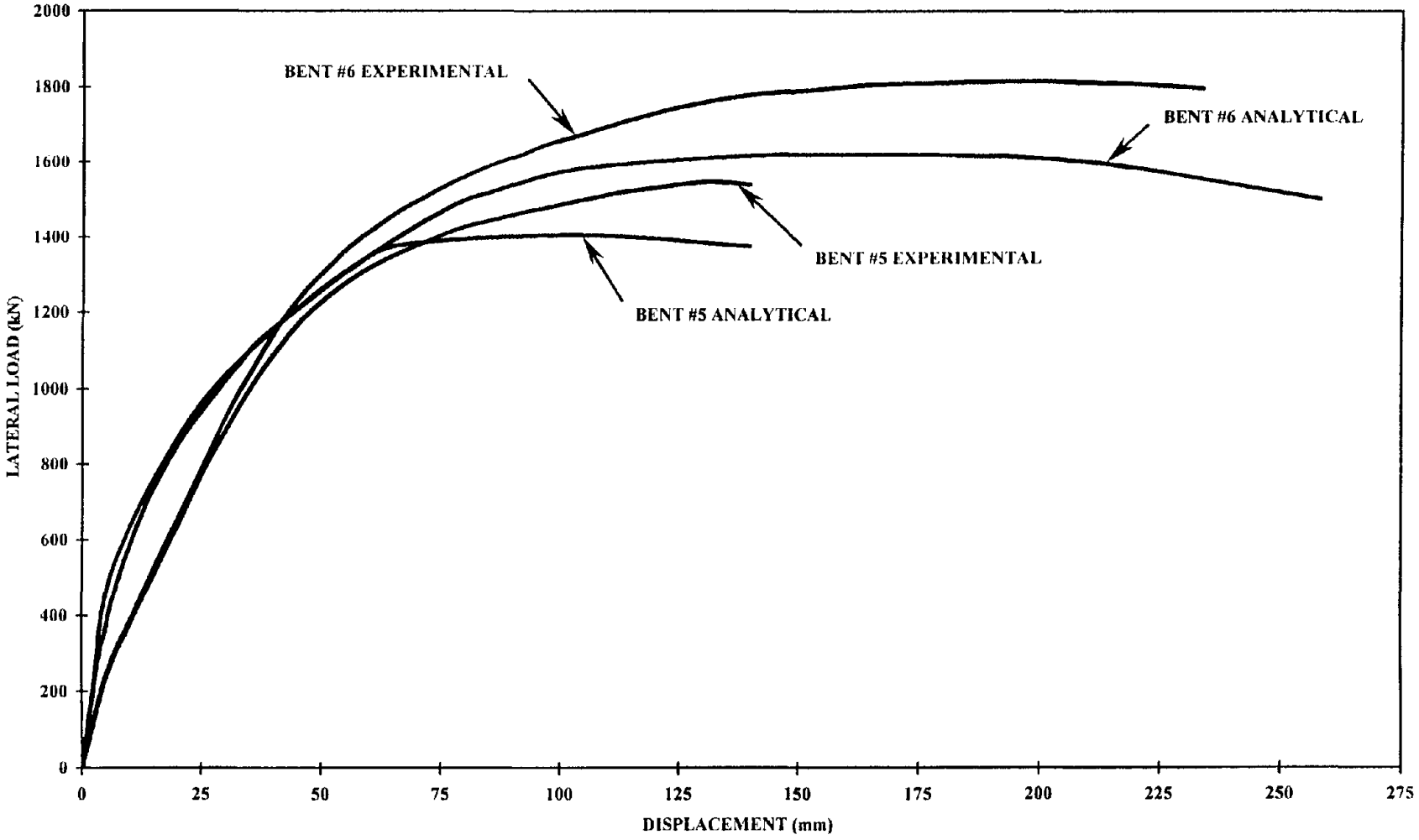

Figure 66. Pushover curves of bents in the as-is and retrofitted condition

Once again, due to the 0.63 MPa compression stress, the principal planes will not be at 45^0 from the horizontal plane. Figure 67a shows an element in the joint area with the shear and the normal stresses acting on the face of the element. If this element is rotated counterclockwise by 42^0 (see Figure 67b), the results are only normal stresses (principal stresses), with the directions parallel to the principal planes.

To identify the sign of the principal stresses, a Mohr's circle is constructed (shown in Figure 67c). Following the sign conventions used in transformation of stresses (a positive shear stress tends to rotate the element clockwise), the shear stress on the vertical planes is positive, and negative for the horizontal planes. The location of these two planes is marked with A and B. By rotating counterclockwise the line AB with 84^0 (two times the actual angle), the principal stresses are found at the points 1 and 2.

If the horizontal load is reversed, only the sign of the shear stress changes. As a result, the direction of the principal tensile stresses will be at 48^0 from the horizontal plane, measured counterclockwise. Thus, to maximize the effect of composite layers, the orientation of the fibers should be at $\pm 48^0$ from the longitudinal axis of the cap beam.

However, in the present study, the sheets were outlined and laid at approximately $\pm 45^0$. This angle is only approximate if one considers the difficulties in measuring angles in a construction project. It is the opinion of the author of the present thesis, that these three degrees fall within the tolerance a designer should accept in composite applications, and no correction was made to the design.

In other applications, when the ratio of shear to normal stresses results in principal planes inclined at an angle much different from 45^0, the actual angle should be specified in the design, and applied to the structural member.

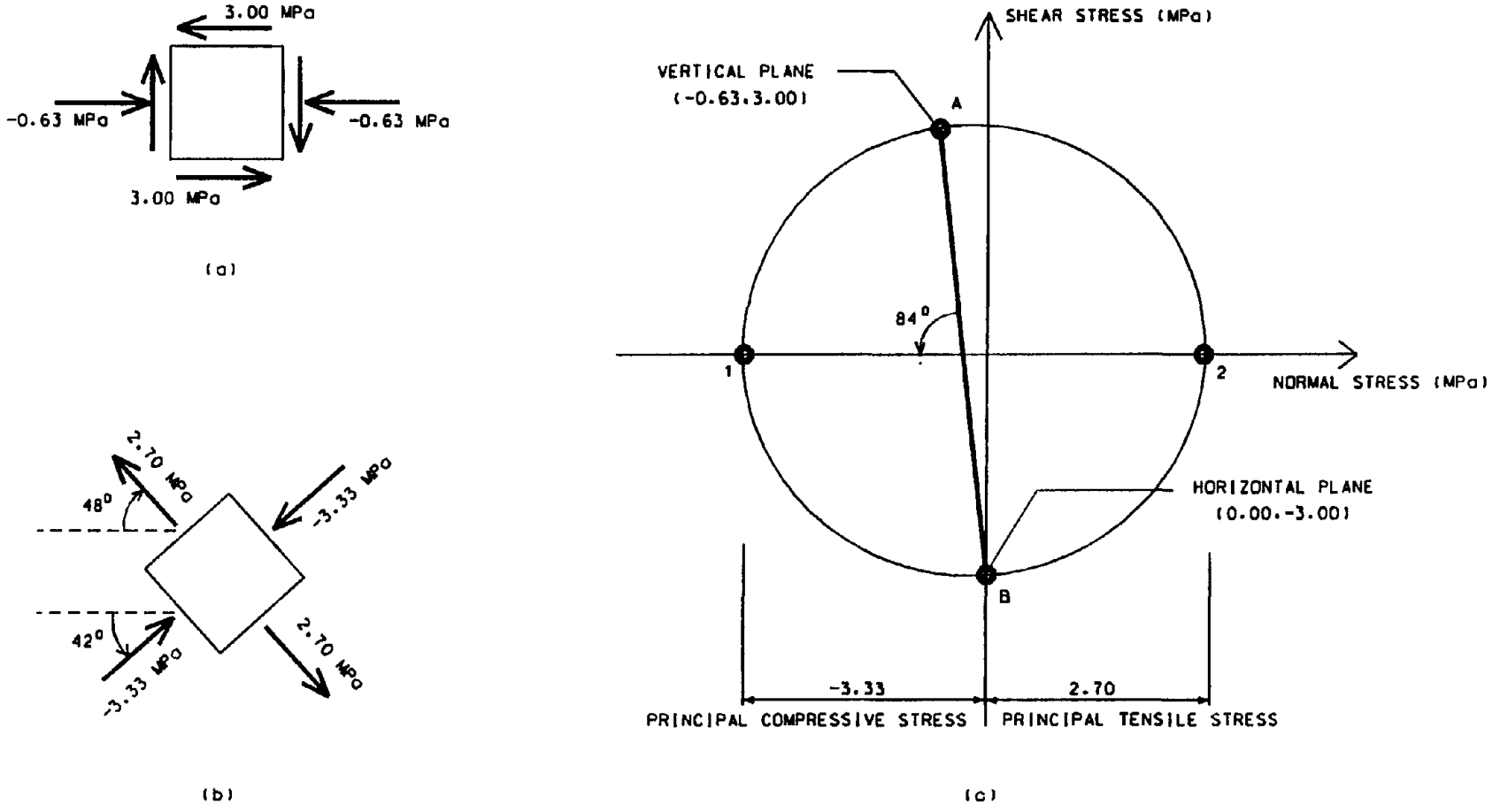

Figure 67. Principal stresses for the bridge joint

It can be seen from the calculations for the retrofitted bridge bent, that with the increase in lateral load capacity of the entire system, the demand for the joint principal tensile stress was increased by $\Delta\sigma_t = 0.72$ MPa, from 1.98 MPa to 2.70 MPa. To find the number of composite layers inclined at 48^0 required to provide a higher shear capacity, a diagonal tension crack in the joint region was analyzed.

Figure 68 shows the column-cap beam joint with the composite layer perpendicular to the crack. The direction of the crack is parallel with the principal compression stresses. The force F acting normal to crack is the total force resisted by the composite layers stressed in the fiber direction. As it can be seen, the dimension of the joint and the inclination of the principal planes control the value of the joint effective depth (d_e). The magnitude of the force F, expressed in kN and as a function of the number of composite layers (n), can be calculated using Equation (31):

$$F = nt\varepsilon_f E_f \frac{d_e}{\cos\beta} = n \times 0.00132 \times 0.0021 \times 64{,}730{,}000 \times \frac{0.823}{\cos 48^0} = 221 \times n \qquad (31)$$

where β is the angle between the longitudinal axis of the member and the fiber direction.

To find the principal tensile stress in the composite (in MPa), the value of the force F is devided by the width of the joint and by the inclined length (along the crack) bordered by the effective depth.

$$\sigma_f = \frac{F\cos\beta}{bd_e} = \frac{221 \times n \times \cos 48^0}{0.914 \times 0.823} = 0.197 \times n \qquad (32)$$

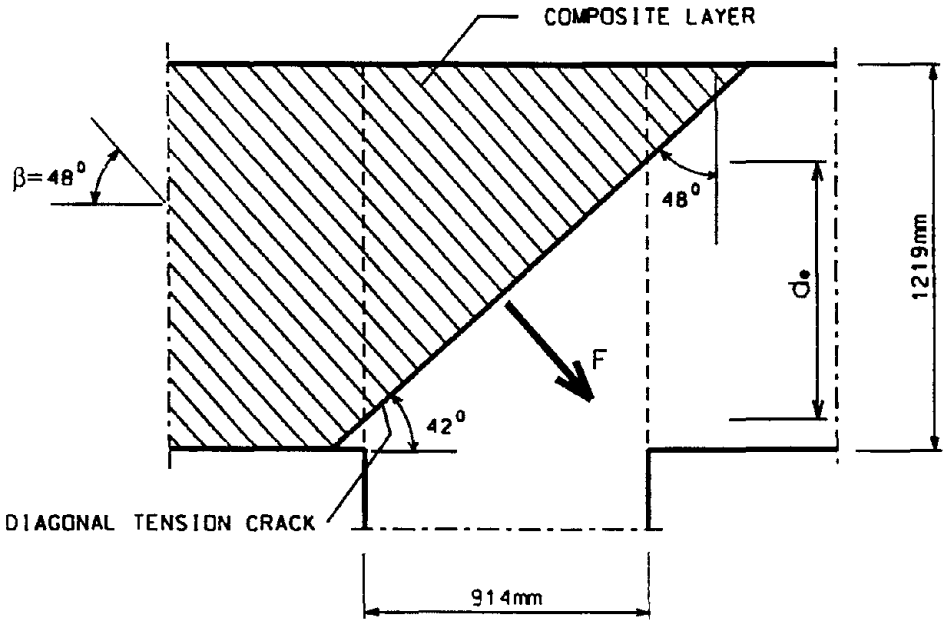

Figure 68. Composite tensile forces in the joint

This principal tensile stress (σ_f) however, has to be equal or grater than the 0.72MPa stress increase. The total number of layers required is given by:

$$n = \frac{\Delta\sigma_t}{\sigma_f} = \frac{0.72}{0.197} = 3.65 layers \tag{33}$$

In order to have a symmetric composite jacket around the joint, four layers of unidirectional fabric material were applied. These layers were provided in both directions to take into account the cyclic nature of the loads (see Figure 63).

6.3 Testing of the retrofitted bent

The test setup, the location of instruments, and the testing procedures are similar to the ones described in Section 6.1. Due to the difficulties in calibrating and reading the strain gages attached to the reinforcement of the columns and cap beam, it was not possible to record and experimentally observe the yielding of the structure.

Therefore, a force-controlled test was performed up to a lateral load of 801 kN, with a corresponding horizontal displacement of 13 mm. After this load segment, a displacement-controlled test was performed by gradually increasing the lateral deflection in each step.

The load-displacement curve for Bent #6 is shown in Figure 69. This is a good example of a ductile behavior, where the lateral capacity is maintained up to 200 mm with no significant damage to the structure. The "backbone curve" (drawn according to the FEMA 273 (1997) guidelines) for the test was included with the analytical pushover curve shown in Figure 65.

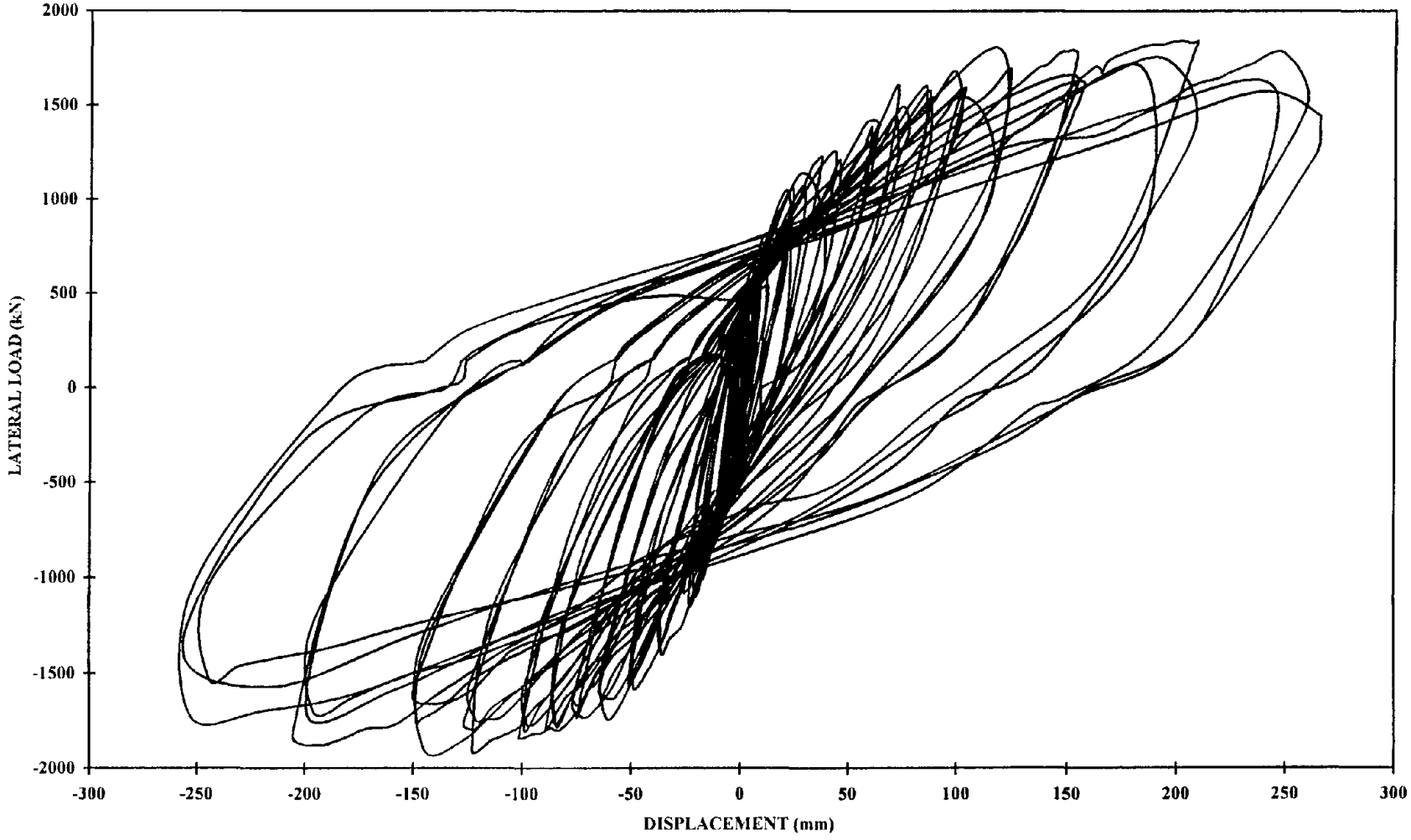

Figure 69. I-15 Bent #6 - Load vs. displacement

The good comparison between analysis and experiment is similar to the results for Bent #5. Based on these reliable analytical results, to determine the yield displacement (Δ_y), the lateral load (from the analysis) at the first yield was identified (P_y = 956 kN). The displacement from the backbone curve, corresponding to this load was then used as the yield displacement (Δ_y = 25 mm).

With an ultimate deflection of Δ_u = 259 mm, the displacement ductility of the system was approximately 10. According to the analytical results, plastic hinges were formed at the same location as the one shown in Figure 59.

The composite layers have been delaminated in the column-cap beam joint region and at the top of the columns. Figure 70 shows the strain readings from two strain gages attached to the composite sheets at the center of the joint. It can be seen that the peak value was approximately 2200 με or 0.22%, about a fifth of the ultimate value of 1% determined in Chapter 2.

This low strain level in the composite proves the validity of the value used in Equation (31) to design the composite layout. Without mechanical anchors, the composite sheets fail by debonding from the concrete surface, rather than by reaching its tensile capacity.

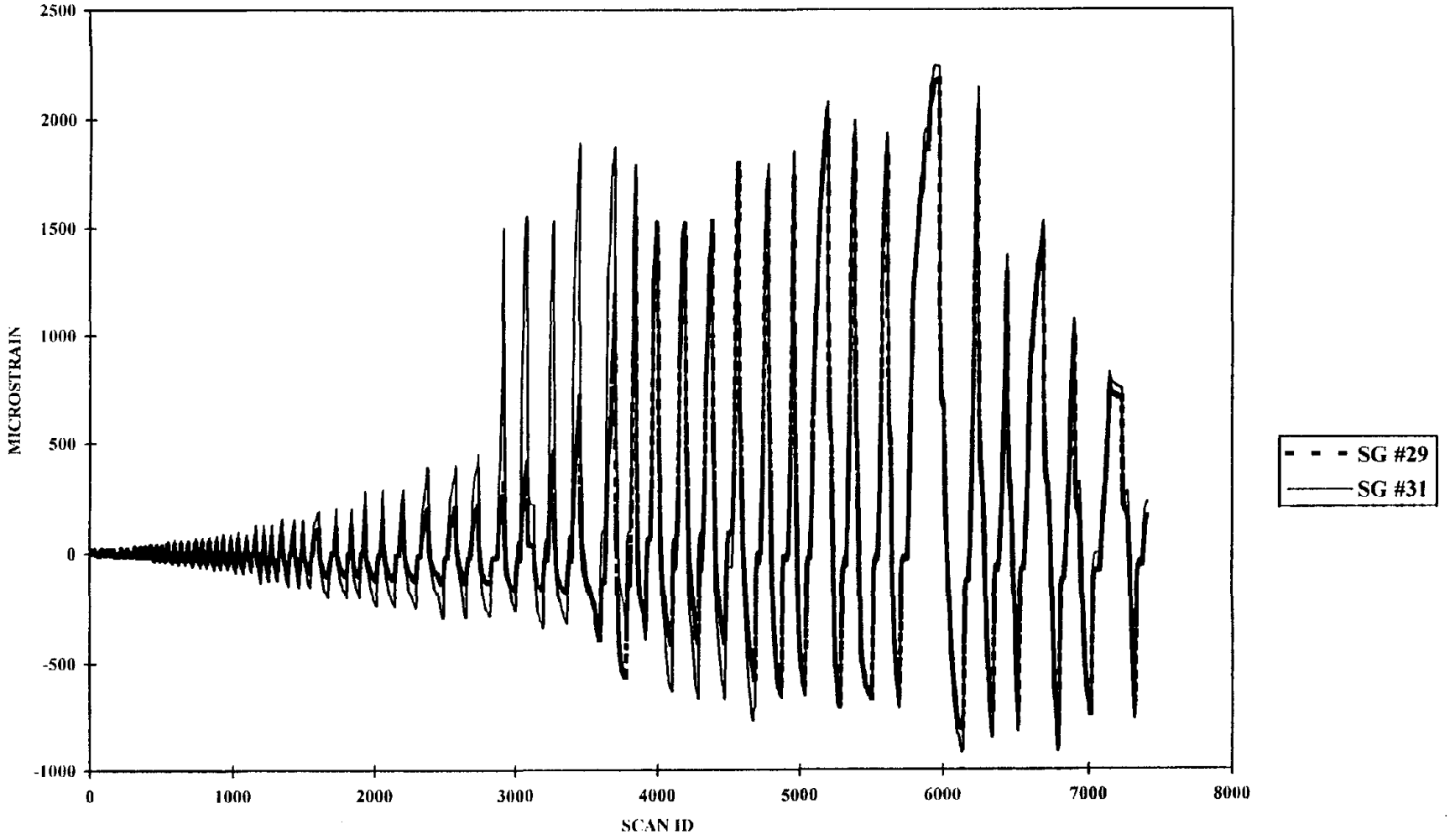

Figure 70. I-15 Bent #6 - Strain readings on the composite

CHAPTER 7

CONCLUSIONS

After performing 15 beam-column joint tests, it is clear that: externally bonded carbon fiber reinforced plastic composite sheets greatly enhance the joint's shear capacity, they improve the overall damage control, and the joints proved to have a minimal residual strength at the end of the test sufficient to support dead load.

Failure of the baseline specimens was identical. Extensive diagonal tension cracks in the joint region, which extended into the beam at the level of the bottom longitudinal reinforcement. The FRP reinforced specimens reached their peak load, but as the composite delaminated, this load level could not be sustained. This caused specimen failures at lower loads and corresponding bending moments than the element's capacity.

To compare the test results, Table 6 provided the recorded peak lateral load for each specimen. Besides the four baseline specimens, there were eleven FRP reinforced specimens tested. In this test program several variables have been monitored with the following results:

- The reinforced concrete specimens' surface preparation: superior performance has been achieved by water jetting the concrete surface, and using a high strength adhesive such as Sikadur 31.

- The resin curing system: there was no evidence of better joint shear improvement by using elevated temperature cure system versus room temperature cure system. However, no specimens have received a special surface preparation (water jet and Sikadur 31) and strengthened by elevated temperature cure system.
- The fiber orientation: the most effective fibers in the joint region were inclined at a 45^0, the direction of the principal planes. By applying the composite at a $\pm 45^0$ angle on both faces, a symmetric and balanced layout was achieved.
- The extension of composite sheets: delamination of the inclined sheets was observed to start from the top and bottom of the joint, which reinforced the importance of proper anchorage. The anchoring of these layers was improved at the face of the beam by providing the transverse layers at those locations.
- The number of layers: the performance of the specimens was a function of the concrete-composite bond. Delamination occurred at stress levels only a fifth of the composite's capacity. It is believed that there would have been no significant increase in joint strength by only adding more inclined layers without enhancing the anchorage of the sheets.
- There were no significant compression stresses recorded in the inclined composite layers, because the concrete in the joint could take the diagonal compression forces. This suggests that in a balanced layout and for joints subjected to cyclic loads, only the layers with similar directions should be counted in the analysis.

From the analysis and experiments performed on the Interstate-15 bridge bents, a few of the following preliminary conclusions are:

- Good correlations between analytical and experimental results. including the yield level, the peak lateral load, and the location of the plastic hinges.
- Due to the horizontal axial stresses applied to the joints, the angle of the principal tensile stresses is steeper than 45^0.
- Bent #5, although suffering substantial damage during the test, maintained a high load until a displacement ductility level of five.
- By retrofitting Bent #6, the objective was to double the ductility reached by the baseline test, and to increase the peak lateral load with a minimum amount of 10%. These objectives were actually met. A 20% higher lateral load was achieved for Bent #6, which resulted in the increase of the joint shear stresses by 35%.

APPENDIX A

DRAIN-2DX INPUT FILE FOR THE T-JOINT SPECIMENS

```
*STARTXX
  TJOINTF2          0 1 1 0                Beam-column joints
*NODECOORDS
C         1          0          0
C         2          4          0
C         3          8          0
C         4         12          0
C         5         16          0
C         6         20          0
C         7         24          0
C         8         28          0
C         9         32          0
C        10         36          0
C        11         40          0
C        12         44          0
C        13         48          0
C        14         52          0
C        15         56          0
C        16         60          0
C        17         64          0
C        18         32          4
C        19         32          8
C        20         32         12
C        21         32         16
C        22         32         20
C        23         32         24
C        24         32         28
C        25         32         32
C        26         32         36
C        27         32         40
C        28         32         44
*RESTRAINTS
S 010     1
S 110    17
*ELEMENTGROUP
   15     1     1              0.0           Type 15
    1     1     2     1     0     0     0     0     2
! Materials
! Unconfined concrete  (C01)
    5     0        0.5        0.1
     0.900     0.0003
     2.600     0.0013
     2.850     0.0020
     1.000     0.0100
     0.001     0.0101
```

```
! Steel reinforcement  (S01)
    1       0.1
      60.0    0.0020
! Element section properties
! Beam
   18
      7.50     11.00  C01
      6.50     14.00  C01
      5.50     12.00  C01
      4.50     14.00  C01
      3.50     14.00  C01
      2.50     14.00  C01
      1.50     14.00  C01
      0.50     14.00  C01
     -0.50     14.00  C01
     -1.50     14.00  C01
     -2.50     14.00  C01
     -3.50     14.00  C01
     -4.50     14.00  C01
     -5.50     12.00  C01
     -6.50     14.00  C01
     -7.50     11.00  C01
      5.50      1.08  S01
     -5.50      1.08  S01
! Column
   18
      7.50     11.00  C01
      6.50     14.00  C01
      5.50     10.00  C01
      4.50     14.00  C01
      3.50     14.00  C01
      2.50     14.00  C01
      1.50     14.00  C01
      0.50     14.00  C01
     -0.50     14.00  C01
     -1.50     14.00  C01
     -2.50     14.00  C01
     -3.50     14.00  C01
     -4.50     14.00  C01
     -5.50     10.00  C01
     -6.50     14.00  C01
     -7.50     11.00  C01
      6.00      3.16  S01
     -6.00      3.16  S01
! Elastic segments
  4779.0   224.0              3043.0
```

```
! Section types
    3
      0.48  F01
      0.04  E01
      0.48  F01
    3
      0.48  F02
      0.04  E01
      0.48  F02
! Element location
    1          1          2          1    1
    2          2          3          1    1
    3          3          4          1    1
    4          4          5          1    1
    5          5          6          1    1
    6          6          7          1    1
    7          7          8          1    1
    8          8          9          1    1
    9          9         10          1    1
   10         10         11          1    1
   11         11         12          1    1
   12         12         13          1    1
   13         13         14          1    1
   14         14         15          1    1
   15         15         16          1    1
   16         16         17          1    1
   17          9         18          9    2
   18         18         19          1    2
   19         19         20          1    2
   20         20         21          1    2
   21         21         22          1    2
   22         22         23          1    2
   23         23         24          1    2
   24         24         25          1    2
   25         25         26          1    2
   26         26         27          1    2
   27         27         28          1    2
*NODALOAD
 HORZ                                    Lateral load
S     1.00        0.0         0.0         27
*STAT
N      HORZ      1.000
D        28          0    1      0.010      0.140    99    99
*STOP
```

APPENDIX B

DRAIN-2DX INPUT FILE FOR THE BRIDGE BENT #5

```
*STARTXX                                        I-15 BRIDGE BENT #5
  I15STF61          0 1 1 0
*NODECOORDS
! Column
C         1           0          0
C         2         286          0
C         3         572          0
C         4           0         72
C         5         286         72
C         6         572         72
C         7           0        144
C         8         286        144
C         9         572        144
C        10           0        216
C        11         286        216
C        12         572        216
! Cap beam
C        13       -77.0        312
C        14         0.0        312
C        15        26.8        312
C        16       130.5        312
C        17       234.2        312
C        18       286.0        312
C        19       337.8        312
C        20       441.5        312
C        21       545.2        312
C        22       572.0        312
C        23       649.0        312
! Pile caps and spring supports
C        24       -24.0          0
C        25       -24.0          0
C        26        24.0          0
C        27        24.0          0
C        28       250.0          0
C        29       250.0          0
C        30       286.0          0
C        31       322.0          0
C        32       322.0          0
C        33       548.0          0
C        34       548.0          0
C        35       596.0          0
C        36       596.0          0
```

```
*RESTRAINTS
! Fixed nodes for connection elements
S 111   25        29          2
S 111   30        36          2
S 100    1         3          1
*ELEMENTGROUP
   15    1    1              0.0           Type 15
    1    1    3    4    0    0    0    2   14
! Materials
! Unconfined concrete  (C01)
    5    0       0.5        0.1
     0.900    0.0003
     2.700    0.0013
     3.000    0.0020
     2.500    0.0040
     0.001    0.0041
! Steel reinforcement  (S01)
    2       0.1
      40.0    0.0014
      46.0    0.0100
! Element section properties
! Beam a
   21
     21.50     32.00  C01
     19.50     81.00  C01
     16.50     96.00  C01
     13.50     96.00  C01
     10.50     96.00  C01
      7.50     96.00  C01
      4.50     96.00  C01
      1.50     96.00  C01
     -1.50     96.00  C01
     -4.50     96.00  C01
     -7.50     96.00  C01
    -10.50     96.00  C01
    -13.50     96.00  C01
    -16.50     96.00  C01
    -19.50     88.00  C01
    -21.50     32.00  C01
     20.75     10.16  S01
     19.50      5.08  S01
      6.92      0.62  S01
     -6.92      0.62  S01
    -20.75      5.08  S01
```

```
! Beam b
   21
     21.50      32.00  C01
     19.50      88.00  C01
     16.50      96.00  C01
     13.50      96.00  C01
     10.50      96.00  C01
      7.50      96.00  C01
      4.50      96.00  C01
      1.50      96.00  C01
     -1.50      96.00  C01
     -4.50      96.00  C01
     -7.50      96.00  C01
    -10.50      96.00  C01
    -13.50      96.00  C01
    -16.50      96.00  C01
    -19.50      83.00  C01
    -21.50      32.00  C01
     20.75       5.08  S01
      6.92       0.62  S01
     -6.92       0.62  S01
    -19.50       3.81  S01
    -20.75       8.89  S01
! Column
   17
     16.50     108.00  C01
     13.50     100.00  C01
     10.50     108.00  C01
      7.50     108.00  C01
      4.50     108.00  C01
      1.50     108.00  C01
     -1.50     108.00  C01
     -4.50     108.00  C01
     -7.50     108.00  C01
    -10.50     108.00  C01
    -13.50     100.00  C01
    -16.50     108.00  C01
     13.38       6.35  S01
      6.69       2.54  S01
      0.00       2.54  S01
     -6.69       2.54  S01
    -13.38       6.35  S01
! Elastic segments
227157.0  1408.0              3321.0
139968.0  1296.0              3321.0
326592.0  3024.0              3321.0
419904.0  3888.0              3321.0
```

```
! Rigid end zones
18.0        0.0
 0.0       24.0
    3                    -1
      0.48   F01
      0.04   E01
      0.48   F01
    3               1
      0.48   F01
      0.04   E01
      0.48   F01
    3
      0.48   F01
      0.04   E01
      0.48   F02
    3
      0.48   F02
      0.04   E01
      0.48   F01
    3                    -1
      0.48   F01
      0.04   E01
      0.48   F01
    3               1
      0.48   F01
      0.04   E01
      0.48   F01
    3
      0.48   F01
      0.04   E01
      0.48   F02
    3
      0.48   F02
      0.04   E01
      0.48   F01
    3                    -1
      0.48   F01
      0.04   E01
      0.48   F01
    3               1
      0.48   F01
      0.04   E01
      0.48   F01
    3
      0.48   F03
      0.04   E02
      0.48   F03
```

```
    1
      1.00  E03
    1
      1.00  E04
    3                -2
      0.48  F03
      0.04  E02
      0.48  F03
! Element location
! Column elements
    1          1          4          3   11
    2          2          5          3   11
    3          3          6          3   11
    4          4          7          3   11
    5          5          8          3   11
    6          6          9          3   11
    7          7         10          3   11
    8          8         11          3   11
    9          9         12          3   11
   10         10         14          4   14
   11         11         18          7   14
   12         12         22         10   14
! Beam elements
   13         13         14          1    1
   14         14         15          1    2
   15         15         16          1    3
   16         16         17          1    4
   17         17         18          1    5
   18         18         19          1    6
   19         19         20          1    7
   20         20         21          1    8
   21         21         22          1    9
   22         22         23          1   10
! Pile cap elements
   23          1         24         23   12
   24          1         26         25   12
   25          2         28         26   13
   26          2         31         29   13
   27          3         33         30   12
   28          3         35         32   12
*ELEMENTGROUP
    4    1    0                              Connection elements
    2
    1  3.50E+03        0.0    3500.0    3500.0  1.0   2    1
    2  1.50E+03        0.0    1500.0    1500.0  1.0   2    1
```

```
1        24          25          1        1
2        26          27          1        1
3        28          29          1        1
4         2          30         28        2
5        31          32          1        1
6        33          34          1        1
7        35          36          1        1
*NODALOAD
 VERT                                      Gravity loads
! Deck, girder and bent cap weight
S       0.0       -54.0         0.0       13
S       0.0       -54.0         0.0       15
S       0.0       -54.0         0.0       16
S       0.0       -54.0         0.0       17
S       0.0       -54.0         0.0       19
S       0.0       -54.0         0.0       20
S       0.0       -54.0         0.0       21
S       0.0       -54.0         0.0       23
! Column weight
S       0.0       -32.4         0.0        1
S       0.0       -32.4         0.0        2
S       0.0       -32.4         0.0        3
*NODALOAD
 HORZ                                      Lateral load
S     1.00         0.0         0.0       13
*STAT
N      VERT         1.0
L       1.0         1.0
*STAT
N      HORZ       1.000
D        13           0    1      0.100       5.50    99    99
*STOP
```

APPENDIX C

DRAIN-2DX INPUT FILE FOR THE BRIDGE BENT #6

```
*STARTXX                                        I-15 BRIDGE BENT #6
  I15STF51          0 1 1 0
*NODECOORDS
! Column
C         1           0          0
C         2         286          0
C         3         572          0
C         4           0         72
C         5         286         72
C         6         572         72
C         7           0        144
C         8         286        144
C         9         572        144
C        10           0        216
C        11         286        216
C        12         572        216
! Cap beam
C        13       -77.0        312
C        14         0.0        312
C        15        26.8        312
C        16       130.5        312
C        17       234.2        312
C        18       286.0        312
C        19       337.8        312
C        20       441.5        312
C        21       545.2        312
C        22       572.0        312
C        23       649.0        312
! Pile caps and spring supports
C        24       -24.0          0
C        25       -24.0          0
C        26        24.0          0
C        27        24.0          0
C        28       250.0          0
C        29       250.0          0
C        30       286.0          0
C        31       322.0          0
C        32       322.0          0
C        33       548.0          0
C        34       548.0          0
C        35       596.0          0
C        36       596.0          0
```

```
*RESTRAINTS
! Fixed nodes for connection elements
S 111   25        29          2
S 111   30        36          2
S 100    1         3          1
*ELEMENTGROUP
   15    1    1              0.0        Beam & column, Type 15
    4    1    5     4     0     0     0     2    15
! Materials
! Unconfined concrete  (C01)
    5    0        0.5        0.1
     0.900    0.0003
     2.700    0.0013
     3.000    0.0020
     2.500    0.0040
     0.001    0.0041
! Confined concrete in columns  (C02)
    5    0        0.5        0.1
     0.900    0.0003
     2.700    0.0013
     3.500    0.0025
     2.500    0.0065
     0.001    0.0105
! Confined concrete in beams  (C03)
    5    0        0.5        0.1
     0.900    0.0003
     2.700    0.0013
     3.500    0.0025
     2.500    0.0065
     0.001    0.0105
! Carbon FRP composite reinforcement  (C04)
    2    2        0.5        0.1
     91.00    0.0100
     0.001    0.0130
     91.00    0.0100
     0.001    0.0130
! Steel reinforcement  (S01)
    2       0.1
      40.0    0.0014
      46.0    0.0100
! Element section properties
! Beam a
   21
     22.50    108.00  C03
     19.50     93.00  C03
     16.50    108.00  C03
     13.50    108.00  C03
```

```
      10.50    108.00  C03
       7.50    108.00  C03
       4.50    108.00  C03
       1.50    108.00  C03
      -1.50    108.00  C03
      -4.50    108.00  C03
      -7.50    108.00  C03
     -10.50    108.00  C03
     -13.50    108.00  C03
     -16.50    108.00  C03
     -19.50    100.00  C03
     -22.50    108.00  C03
      20.75     10.16  S01
      19.50      5.08  S01
       6.92      0.62  S01
      -6.92      0.62  S01
     -20.75      5.08  S01
! Beam b
   21
      22.50    108.00  C01
      19.50    100.00  C01
      16.50    108.00  C01
      13.50    108.00  C01
      10.50    108.00  C01
       7.50    108.00  C01
       4.50    108.00  C01
       1.50    108.00  C01
      -1.50    108.00  C01
      -4.50    108.00  C01
      -7.50    108.00  C01
     -10.50    108.00  C01
     -13.50    108.00  C01
     -16.50    108.00  C01
     -19.50     95.00  C01
     -22.50    108.00  C01
      20.75      5.08  S01
       6.92      0.62  S01
      -6.92      0.62  S01
     -19.50      3.81  S01
     -20.75      8.89  S01
! Column bottom
   17
      16.50    108.00  C02
      13.50    100.00  C02
      10.50    108.00  C02
       7.50    108.00  C02
       4.50    108.00  C02
```

```
      1.50     108.00  C02
     -1.50     108.00  C02
     -4.50     108.00  C02
     -7.50     108.00  C02
    -10.50     108.00  C02
    -13.50     100.00  C02
    -16.50     108.00  C02
     13.38       6.35  S01
      6.69       2.54  S01
      0.00       2.54  S01
     -6.69       2.54  S01
    -13.38       6.35  S01
! Column middle
   17
     16.50     108.00  C01
     13.50     100.00  C01
     10.50     108.00  C01
      7.50     108.00  C01
      4.50     108.00  C01
      1.50     108.00  C01
     -1.50     108.00  C01
     -4.50     108.00  C01
     -7.50     108.00  C01
    -10.50     108.00  C01
    -13.50     100.00  C01
    -16.50     108.00  C01
     13.38       6.35  S01
      6.69       2.54  S01
      0.00       2.54  S01
     -6.69       2.54  S01
    -13.38       6.35  S01
! Column top
   19
     16.50     108.00  C02
     13.50     100.00  C02
     10.50     108.00  C02
      7.50     108.00  C02
      4.50     108.00  C02
      1.50     108.00  C02
     -1.50     108.00  C02
     -4.50     108.00  C02
     -7.50     108.00  C02
    -10.50     108.00  C02
    -13.50     100.00  C02
    -16.50     108.00  C02
     13.38       6.35  S01
      6.69       2.54  S01
```

```
      0.00       2.54   S01
     -6.69       2.54   S01
    -13.38       6.35   S01
     12.00       3.74   C04
    -12.00       3.74   C04
! Elastic segments
331776.0  1728.0                3321.0
139968.0  1296.0                3321.0
326592.0  3024.0                3321.0
419904.0  3888.0                3321.0
! Rigid end zones
18.0        0.0
 0.0       24.0
    3                  -1
      0.48  F01
      0.04  E01
      0.48  F01
    3              1
      0.48  F01
      0.04  E01
      0.48  F01
    3
      0.48  F01
      0.04  E01
      0.48  F02
    3
      0.48  F02
      0.04  E01
      0.48  F01
    3                  -1
      0.48  F01
      0.04  E01
      0.48  F01
    3              1
      0.48  F01
      0.04  E01
      0.48  F01
    3
      0.48  F01
      0.04  E01
      0.48  F02
    3
      0.48  F02
      0.04  E01
      0.48  F01
```

```
     3                  -1
       0.48  F01
       0.04  E01
       0.48  F01
     3              1
       0.48  F01
       0.04  E01
       0.48  F01
     3
       0.48  F03
       0.04  E02
       0.48  F03
     1
       1.00  E03
     1
       1.00  E04
     3                  -2
       0.48  F03
       0.04  E02
       0.48  F05
     3
       0.48  F04
       0.04  E02
       0.48  F04
! Element location
! Column elements
     1          1          4          3   11
     2          2          5          3   11
     3          3          6          3   11
     4          4          7          3   15
     5          5          8          3   15
     6          6          9          3   15
     7          7         10          3   15
     8          8         11          3   15
     9          9         12          3   15
    10         10         14          4   14
    11         11         18          7   14
    12         12         22         10   14
! Beam elements
    13         13         14          1    1
    14         14         15          1    2
    15         15         16          1    3
    16         16         17          1    4
    17         17         18          1    5
    18         18         19          1    6
    19         19         20          1    7
    20         20         21          1    8
```

```
   21         21         22          1    9
   22         22         23          1   10
! Pile cap elements
   23          1         24         23   12
   24          1         26         25   12
   25          2         28         26   13
   26          2         31         29   13
   27          3         33         30   12
   28          3         35         32   12
*ELEMENTGROUP
    4    1    0                              Connection elements
    2
    1  3.50E+03     0.0  3500.0  3500.0        1.0    2    1
    2  1.50E+03     0.0  1500.0  1500.0        1.0    2    1
1        24          25          1         1
2        26          27          1         1
3        28          29          1         1
4         2          30         28         2
5        31          32          1         1
6        33          34          1         1
7        35          36          1         1
*NODALOAD
 VERT                                        Gravity loads
! Deck, girder and bent cap weight
S      0.0      -54.0        0.0         13
S      0.0      -54.0        0.0         15
S      0.0      -54.0        0.0         16
S      0.0      -54.0        0.0         17
S      0.0      -54.0        0.0         19
S      0.0      -54.0        0.0         20
S      0.0      -54.0        0.0         21
S      0.0      -54.0        0.0         23
! Column weight
S      0.0      -32.4        0.0          1
S      0.0      -32.4        0.0          2
S      0.0      -32.4        0.0          3
*NODALOAD
 HORZ                                       Lateral load
S     1.00        0.0        0.0         13
*STAT
N     VERT        1.0
L      1.0        1.0
*STAT
N     HORZ      1.000
D       13          0    1     0.100       9.20   99   99
*STOP
```

REFERENCES

ACI Committee 318 (1995). "Building Code Requirements for Reinforced Concrete (ACI 318-95) and Commentary (ACI 318R-95)." *American Concrete Institute*, Detroit, MI.

ACI Committee 352 (1991). "Recommendations for design of beam-column joints in monolithic reinforced concrete structures (ACI 352R-91)." *American Concrete Institute*, Detroit, MI.

Alcocer, S. M., and Jirsa, J. O. (1993). "Strength of reinforced concrete frame connections rehabilitated by jacketing." *ACI Structural Journal*, 90(3), 249-261.

Al-Salloum, Y. A., Alsayed, S. H., Almusallam, T. H., and Amjad, M. A. (1996). "Some design considerations for concrete beams reinforced by GFRP bars." *Proc., First International Conference on Composites in Infrastructure*, ICCI'96, Tucson, Arizona, 318-331.

An, W., Saadatmanesh, H., and Ehsani, M. R. (1991)."RC beams strengthened with FRP plates. I: Analysis and parametric study." *J. of Structural Engineering*, ASCE, 117(11), 3434-3455.

Arduini, M., Di Tommaso, A., and Giacani, S. (1996). "Modelling of concrete beams reinforced with external FRP prestressed tendons." *Proc., First International Conference on Composites in Infrastructure*, ICCI'96, Tucson, Arizona, 481-490.

ASTM D 3039 (1996). "Standard test method for tensile properties of polymer matrix composite materials." *ASTM D 3039/D 3039M-95a.*

ASTM D 3171 (1996). "Test method for fiber content of resin-matrix composites by matrix digestion." *ASTM D 3171.*

Biddah, A., Ghobarah, A., and Aziz, T. S. (1997). "Upgrading of nonductile reinforced concrete frame connections." *J. of Structural Engineering*, ASCE, 123(8), 1001-1010.

Bollo, M. E., Mahin, S. A., Moehle, J. P., Stephen, R. M., and Qi, X. (1990). "Observations and implications of tests on the Cypress Street viaduct test structure." *Report No. UCB/SEMM-90/21*, University of California, Berkeley, CA.

Chajes, M. J., Januszka, T. F., Mertz, D. R., Thomson, T. A. Jr., and Finch, W. W. Jr. (1994). "Shear strengthening of reinforced concrete beams using externally applied composite fabrics." *Research Report No. CIEG94-1*, University of Delaware, Newark, Delaware.

Chajes, M. J., Kaliakin, V. N., and Meyer, A. J. Jr. (1996). "Behavior of engineered wood-CFRP beams." *Proc., First International Conference on Composites in Infrastructure*, ICCI'96, Tucson, Arizona, 870-877.

Dolan, C. W., Galloway, T. L., and Tsunemori, A. (1997). "Prestressed glued-laminated timber beam – pilot study." *J. of Composites for Construction*, ASCE, 1(1), 10-16.

Domenico, N. G., Mahmoud, Z. I., and Rizkalla, S. H. (1998). "Bond properties of carbon fiber composite prestressing." *ACI Structural Journal*, 95(3), 281-290.

Earthquake Engineering Research Institute (1995). "Northridge earthquake of January 17, 1994 – Reconnaissance report." *Earthquake Spectra*, Supplement C to Volume 11, Oakland, CA.

Ehsani, M. R., and Saadatmanesh, H. (1997). "Fiber composites: An economical Alternative for retrofitting earthquake damaged precast-concrete walls." *Earthquake Spectra*, Earthquake Engineering Research Institute, Oakland, CA, 13(2), 225-241.

"ENR Special advertising section, Plastics and composites in construction." (1995). *Engineering News Record*, The McGraw-Hill Companies.

Federal Emergency Management Agency (1997)."NEHRP Guidelines for the Seismic Rehabilitation of Buildings." *FEMA 273 and 274*, Washington, DC.

Gamble, W. L., and Hawkins, N. M. (1996). "Seismic retrofitting of bridge pier columns." *Proc., Structures Congress XIV*, ASCE, Chicago, Illinois, 16-23.

Gergely, I. (1996). "Linear and nonlinear procedures for seismic evaluation of existing buildings." M. Sc. Thesis, University of Utah, Salt Lake City, UT.

Gergely, I., Pantelides, C. P., Reaveley, L. D., and Nuismer, R. J. (1997). "Application of advanced composite materials to the repair and retrofit of highway bridge bents." *Research Report UUCVEEN 97-01*, University of Utah, Salt Lake City, UT.

Gergely, I., Pantelides, C. P., Nuismer, R. J., and Reaveley, L. D. (1998). "Repair of a bridge pier with carbon fiber composites." *J. of Composites for Construction*, ASCE, accepted.

Hoppel, C. P. R., Bogetti, T. A., Gillespie, J. W. Jr., Howie, I., and Kharbari, V. M. (1994). "Analysis of a concrete cylinder with a composite hoop wrap." *Proc., Third Engineering Materials Conference*, ASCE, San Diego, CA., 191-198.

Howie, I., and Karbhari, V. M. (1995). "Effect of tow sheet composite wrap architecture on strengthening of concrete due to confinement: I – Experimental studies." *J. of Reinforced Plastics and Composites*, 14(9), 1008-1030.

Innamorato, D. (1994). "The repair of reinforced structural masonry walls using a carbon fiber, polymeric matrix composite overlay." M. Sc. Thesis, University of California. San Diego, La Jolla, CA.

Karbhari, V. M. (1996). "Issues in joining composites to concrete – rehabilitation and retrofit." *Proc., Composites '96 Manufacturing and Tooling Conference*, Anaheim. CA., 345-363.

Karbhari, V. M., and Engineer, M. (1996). "Effect of environmental exposure on the external strengthening of concrete with composites – short term bond durability." *J. of Reinforced Plastics and Composites*, 15(12), 1194-1216.

Lowes, L. N., and Moehle, J. P. (1995). "Seismic behavior of retrofit of older reinforced concrete bridge T-joints." *Report No. UCB/EERC-95/09*, University of California. Berkeley, CA.

MacGregor, J. G. (1998). *Reinforced concrete – mechanics and design*. Prentice Hall. New Jersey.

Nanni, A., and Norris, M. S. (1995). "FRP jacketed concrete under flexure and combined flexure-compression." *Construction and Building Materials*, 9(5), 273-281.

Nilsson, I. H. E., and Losberg, A. (1976). "Reinforced concrete corners and joints subjected to bending moment." *J. of the Structural Division*, ASCE, 102(ST6), 1229-1254.

Norris, T., Saadatmanesh, H., and Ehsani, M. R. (1997). "Shear and flexural strengthening of R/C beams with carbon fiber sheets." *J. of Structural Engineering*, ASCE, 123(7), 903-911.

Pantelides, C. P., Reaveley, L. D., Gergely, I., Hofheins, C., and Volnyy, V. (1998). "Testing of precast wall connections." *Research Report UUCVEEN 98-01*, University of Utah, Salt Lake City, UT.

Paulay, T., and Priestley, M. J. N. (1992). *Seismic design of reinforced concrete and masonry buildings*. John Wiley & Sons, Inc., New York, N.Y.

Picher, F., Rochette, P., and Labossiere, P. (1996). "Confinement of concrete cylinders with CFRP." *Proc., First International Conference on Composites in Infrastructure*, ICCI'96, Tucson, Arizona, 829-841.

Policelli, F. (1995). "Carbon fiber jacket wrapping of five columns on the Santa Monica viaduct Interstate 10, Los Angeles." *Report No. ACCT/BIR-95/14*, Advanced Research Projects Agency, Arlington, VA.

Prakash, V., Powell, G. H., and Filippou, F. C. (1992). "DRAIN-2DX Base Program User Guide." *Report No. UCB/SEMM-92/29*, University of California, Berkeley, CA.

Priestley, M. J. N., Seible, F., and Calvi, G. M. (1996). *Seismic design and retrofit of bridges*. John Wiley & Sons, Inc., New York, N.Y.

Priestley, M. J. N., Seible, F., MacRae, G. A., and Chai, Y. H. (1997). "Seismic assessment of the Santa Monica viaduct bent details." *ACI Structural Journal*, 94(5), 513-524.

Ritchie, P. A., Thomas, D. A., Lu, L. W., and Conelly, G. M. (1991). "External reinforcement on concrete beams using fiber reinforced plastics." *ACI Structural Journal*, 88(4), 490-500.

Saadatmanesh, H., and Ehsani, M. R. (1991). "RC beams strengthened with GFRP plates. I: Experimental studies." *J. of Structural Engineering*, ASCE, 117(11), 3417-3433.

Seible, F., Priestley, M. J. N., Innamorato, D., Weeks, J., and Policelli, F. (1994). "Carbon fiber jacket retrofit test of circular shear bridge column, CRC-2." *Report No. ACTT-94/02*, University of California, San Diego, CA.

Seible, F., Hegemier, G., Priestley, M. J. N., and Innamorato, D. (1995). "Earthquake retrofit of bridge columns with continuous carbon fiber jackets." *Report No. ACTT-95/08*, University of California, San Diego, CA.

Seible, F., Priestley, M. J. N., Hegemier, G. A., and Innamorato, D. (1997). "Seismic retrofit of RC columns with continuous carbon fiber jackets." *J. of Composites for Construction*, ASCE, 1(2), 52-62.

Saadatmanesh, H., Ehsani, M. R., and Jin, L. (1996). "Behavior of concrete columns retrofitted with fiber composite straps under cyclic loading." *Proc., First International Conference on Composites in Infrastructure*, ICCI'96, Tucson, Arizona, 842-856.

Sun, Z., Seible, F., and Priestley, M. J. N. (1993). "Diagnostics and retrofit of rectangular bridge columns for seismic loads." *Report No. SSRP-93/07*, University of California, San Diego, La Jolla, CA.

Swanson, S. R. (1997). *Introduction to design and analysis with advanced composite materials*. Prentice Hall, New Jersey.

Thomas, J., Kline, T., Emmons, P., and Kliger, H. (1996). "Externally bonded carbon fiber for strengthening concrete." *Proc., 4th Materials Engineering Conference*, ASCE, Washington, DC, 924-931.

Triantafillou, T. C. (1998). "Shear strengthening of reinforced concrete beams using epoxy-bonded FRP composites." *ACI Structural Journal*, 95(2), 107-115.